Differential impact of hypothalamic and hippocampal corticotropin-releasing hormone neurons on stress, cognition, and seizure susceptibility

A thesis

submitted by

Andrew Hooper

in partial fulfillment of the requirements

for the degree of

Doctor of Philosophy

In

Neuroscience

TUFTS UNIVERSITY

Sackler School of Graduate Biomedical Sciences

October 2016

ADVISER: Jamie Maguire, Ph.D.

Abstract

Proper regulation of the hypothalamic-pituitary-adrenal axis permits the adaptive, integrated response to stress. Corticotropin-releasing hormone neurons in the paraventricular nucleus of the hypothalamus reside at the apex of this stress signaling axis, so any genetic or environmental insult to the normal modulation of their activity can profoundly disrupt healthy stress signaling. Additionally, there exist corticotropin-releasing hormone neurons in other brain regions, notably the hippocampus. Much less is known about the function of this population, but it is thought to be critical for stress effects on cognition. The main focus of my thesis work has been twofold: first, to investigate the cellular mechanisms that regulate the activity of hypothalamic corticotropin-releasing hormone neurons involving robust inhibitory constraint by GABA and the rapid erosion of inhibition; and second, to explore the characteristics and functional relevance of hippocampal corticotropin-releasing hormone neurons, with particular emphasis on their stress-reactivity and impact on the excitability of the hippocampal network.

The relatively recent advent of genetic tools to isolate specific cell types in the brain for identification and manipulation provided the foundation for my investigations of these two neuronal populations: specifically, a transgenic mouse line that expresses Cre recombinase under the control of the promoter for the corticotropin-releasing hormone gene. For my investigations in the hypothalamus, I combined this line with a Cre-dependent mouse line that abolishes the chloride-extruding capacity of KCC2, in order to generate a mouse model exhibiting impaired inhibitory constraint of the neuroendocrine stress response, enabling me to study stress-related physiology and behavior which depend on this inhibitory constraint. For my investigations in the hippocampus, I combined the Cre recombinase line with a number of Cre-dependent molecular tools, including tracer viruses to study anatomical connectivity, the light-activated cation channel

Channelrhodopsin to study functional connectivity and circuit-level effects, and Designer Receptors Exclusively Activated by Designer Drugs to study effects of manipulating this population's activity on hippocampal-dependent behavior and seizure susceptibility.

I confirmed that inhibitory constraint of hypothalamic corticotropin-releasing hormone neurons is critical for regulating stress-reactive emotional behaviors, and helped to reveal that this inhibitory constraint is compromised following seizures. Unexpectedly, I also uncovered a novel projection from the hypothalamic population to the tuberal nucleus of the lateral hypothalamus, as well as a possible functional role for this population in body weight homeostasis. In the course of my hippocampus-oriented project, I characterized back-projecting corticotropin-releasing hormone neurons as a novel interneuron population. In addition to extensively characterizing the intrinsic properties of this population, I also uncovered their functional relevance in hippocampal-dependent learning and memory, excitability of the hippocampal network, and seizure susceptibility.

My results from studying hypothalamic chloride plasticity helped to identify a mechanism that gives rise to the vicious cycle of mutual reinforcement between pathological stress and seizures. This mechanism highlights KCC2 as a drug target with great potential for alleviating stress-related disorders and seizures, and breaking the vicious cycle between them. My characterization of back-projecting CRH interneurons adds another layer of complexity to the circuitry of the hippocampus. Additionally, my findings on CRH interneurons' impact on both the physiological function of learning and memory, and the pathophysiology of seizure susceptibility, highlight the importance of this interneuron class in hippocampal function. Finally, my results on the circuit-level impact of manipulating these interneurons provide the beginning of a mechanistic framework for how this single cell type contributes to a complex

behavior, while raising exciting new questions about the differential effects of synaptic versus peptidergic transmission.

Acknowledgements

I am first and foremost grateful to my advisor, Dr. Jamie Maguire, for taking me on as a doctoral student and providing constant support, guidance, and encouragement over the last four years. Apart from being the creative force behind all of the projects in which I was fortunate enough to play a part, Jamie has maintained a constant positive mental attitude that makes it a genuine pleasure to work in her laboratory, supported my pursuit of a career in science policy every step of the way, repeatedly lift my spirits in stressful times, and intensified my passion for neuroscience with her own. Thanks to Jamie I have had amazing opportunities to not only learn a host of techniques in the lab, but also travel to academic conferences and broaden my scientific horizons, stay on the cutting edge by learning about new techniques and hypotheses, receive critical feedback directly from the world's leading experts in the stress and epilepsy fields, and establish contacts with researchers with whom I hope to maintain productive, lifelong working relationships. I cannot imagine a better mentor and role model for an aspiring scientist than Jamie, and no words can adequately capture how fortunate I feel to have been her student.

My thesis advisory committee – Drs. Maribel Rios, Stephen Moss, and Leon Reijmers – have provided a constant source of critical guidance and creative solutions. To gain an education is to constantly grow in appreciation of how much there is to know and, by extension, how relatively little I know: in this sense every member of my committee has been absolutely instrumental to my education. I thank Dr. Rios for lending her expertise on hypothalamic function, Dr. Moss (sorry – Steve) for his expertise on all things GABA-related, Dr. Reijmers for his insights into the molecular basis of learning and memory – and all three for their extraordinary commitment of time and patience. I am also very grateful to my external thesis examiner, Dr. Kerry Ressler at Harvard Medical School. It was a great honor to have one of the

planet's foremost authorities on the neurobiology of traumatic stress critically assess my thesis work, and I thank Dr. Ressler for his time and valuable feedback towards greatly improving my dissertation.

Members of the Sackler Neuroscience Program too numerous to do full justice here have been central not only to the success of my graduate work, but also to my enjoyment of the same. I am grateful to the Neuroscience Department Chair Dr. Philip Haydon for his inspiring leadership and tireless work in maintaining a high standard of excellence across the board; to Drs. Rob Jackson, Michele Jacob, and Chris Dulla for running so many aspects of the Program and keeping the students informed, but more importantly for taking so many extra steps to ensure our personal well-being; to my former rotation mentor Dr. Yongjie Yang for a wonderfully educational rotation that made me almost as excited about astroglia as I am about interneurons; and to the entire administrative staff – Jose, Brian, Shelley, Alison, and Layla – for keeping the lights on, making sure I know where I'm supposed to be and when, and understanding how finance works (because I sure don't). I must also acknowledge both personally and professionally just a few of the many postdoctoral scholars and fellow students whose countless contributions to morale and experiments over the years made my experience an unequivocally positive one: Drs. Tarek Deeb, Sudhir Sivakumaran, Thomas Papouin, Yasuko Nakamura, Adema Ribic, Haruki Higashimori, Laverne Melon, Georgina MacKenzie, and Stephanie Miller-Smith; and of course Alex Jones, Jaclyn Dunphy, Vallent Lee, Patrick Davis, Laura Darnieder, Julie Hewitt, and Liz Hanson.

I am extremely grateful to all my brothers and sisters from C CO, 205th MI BN for the kind of loyalty that no amount of money can buy, for their boundless patience with someone who is in the bottom 1% of the world's "Keep in Touch" rankings, and for continuing to share

with me their votes of confidence and war stories over the years. In particular I thank Bergeman, Settles, Robinson, Bauchat, and Panitzke for encouraging me to pursue my dream of studying neuroscience when I had just about given up hope.

Finally, I am grateful to my mother Melodye, father Thomas, and sister Katie, the only three constants in my life, for – among many other things – never doubting me no matter how much I've doubted myself. I'll never stop, but I know that you won't either, which is an essential source of reassurance when the going gets tough.

"We are not so absurd as to propose that the teacher should not set forth his own opinions as the true ones and exert his utmost powers to exhibit their truth in the strongest light. To abstain from this would be to nourish the worst intellectual habit of all, that of not finding, and not looking for, certainty in any teacher. But the teacher himself should not be held to any creed; nor should the question be whether his own opinions are the true ones, but whether he is well instructed in those of other people, and, in enforcing his own, states the arguments for all conflicting opinions fairly."

John Stuart Mill, "Civilization," *London and Westminster Review* (1836)

Table of Contents

List of Tables

List of Figures

List of Abbreviations

ACTH	adrenocorticotropic hormone
AVP	arginine vasopressin
BNST	bed nucleus of the stria terminalis
CeA	central nucleus of the amygdala
CORT	corticosterone (rodents); cortisol (humans)
CRH	corticotropin-releasing hormone
DGGC	dentate gyrus granule cell
EPSC	excitatory postsynaptic current
EPSP	excitatory postsynaptic potential
GABA	gamma-amino butyric acid
$GABA_AR$	GABA-A receptor
Gabrd	GABA-A receptor δ (delta) subunit
GR	glucocorticoid receptor
IPSC	inhibitory postsynaptic current
IPSP	inhibitory postsynaptic potential
KA	kainic acid
LTP	long-term potentiation
MDD	major depressive disorder
mEPSC	miniature EPSC
mIPSC	miniature IPSC
MR	mineralocorticoid receptor
Pomc	pro-opiomelanocortin

PVN	paraventricular nucleus
SST	somatostatin
TLE	temporal lobe epilepsy

Copyright Release

This volume contain figures and figure legends reproduced from three copyrighted publications (O'Toole et al., 2014;Lee et al., 2016;Hooper and Maguire, 2014) and one forthcoming publication (Fuchs et al., 2016). I have obtained written permission from the respective rights holders to reproduce these copyrighted materials in my dissertation.

Differential impact

of hypothalamic and hippocampal

corticotropin-releasing hormone

neurons

on stress, cognition, and seizure

susceptibility

Introduction

1.1. Stress and epilepsy: Overarching research goals

The epilepsies are a cluster of neurological disorders characterized by bouts of highly synchronous neuronal discharges termed seizures, the clinical manifestations of which vary as a function of their anatomical locations in the brain. Epilepsy afflicts 2.2 million people in the US and 50 million people globally (Hirtz et al., 2007;Meyer et al., 2010), causing incalculable suffering and disruption in its own right but also co-occurring at high rates with neuropsychiatric syndromes in general (35% among patients with epilepsy vs 21% with no epilepsy), and with major depressive disorder in particular (17% vs 10%) (Tellez-Zenteno et al., 2007;Vargas-Perez et al., 2014). Additionally, stress is the most commonly reported trigger for seizures among patients with epilepsy (Sperling et al., 2008), strongly suggesting a mechanistic link between epilepsy and stress. Stress-related disorders include mood and anxiety disorders, which respectively affect 30.7% and 41.7% of people in the US over the course of their lives (Kessler et al., 2012). Like epilepsy, stress-related disorders carry a massive cost in terms of treatment and work impairment (Greenberg et al., 2015;Greenberg et al., 1999;Allers et al., 2015) as well as a substantially increased risk for suicide (Uebelacker et al., 2013;Miret et al., 2013;Tian et al., 2016). While a subset of individuals with epilepsy and stress-related disorders are able to manage their symptoms with currently available treatments (Goldenberg, 2010;Rush et al., 1998), drug-resistant seizures and treatment-refractory mood disorders remain major obstacles to effective treatment. In short, our understanding of the neural circuitry mediating maladaptive effects of stress on brain physiology – including seizure susceptibility – is far from complete.

The goal of my thesis work has been to uncover novel targets and strategies for treatment by shedding light on cellular mechanisms underlying seizure susceptibility, stress signaling, and interactions between the two. I have primarily focused on inhibitory (GABAergic)

neurotransmission in two neuronal populations with discrete functions in stress reactivity: first, corticotropin-releasing hormone (CRH) neurons in the paraventricular nucleus (PVN) of the hypothalamus, which act as gatekeepers for the systemic (neuroendocrine) response to stress and are tightly regulated by GABAergic inhibition; and second, CRH neurons in area CA1 of the hippocampus, which I have identified as a novel interneuron subtype, and which are thought to mediate the deleterious effects of stress on spatial learning and memory. Throughout both projects, I have striven to test the functional relevance of pathology-associated genes and neuronal populations by progressing from the micro- level of gene expression and physiology of individual classes of neurons, to the meso- level of local neuronal circuits, to the macro- level of physiology and behavior. My overarching goal has been to accurately advance our understanding of cell signaling mechanisms in the adaptive stress response and investigate how these native mechanisms can be corrupted to give rise to pathology in the form of seizures and stress-related pathological behavior. My hope is that this progress will soon be integrated into a comprehensive understanding of stress neurobiology, giving rise to powerful preventative and restorative power against pathological hyperexcitability and stress.

1.2. Stress and epilepsy: Operational definitions

"Stress" is an intuitively useful but imprecise word, as it is used interchangeably with "anxiety" in common parlance, but can describe any of a wide range of insults to homeostasis, carried through a living subject's system by disparate complex signaling pathways. For example, oxidative stress refers to a stimulus that disrupts physiological or structural integrity at the level of cells and tissue: mechanical trauma, ultraviolet radiation, nutrient deprivation, and sharp alterations in osmolarity can all trigger distinct but overlapping cell signaling cascades to alter transcription and translation, perturb ionic homeostasis, and even trigger cell death (Ikonomidou and Kaindl, 2011;Erler and Monaghan, 2015;Panich et al., 2016;Venza et al., 2015;Rani et al., 2016). At the other end of the "stress" spectrum, psychological stress describes any stimulus or situation that gives a subject the perception that their well-being is in imminent jeopardy (Ulrich-Lai and Herman, 2009;Feodorova and Sarafian, 2012;Yang et al., 2015a). Examples of psychological stress in humans include the anxiety of preparing for a consequential exam or job interview, the grief of losing a loved one, the trauma of surviving a natural disaster, or the pain and sense of helplessness from being the victim of a violent crime. The duration, severity, and predictability of a stressor determine its physiological consequences, which in turn can be gated by resilience factors and coping mechanisms. Accordingly, stress researchers employ a wide variety of animal models of psychological stress to isolate its myriad consequences and signaling pathways (Gregus et al., 2005;de Andrade et al., 2012;de Andrade et al., 2013). Importantly, one unifying feature of these models is a highly reproducible increase in circulating stress hormones via activation of hypothalamic CRH neurons (Feodorova and Sarafian, 2012;Juruena, 2014). *Throughout this volume, I apply several paradigms of psychological stress and detail each in turn; where I simply use the term "stress," I refer specifically to the psychological variety.*

Similarly, "epilepsy" is a somewhat opaque term given the diverse etiologies and substrates of the epilepsy syndromes. The primary accepted clinical definition of epilepsy is the occurrence of at least two spontaneous seizures – that is, seizures not directly provoked by traumatic brain injury, infection, anoxia, or other insults – at least 24 hours apart (Fisher et al., 2014). The diagnosis of a specific epilepsy syndrome depends on the putative anatomical point of initiation (focus) of seizures, age of onset, causal neuropathological features like tubers, and involvement of genetic risk factors (Park et al., 2015;Guerrini et al., 2014;Saxena and Sampson, 2015;Dravet and Oguni, 2013). Among the dozens of distinct epilepsy syndromes, the most common is partial-complex temporal lobe epilepsy (TLE), comprising a majority of partial-onset epilepsies which in turn account for more than half of all epilepsy cases (Tellez-Zenteno and Hernandez-Ronquillo, 2012). Partial-complex TLE is characterized by foci in the hippocampus or hippocampus-adjacent neocortical regions, and the tendency of seizures to impact a limited brain region – and hence a single function or restricted subset of functions – upon initiation, before spreading across a wider swath of cortex as they progress (Tatum, 2012). This syndrome is also characterized by a conspicuously high incidence of drug-resistant seizures for reasons that remain poorly understood (Laxer et al., 2014;Albus et al., 2008). As in the case of stress, a wide variety of animal models exist to experimentally access distinct epilepsy syndromes or to capture specific features of the disease. The WAG/Rij strain of rat, and more recently, TRIP8b knockout mice, were found to have spontaneous absence seizures and are thus being used to study absence epilepsy etiology (Sarkisova and van, 2011;Heuermann et al., 2016); another genetic model – mice with a point mutation in a sodium channel subunit – demonstrates hippocampal hyperexcitability and spontaneous seizures (Hatch et al., 2014); and even the comparatively simple nervous system of the zebrafish has been utilized to great effect in

studying gene mutations associated with epilepsy (Griffin et al., 2016). Turning away from genetic models of epilepsy, there also exist a variety of experimental means of inducing seizures, each with strengths and limitations. For example, in the amygdala kindling model, repetitive electrical stimulation is used promote hyperexcitability of the limbic forebrain, producing spontaneous seizures (Casillas-Espinosa et al., 2015;Cota et al., 2016). Systemic infusion of the chemoconvulsant pilocarpine, or intrahippocampal infusion of another chemoconvulsant, kainic acid (KA), can also reliably produce robust spontaneous seizures after a defined latent period (Kandratavicius et al., 2014;Curia et al., 2008;Chen et al., 2013a). Throughout my thesis work, I applied the single-dose systemic KA and pilocarpine models. Both of these are widely-used models of TLE, but the systemic KA model can be more narrowly defined as a model of robust, acute temporal lobe seizures (Levesque and Avoli, 2013). Since the systemic KA model does not give rise to subsequent spontaneous seizures after just one dose, it holds less validity for epileptogenesis, the generation of spontaneous seizures on a days-to-weeks timescale, but rather is very useful for studying ictogenesis, the generation of individual seizures on the order of milliseconds to minutes. ***Throughout this volume, I use the term "epilepsy" specifically in reference to clinical studies or animal models involving epileptogenesis and the development of spontaneous seizures, and instead the term "acute seizures" when dealing with the systemic KA model.***

1.3. Corticotropin-releasing hormone: Discovery and relevance to stress

In 1981 Wylie Vale and colleagues isolated a 41-amino acid peptide from ovine hypothalamus, dubbing this peptide "corticotropin-releasing factor" (hereinafter referred to as corticotropin-releasing hormone, CRH, since it has since been established to act as a hormone) based on its ability to potently stimulate release of the primary stress hormone secretagogue adrenocorticotropic hormone (ACTH) from cultured rat pituitary cells (Vale et al., 1981). The Vale group then used an antiserum against CRH to histologically identify the critical CRH-producing brain region for the neuroendocrine stress response: the parvocellular division of the paraventricular nucleus (PVN) of the hypothalamus (Bloom et al., 1982). Using the same antiserum, Vale and colleagues next revealed that the cerebrospinal fluid (CSF) of patients with major depressive disorder (MDD) contained significantly higher levels of CRH than the CSF of healthy control subjects or patients with schizophrenia or senile dementia (Nemeroff et al., 1984), implicating hypersecretion of CRH as a key culprit in stress-related psychiatric disorders. This landmark series of studies represented a giant leap forward in defining the anatomical substrates for the neuroendocrine response to stress. Indeed, it is now well-established that PVN CRH neurons are the master regulators of the hypothalamic-pituitary-adrenal (HPA) axis, the endocrine signaling pathway that translates visceral or sensory information about stressful stimuli into an elevation of circulating stress hormones. Stress hormones (cortisol in humans or its counterpart in rodents, corticosterone, hereinafter CORT) in turn relay the effects of physical or psychological stress, not only back to the brain but also to organ systems throughout the body.

In the ensuing years, researchers added to Vale and colleagues' initial discoveries by uncovering CRH's cognate receptors and other related genes, and by probing their respective functions in the stress signaling pathway. The principle receptor for CRH, CRH receptor 1 (CRHR1, also known as CRF1), is highly expressed on corticotrophs in the anterior lobe of the pituitary gland, where it mediates the pro-secretory action of CRH on ACTH (Drolet and Rivest, 2001;Bittencourt and Sawchenko, 2000). Its other receptor, CRHR2 (also known as CRF2), acts in opposition to CRHR1 to attenuate HPA axis output (Bale et al., 2000;Hashimoto et al., 2001). Yet another related gene encodes a secreted protein, CRH-binding protein (CRH-BP, also known as CRF-BP), which binds extracellular CRH to buffer its local concentration and seems to play an especially important role in modulating CRH signaling during pregnancy (Behan et al., 1995;Petraglia et al., 1996). Finally, several other ligands with comparable affinities for the CRHRs and CRH-BP have joined CRH to form the family of CRH-related peptides: Urocortins I, II, and III (Lovejoy and de, 2013;Hemley et al., 2007;Weninger et al., 1999). While the identification of new auxiliary players and modulatory pathways for the stress response highlights the intricacy of the stress signaling pathway, one fundamental point from Vale and colleagues' pioneering work remains clear: hypersecretion of CRH drives the neuroendocrine stress response into disarray. Therefore, understanding the connectivity and physiology of CRH neurons is a critical means to the end of correcting the pathological HPA axis.

In the following section I will elaborate in detail on the sequence of cellular events along the circuitry impinging on the HPA axis, from the perception of a stressor to the increase in circulating CORT, with an emphasis on PVN CRH neurons' role in this circuit.

1.4. Hypothalamic CRH neurons: Neuroendocrine stress response gatekeepers

Stress signaling in the brain begins with perception: visual, olfactory, proprioceptive, and other sensory information entering via sensory organs to be processed into a coherent representation of the subject's present state and context. A representation that indicates a present threat to well-being or triggers memories of past threats initiates the stress signaling cascade, a system-wide signal that varies in detail according to the subject and the stressor, but whose general sequence is highly conserved. Within seconds of perceiving a stressor, preganglionic sympathetic neurons of the spinal cord activate the fight-or-flight response via cholinergic stimulation of the sympathetic nervous system (Ulrich-Lai and Herman, 2009). This division of the autonomic nervous system gives rise to the many peripheral responses to acute stress: a surge in circulating adrenaline from the adrenal medulla, vasodilation, mobilization of stored energy, and increased heart rate and respiration, to name a few (Ulrich-Lai and Herman, 2009). At the same time, noradrenergic brainstem neurons initiate the central response to stress via ascending projections throughout the midbrain and forebrain (Joels and Baram, 2009). Some of these extensive central projections give rise to psychological aspects of the fight-or-flight response, such as the subjective experience of fear, anxiety, or exhilaration, via ascending projections to the principle emotion center of the brain, the limbic forebrain (McKlveen et al., 2015). Others – including projections to PVN CRH neurons – work in opposition to the fight-or-flight response, acting collectively as a delayed feedback-inhibitory circuit to ensure that the acute stress state has a finite duration (Pacak et al., 1995;Fuzesi et al., 2016;Wamsteeker and Bains, 2010).

Elements of the feedback-inhibitory neuroendocrine stress circuit ultimately converge on the HPA axis, at the apex of which are CRH neurons concentrated in the medial parvocellular division of the PVN (Smith and Vale, 2006;Wamsteeker and Bains, 2010). The majority of glutamatergic afferents to PVN CRH neurons arise from the brainstem and hypothalamus, specifically the nucleus of the solitary tract, dorsomedial nucleus, medial preoptic area, and lateral hypothalamus (Herman et al., 2004). The medial parvocellular division of the PVN also receives extensive GABAergic projections, most of which arise from the anterior perifornical nucleus, perinuclear supraoptic area, anterior hypothalamic area, and anterior PVN (Roland and Sawchenko, 1993). In addition to these direct synaptic connections and the modulatory brainstem noradrenergic projections mentioned above, the neuroendocrine stress circuit also consists of descending modulatory pathways coursing through the limbic forebrain, the aforementioned emotional information-processing network, which is comprised of the prefrontal cortex, hippocampus, and amygdala. Projections from the prefrontal cortex and hippocampus indirectly suppress HPA axis output, likely through a network incorporating the BNST and multiple PVN-adjacent hypothalamic nuclei which in turn innervate PVN CRH neurons (Forray and Gysling, 2004;Jankord and Herman, 2008). The amygdala also projects to the PVN indirectly through the BNST, but unlike the cortical projections, these amygdalar projections ultimately activate the HPA axis (Herman et al., 2005). Hypothalamic CRH neurons' principle output is to the median eminence, where they release CRH onto the pituitary gland through the hypophyseal portal system (Swanson et al., 1983;Chen et al., 2015). Parvocellular neuroendocrine cells in the PVN also release arginine-vasopressin (AVP), which is primarily important for regulating vasoconstriction and kidney function, but also acts as a less-potent secretagogue for ACTH, thus playing a subordinate, modulatory role in the neuroendocrine stress response (Makara, 1992;Rotondo et al., 2016). Corticotrophs of the anterior pituitary then

release ACTH into the bloodstream to stimulate secretion of CORT from the adrenal cortex (Aguilera et al., 2001). In addition to PVN CRH neurons' critical peptidergic output to the median eminence, the PVN also contains a distinct population of neurons that form synaptic contacts with preganglionic sympathetic neurons of the spinal cord (Sawchenko and Swanson, 1982). Though they remain sparsely characterized, these projections are thought to play a similar delayed feedback-inhibitory role on the sympathetic nervous system (Pacak et al., 1995). A recent study even revealed that PVN CRH neurons themselves project collaterals to the lateral hypothalamus, and evidently these synaptic contacts contribute to stress-reactive behaviors like grooming (Fuzesi et al., 2016). The most important role of PVN CRH neurons, though, is best understood as the gateway connecting brain to body *vis a vis* the neuroendocrine stress response: the final opportunity for modulatory forebrain circuits to exert a direct influence on systemic stress signaling.

The principle output of the HPA axis, CORT, signals primarily through activation of the transcription-repressing glucocorticoid and mineralocorticoid receptors (GR and MR). Effects of GR and MR activation vary across tissue types, and their myriad actions in the periphery fall outside the scope of my project (for review see (Rashid and Lewis, 2005;Nicolaides et al., 2015)). Centrally however, CORT's stress-related actions are thought to be mediated almost exclusively by GRs: since MRs have a 10-fold higher affinity for CORT, they are highly occupied basally, so the stress-induced increase in CORT levels has minimal effect on MR-mediated gene regulation (de Kloet et al., 2005;Reul and de Kloet, 1985). Instead, MR-mediated genomic effects are mainly important for sensing fluctuations of hippocampal CORT within its low, basal concentration range to regulate tonic HPA axis activity (de Kloet et al., 1998;Atkinson et al., 2008). Interestingly, there is evidence that hippocampal MRs can also act on a much shorter time

scale through a distinct mechanism impacting glutamate release (Karst et al., 2005). The primary mechanism of action for GRs, on the other hand, is as follows: membrane-permeant CORT enters the cell and binds to monomeric GR, causing GRs to dimerize, translocate to the nucleus, and bind DNA on GR-response elements found in the promoter region of many genes; finally, response element-bound GR dimers suppress transcription of these genes by obstructing the binding of activator proteins and transcription factors (Lu et al., 2006). Among the many central systems impacted by GR signaling are the PVN and the anterior pituitary, where CORT acts in a feedback-inhibitory fashion to terminate its own secretion by downregulating CRH and pro-opiomelanocortin (POMC) transcription, respectively (Keller-Wood, 2015). In area CA1 and the dentate gyrus of the hippocampus, stress levels of CORT reversibly reduce long-term potentiation (LTP) (Foy et al., 1987;Shors and Dryver, 1994), while in area CA3, stress-induced CORT degrades the apical dendrites of pyramidal neurons (McEwen, 2000). Unfortunately, the specific genomic actions of activated GRs that underlie these changes in hippocampal excitatory signaling have yet to be precisely determined. Further complicating the problem of stress effects on cognition, recent evidence indicates that hippocampal GRs also have a fast, non-genomic mechanism of action that impinges on N-methyl-D-aspartate (NMDA) receptor function (Zhang et al., 2012). Nevertheless, it is currently widely accepted that GR signaling primarily affects cognition through the suppression of hippocampal synaptic plasticity and dendritic spine maturation ((Joels and Baram, 2009;Kim and Diamond, 2002) but see also (Duvarci and Pare, 2007)).

In summary, the stress response consists of sympathetic nervous system induction, which is driven by activation of the adrenal medulla and preganglionic sympathetic neurons to elevate circulating epinephrine (EP) and norepinephrine (NE), respectively (Ulrich-Lai and

Herman, 2009). This activation happens on a time scale of seconds, allowing immediate emergence of the acute stress state (increased heart rate, perspiration, mobilization of stored energy, feelings of excitement, fear, and anxiety, *et cetera*). The acute stress state is a transient shift away from homeostasis, redirecting resources to survive an imminent threat but imposing an allostatic load on the system the longer the shift persists. The delayed elevation of CORT, on the other hand, acts not only to terminate its own secretion, but also to counterbalance the acute stress state at multiple levels in parallel – for example, reversing the enhanced plasticity of the hippocampus and the enhanced excitability of brainstem catecholaminergic neurons, and suppressing learned anxiety in the central amygdala (Joels et al., 2007;Kolber and Muglia, 2009). Thus, it is misleading to simply call CORT a stress hormone, since it also acts as an *anti*-stress hormone in the sense that it works in direct opposition to the acute stress state-mobilizing actions of EP and NE. Maladaptive effects of CORT are thought to emerge only when there is an abnormally large or prolonged secretion, due either to a particularly grievous stressor or to intrinsic deficits in the stress-modulatory network (de Kloet et al., 2005;Joels, 2011). Therefore, considering CORT's essential role in pulling the acutely-stressed system back into homeostatic equilibrium, proper modulation of the HPA axis is necessary to mount and terminate the stress response in a way that minimizes lasting harm to the system. In Section 1.6, I will justify my work concerning hypothalamic CRH neurons by discussing synaptic inhibitory constraint of PVN CRH neurons, and by providing evidence that this constraint is an absolutely critical component of adaptive HPA axis modulation.

1.5. Extrahypothalamic CRH neuron populations

Many questions remain regarding the function and regulation of CRH signaling throughout the brain, including a crucial one originally raised by Vale and colleagues in their 1984 study of depressed patients' CSF: does the elevation in CSF CRH result solely from increased CRH secretion from the PVN, or do other CRH-producing brain regions contribute? We don't yet have an absolutely definitive answer, and the identity and functional relevance of extrahypothalamic CRH neurons remain topics of intense interest. Indeed, we have only begun to uncover the roles of these populations in regulating various aspects of the stress response. In addition to the canonical CRH neurons that Vale and colleagues identified in the PVN, there exist CRH neuron populations in the ventral tegmental area (VTA), central amygdala (CeA), bed nucleus of the stria terminalis (BNST), neocortex, and hippocampus. Each of these has been studied to a limited extent, and there may be additional functionally distinct populations that have yet to be described. In this section I will discuss our current understanding of extrahypothalamic CRH neurons, including experimental evidence both for and against the notion that each population shares with PVN CRH neurons a vital role in mediating the effects of stress on cognition and behavior.

The VTA is a key component of the reward circuit, and has primarily been studied for its role in drug-taking and withdrawal (Vargas-Perez et al., 2014;Morisot et al., 2015;Albrechet-Souza et al., 2015). Corticotropin-releasing hormone signaling in the VTA mediates stress-induced reinstatement of drug-seeking behavior via CRHR2 (Wise and Morales, 2010). Specifically, after rats learned to self-administer cocaine and subsequently had this behavior extinguished over time, the behavior could be rapidly reinstated by a foot-shock stress. This reinstatement was blocked by infusing a CRHR2-specific antagonist into the VTA, lending

strong support to the notion that CRH is directly relevant to stress signaling in this brain region. On the other hand, CRHR1 is also expressed on dopaminergic neurons in this VTA, and local infusion of CRHR1-selective antagonists had no effect on stress-induced reinstatement in this study. In contrast, other investigators more recently demonstrated a critical role for VTA CRHR1 in social stress-induced escalation of both alcohol consumption and cocaine self-administration (Boyson et al., 2014;Hwa et al., 2016). Thus, despite divergent findings on the particular molecular mechanisms involving CRH-related proteins, it is well-established that the VTA is specialized for mediating stress effects on the reward pathway, and evidence for the overarching importance of CRH in this region is quite robust.

The extended amygdala, consisting principally of the basolateral and central nuclei of the amygdala (BLA and CeA) and the bed nucleus of the stria terminalis (BNST), is a highly conserved, critical substrate for the emotional component of information processing (Janak and Tye, 2015;Keifer, Jr. et al., 2015;Ressler, 2010). Thus CRH receptor pharmacology has been employed in both the CeA and BNST to investigate emotionally salient behaviors such as bright light avoidance and fear conditioning (Walker et al., 2009;Gafford and Ressler, 2015). Additionally, similar to the VTA, CRH signaling in the BNST is an important mediator of stress effects on reward-associated behaviors like binge eating and drug-seeking reinstatement (Silberman and Winder, 2013;Micioni Di Bonaventura et al., 2014). Less is currently known about the role of CRH signaling in the CeA, but recent investigations have successfully isolated them and begun to characterize their functional connectivity, as well as confirming that stress has a significant impact on their activity (De Francesco et al., 2015;Partridge et al., 2016). Finally, in addition to the supporting evidence above, the hypothesis of stress-related function for CRH in the extended amygdala is further strengthened by the fact that the BNST receives synaptic

input from the CeA and in turn forms synaptic contacts in the PVN (Herman et al., 1994;Forray and Gysling, 2004).

Much less is known about neocortical CRH neurons than the populations discussed above, but they appear diffusely throughout the entire cortex and more densely in the olfactory bulb and piriform cortex (Swanson et al., 1983;Kono et al., 2016). Early immunohistochemical and morphological assessment of neocortical CRH neurons suggests that they are chandelier cells, a class of GABAergic interneuron (Lewis and Lund, 1990). At the cellular level, exogenous CRH has the predictable effect of depolarizing CRHR1-expressing pyramidal neurons (Gallopin et al., 2006). Neocortical CRHR1 has also been implicated in mediating adverse effects of early-life stress (Yang et al., 2015b). Otherwise, this population has been sparsely studied and so far no successful attempt has been made to selectively manipulate or fully characterize neocortical CRH neurons. Additionally, given the diffuse expression of CRH throughout neocortex and the anatomical specialization of neocortical regions, the evidence for a specific, critical role for CRH in stress signaling throughout this region is currently tenuous.

Like the neocortex, the hippocampus is a region where the hypothesis of stress-related function for CRH is not entirely straightforward. Early investigations of hippocampal CRH neurons relied on immunostaining and *in situ* hybridization to probe their molecular profile, and pharmacology of the CRH receptors to infer their function. Immunoreactivity for CRH permeates the hippocampus diffusely and colocalizes in a subset of cells with GAD67 mRNA (Chen et al., 2001). Previous investigations also show colocalization between CRH and parvalbumin (PV) immunoreactivity in the developing hippocampus (Yan et al., 1998), suggesting that hippocampal CRH neurons are PV-positive interneurons. An important caveat

to this is that immunostaining cannot distinguish CRH in the extracellular space from CRH inside cells (for example, in secretory granules of CRH-producing neurons), so precise localization of hippocampal CRH neurons remains elusive. On the other hand, CRHR1, the predominant hippocampal receptor for CRH, has been precisely localized via immunogold electron microscopy (EM) to spines along the basal dendrites of pyramidal neurons particularly in CA3 (Chen et al., 2004). Application of exogenous CRH or CRHR antagonists to hippocampal slices reveals a role for CRH in modulating long term potentiation (LTP) of the Schaffer collateral-CA1 synapse (Blank et al., 2002). Additionally, *in vivo* CRHR pharmacology reveals that CRH impacts spine stability through an NMDA receptor- and calpain-dependent pathway (Chen et al., 2008;Chen et al., 2013b;Andres et al., 2013). Psychological stress can activate this pathway to degrade spines and impair learning and memory, and blockade of CRHR1 following stress ablates this effect of stress (Chen et al., 2004;Chen et al., 2010). While the evidence for hippocampal CRH mediation of stress effects on learning and memory is compelling, these pharmacology studies are limited in an important way: nobody has yet directly measured local CRH release in the hippocampus, so extra-hippocampal sources of CRH cannot be ruled out, nor can signaling by CRH-like peptides including urocortin (Weninger et al., 1999). Until recently, technical hurdles also made studying the synaptic connectivity and function of hippocampal CRH neurons impossible. However, with the advent of cell-specific labeling and manipulation – for instance, using the Cre-lox system to express the light-activated cation channel Channelrhodopsin in a single cell type (Cardin et al., 2010) – the way for such studies has been opened wide. Such tools form the foundation for the primary project in my investigations of hippocampal inhibitory neurotransmission: probing the synaptic connectivity and functional relevance of hippocampal CRH neurons.

I have established in this section that, in the course of investigating extrahypothalamic CRH neurons' functional relevance, it is important to recognize that the name of the neuropeptide is misleading on its face, considering that in extrahypothalamic regions there are no sources of cortictropin (ACTH) from which CRH can evoke systemic release. Rather, CRH is simply a ligand for its cognate G-protein coupled receptors (GPCRs) wherever they are expressed. In fact, as previously mentioned, CRH is only one of a family of ligands with comparable affinities and efficacies for these same binding partners. Coticotropin-releasing hormone happens to have corticotropin-releasing properties when released into the hypophyseal portal system because activated stimulatory GPCRs (CRHR1) on pituitary corticotrophs depolarize these cells, increasing their secretory activity. The same GPCRs on dendritic spines of hippocampal pyramidal neurons, on the other hand, will have effects on the hippocampal network consistent with the local concentration of CRH: raising or lowering the pyramidal neurons' relative excitability accordingly and *by no means necessarily resembling a stress state switch*, a rationale that applies equally to CRH receptors in every region outside of the anterior pituitary. While this point may seem excessively obvious, it does bear keeping in mind as a safeguard against confirmation bias when interrogating the function of CRH signaling in extrahypothalamic regions: there is nothing intrinsically "corticotropin-releasing" about the neuropeptide, rather, it is simply a GPCR ligand. Another critical point to recall is that CRH-producing neurons throughout the brain also form glutamatergic or GABAergic synapses, and in the future we will need to characterize still other signaling molecules like endocannabinoids that these neurons may also release. Thus pharmacological manipulations of a neuropeptide's receptors may be informative about the source population's putative function, but such studies only capture one aspect of CRH neurons' function, whereas cell type-specific manipulations of

activity are more likely to capture both modes of exocytosis: CRH or other large signaling molecules from secretory granules, and neurotransmitters from synaptic vesicles.

In Section 1.7, I will justify my investigations of inhibitory neurotransmission in the hippocampus by discussing its known importance in physiological functions, such as emotional behavior and learning and memory, then providing experimental evidence from animal models of pathological conditions that dysregulation of hippocampal inhibitory signaling is a prime pathogenic suspect.

1.6. Inhibitory neurotransmission in the paraventricular nucleus of the hypothalamus

It is important that CRH release from the PVN remain low in the absence of stress to avoid the harmful effects of prolonged CORT exposure, suggesting robust inhibitory constraint basally. Conversely, PVN CRH neurons must quickly and transiently escape this constraint, given the time-sensitivity of responding adaptively to stressors. Characterizing the inhibitory and excitatory inputs impinging on CRH neurons, and identifying the intrinsic mechanism by which CRH neurons rapidly modulate their activity, will provide critical insight into how these synaptic connections and signaling pathways go awry under pathological conditions.

Chloride plasticity in the neuroendocrine stress response

A fundamental property of neurons is that their release of signaling molecules from synaptic vesicles and secretory granules relies on Ca^{2+} influx, which in turn is driven by action potentials (Sudhof and Rizo, 2011;Burgoyne and Morgan, 2003). A neuron's rate of release is therefore determined by its probability of firing an action potential (AP), which in turn depends on the integration of excitatory and inhibitory currents passing through a neuron at any given moment (Takagi, 2000). Basally, parvocellular neuroendocrine cells in the hypothalamus release CRH at a very low rate as revealed by *in vivo* microdialysis (Cook, 2004). Accordingly, imaging studies reveal that one unique feature of PVN CRH neurons is that 46.2% of the synaptic contacts they receive are GABAergic, indicating powerful inhibitory constraint (Miklos and Kovacs, 2002). Consider by contrast that GABAergic synapses comprise just 2.6% and 6.1% of inputs on neurons in the CA1 region of the hippocampus and primary visual cortex, respectively (Hiscock et al., 2000). How, then, do PVN CRH neurons overcome this formidable inhibition to rapidly

increase their AP firing rate following stress? Two obvious possible mechanisms are a transient increase in the frequency of incoming excitatory postsynaptic currents (EPSC) or a decrease in inhibitory postsynaptic current (IPSC) frequency. However, recent work from our lab and others indicates a more elegant alternative mechanism: chloride plasticity.

The efficacy of inhibitory neurotransmission relies on high levels of extracellular [Cl^-] and low intracellular [Cl^-], permitting an inward, hyperpolarizing flux of chloride ions in response to $GABA_AR$ activation (Maguire and Salpekar, 2013;Ben-Ari et al., 2012). Thus the driving force for chloride, expressed as the reversal potential for $GABA_ARs$ (E_{GABA}), a neuron's resting membrane potential (E_M), and its threshold potential for opening voltage-gated Na^+ channels to fire an action potential ($E_{Threshhold}$), together determine the nature of GABA's action: hyperpolarizing-inhibitory when $E_{GABA}<E_M$; shunting-inhibitory when $E_{GABA}=E_M$; depolarizing when $E_{GABA}>E_M$; and excitatory when $E_{GABA}>E_{Threshhold}$. The driving force for chloride is set primarily by the equilibrium established between the K^+/Cl^- cotransporters, KCC2 and NKCC1, which pump chloride out of and into the cell, respectively ((Ben-Ari et al., 2012;Kahle et al., 2013;Deeb et al., 2011) but see also (Glykys et al., 2014)). This dynamic equilibrium gives rise to the aforementioned alternative mechanism for overcoming inhibitory constraint: modulating KCC2 and/or NKCC1 functional expression to collapse the [Cl^-] gradient and erode inhibitory efficacy.

This hypothetical mechanism is attractive for several reasons. First, it reconciles findings from $GABA_AR$ pharmacology in the PVN that would otherwise be highly counterintuitive: $GABA_AR$ agonists *enhance* the stress-induced increase in PVN excitability, amplifying the neuroendocrine stress response, and concordantly, $GABA_AR$ antagonists suppress stress-

induced HPA axis activation (Ulrich-Lai and Herman, 2009;Wamsteeker and Bains, 2010). Second, it is well-established that the developmental maturation of inhibitory currents corresponds with the developmental profile of KCC2 expression (Chudotvorova et al., 2005;Blaesse et al., 2009). Third, given the sheer number of inhibitory projections and diversity of postsynaptic GABAARs, it would be difficult and energetically wasteful to rapidly, reversibly modulate inhibition at the level of presynaptic release or postsynaptic receptor expression. Fourth and finally, as noted previously the PVN receives projections from brainstem noradrenergic neurons, and the proposed mechanism offers a straightforward explanation for how the stress-induced surge of NE onto the PVN translates into a subsequent increase in PVN CRH neuron activity: α1 adrenoceptor-mediated posttranslational modifications of KCC2 negatively modulate its transporter function and/or stability at the cell surface (Wamsteeker and Bains, 2010;Dayas et al., 2001;Pacak et al., 1995;Silayeva et al., 2015).

1.7. Inhibitory neurotransmission in the hippocampus

The foundation of our understanding of hippocampal function was laid by the tragic case of the late Henry Molaison ("patient H.M."), who underwent bilateral temporal lobectomy including complete removal of the hippocampus as a last-ditch surgical effort to control his extremely severe partial-complex mesial temporal lobe epilepsy (for review see (Eichenbaum, 2013)). Removal of both hippocampi resulted in anterograde amnesia: a complete inability to form new semantic memories. As a result we now understand that the hippocampus acts as a template for retaining semantic representations of events, organizing them across time, and tying them to specific locations. Without the hippocampal template to temporarily represent events and re-encode them across diffuse neocortical semantic networks as stable, long-term memories, these events can only be retained in short-term or working memory while attention is actively focused on them. Of note, not all forms of learning and memory rely on the hippocampus. For example, Mr. Molaison was able to increase his proficiency at challenging, specialized motor coordination tasks and retain this proficiency across long intervals: while he subsequently had no memory of the training, his learning of novel motor programs evidently happened at the level of motor association cortex, independent of hippocampal templates or conscious semantic awareness. Such procedural memory is an instance of an implicit memory task; in contrast, the explicit memory task of recalling events and when and where they occurred depends on intact hippocampal function.

The human hippocampus contains roughly 40 million neurons, of which only 4 million are inhibitory interneurons (West and Gundersen, 1990;Freund and Buzsaki, 1996). Each hippocampal interneuron gives rise to 3,000 to 10,000 synaptic contacts, innervating as many as 2,500 pyramidal neurons, so despite being greatly outnumbered, they play a critical role in the

function of the hippocampal network (Freund and Buzsaki, 1996). Fundamentally, the hippocampus serves learning and memory by functioning as an anatomical coincidence detector, integrating sensory information about a salient stimulus with sensory information about the surrounding context from many different neocortical regions, then projecting this integrated information back to the neocortex to encode, consolidate, or retrieve episodic memories (Howard and Eichenbaum, 2015). Accordingly, hippocampal principal neurons can be thought of as millions of cellular coincidence detectors functioning in parallel: each receives a unique fragment of information, and the summation of its incoming excitatory and inhibitory currents determine whether that particular neuron joins an ensemble of other, synchronously active principal neurons to integrate its fragments with theirs. The precise timing of activity required to accomplish this daunting task relies on a rich variety of interneurons subtypes providing inhibitory GABAergic input, with each subtype innervating specific subcellular domains of principal cells in specific regions of the hippocampus. Additionally, several interneuron subtypes are specialized to entrain large ensembles of principal cells to a specific range of firing frequencies. Precisely how the resulting hippocampal network oscillations function to facilitate memory formation is not yet fully understood, but *in vivo* electrocorticogram recording during exploration and learning paradigms, as well as experimental manipulation of oscillations, indicate that they are important for both online information processing and consolidation of long-term memories . Finally, death of hippocampal interneurons is a hallmark neuropathological feature of temporal lobe epilepsy and Alzheimer's disease, and implanted grafts of interneuron precursors are able to markedly alleviate pathology in animal models of both of these disorders (Hunt et al., 2013).

Hippocampal interneurons in cognition, stress, and epilepsy

To-date 21 distinct classes of interneuron have been identified in the hippocampus (Klausberger and Somogyi, 2008). Given the complexity of the meaningful coincidence detection that underlies hippocampus-dependent learning and memory, the abundance of specialization among interneurons is not surprising, and numerous reviews of interneuron subtypes in the hippocampus detail their connectivity and intrinsic properties (Freund and Buzsaki, 1996;Klausberger and Somogyi, 2008;Szilagyi et al., 2011). Here I will highlight only a few of the observations these reviews provide on hippocampal interneuron classes. Generally, hippocampal interneurons project locally to nearby pyramidal neurons: for example, the chandelier cell extends approximately 400 μm along its longest axis (Freund and Buzsaki, 1996). Morphologically, they are generally free of dendritic spines, instead receiving mostly-glutamatergic inputs along the shafts of their dendrites. They express at least one of the two isoforms of the GABA-synthesizing enzyme gamma-amino decarboxylase (GAD), as well as the vesicular GABA transporter (VGAT; also known as vesicular inhibitory amino acid transporter, VIAAT) (Soghomonian and Martin, 1998;Anne and Gasnier, 2014). As such, they primarily signal via GABA receptors on pyramidal neurons: ionotropic $GABA_A$Rs conducting inward, inhibitory flux of chloride ions through both synaptic receptors mediating fast phasic currents, and extrasynaptic receptors mediating slow tonic currents (Moss and Smart, 2001;Coulter and Carlson, 2007); and metabotropic $GABA_B$Rs which generally inhibit the target cell through slower, G protein-coupled signaling cascades – for example, increasing postsynaptic potassium channel conductance through $G_{\beta\gamma}$ subunit activation (Couve et al., 2000). Different classes of interneurons can also express a variety of other signaling molecules. Prominent among these are the peptides somatostatin and cholecystokinin, though these are generally used as markers of the interneurons themselves rather than studied for their effects on cognate peptide receptors. Additionally, classes of interneurons can be distinguished based on the subcellular localization of

the synaptic contacts they form, favoring either the cell body (perisomatic), axon initial segment (axo-axonic), or specific dendritic domains (basal vs apical). Finally, each interneuron type has a distinctive electrophysiological profile: an extensive set of parameters determined by relative expression of calcium-binding proteins, leak conductance channels, connexins, and many other molecular sources. Briefly these parameters include resting membrane potential, input resistance, action potential wave form, firing rate, and firing pattern, as well as phase-locking to the various hippocampal oscillations mentioned above.

The role of interneurons in cognition is clear yet complex: on the one hand, ensembles of pyramidal neurons require inhibitory inputs to synchronize their timing; on the other hand, each neuron can form over 10,000 synapses across thousands of postsynaptic target cells, so the details of how each class of interneuron specifically contributes to synchrony and how this synchrony in turn comprises semantic memories remain extremely convoluted yet extensively studied.

Stress has a bidirectional influence on hippocampus-dependent cognition: CRH and other stress-associated modulators can enhance synaptic plasticity and cognitive performance in a setting of acute stress, while chronic exposure to stress leads to impaired learning, evidently through CORT- and CRH-dependent mechanisms that reduce plasticity and destroy dendritic spines on pyramidal neurons (Maras and Baram, 2012;Joels and Baram, 2009). So far, pyramidal neurons and especially plasticity of glutamatergic synapses have received most of the attention in investigations of stress effects on hippocampal function, whereas more work is still needed to uncover the mechanisms modulating GABAergic signaling in the stressed hippocampus.

Finally, I mentioned previously the evidence for loss of hippocampal GABAergic signaling as a potential mechanism underlying temporal lobe epilepsy. In principle then, it is unsurprising that historically medications directed at epilepsy tend to be GABA agonists; however, given the persistence of drug-resistant seizures particularly in TLE, we are in dire need of a new approach with a more effective target. Still, while it is not quite accurate to say that epilepsy is a straightforward problem of imbalance between excitatory and inhibitory activity, there is definitely strong evidence for dysregulation of GABA underlying epilepsy in general (Scharfman and Brooks-Kayal, 2014), and drug-resistant seizures in particular through downregulation of benzodiazepine-sensitive $GABA_A$Rs (Deeb et al., 2012). The difficulty is that, similar to their contribution to oscillations serving cognition, the role of GABAergic signaling in epilepsy is clear but complex: interneuron activity is necessary to generate synchronous oscillations, and one of the key problems in the seizure state is an overabundance of synchrony; at the same time, inhibitory neurotransmission suppresses excitation of pyramidal neurons, and the other key problem during a seizure is an overabundance of excitation. Thus there appears to be a distinct middle ground, below which inhibition-mediated synchrony is insufficient for adaptive coincidence detection, but above which the hippocampal network enters the runaway hypersynchronous state of a seizure. Understanding how distinct interneuron classes contribute to the maintenance of this adaptive middle ground is a critical issue, as this holds the promise of more effective, novel – perhaps cell type-specific – therapeutic interventions to prevent runaway hippocampal excitability while sparing or even optimizing its physiological functions.

Materials and Methods

Throughout this volume I take care to state explicitly which experiments I conducted (as opposed to other members of the laboratory or collaborators). Accordingly, in this section I list the methods used in the published and unpublished projects described in Sections 3 through 8, but provide detailed descriptions primarily for those methods that I myself employed. Where available, I cite additional technical details from the respective publications.

2.1. Animals

Except where otherwise specifically noted, an approximately equivalent number of male and female animals were used for all experiments. All results reported below reflect merged male and female data; however, results were also separated and analyzed for any sex-specific variations. Any such variations found are also reported below.

All animals were bred and housed at the Tufts University School of Medicine, Division of Laboratory Animal Medicine. The animals (4 adults/cage) were housed in clear plastic cages in a temperature- and humidity-controlled environment with a 12 hr light/dark cycle (light on at 7:00 AM) and were maintained on an *ad libitum* diet of lab chow and water. Animals were handled according to protocols approved by the Institutional Animal Care and Use Committee of the Tufts University School of Medicine.

2.2. Transgenic lines

KCC2$^{f/f}$: KCC2$^{f/f}$ mice were a gift from Dr. Steven Moss at Tufts University School of Medicine. The KCC2 gene of these mice has been modified to contain two loxP sites: one immediately upstream of exon 22, and one immediately downstream of exon 25. Recombination of the loxP sites by Cre recombinase causes excision of the flanked exons, producing a truncated from of KCC2 that lacks residues Q911 through Q1096. KCC2$^{f/f}$ mice were genotyped using the following primers:

5': ATGAGTAGCAGATCCCATAGGCGAACC

3': CTGCCAAGAGCCATTACTACAGTGGATG

CRH-Cre: Tg(Crh-cre)KN282Gsat mice, hereinafter referred to as CRH-Cre mice, were obtained from the Mutant Mouse Regional Research Center (MMRC). This mouse line was generated by bacterial artificial chromosome transgene insertion of the bacteriophage P1 Cre recombinase gene under control of the CRH promoter. Because transgene insertion into the host genome is random, it is unlikely to disrupt native CRH expression. Additionally, GenSat characterized Cre recombinase expression in this line and found that it matched *in situ* hybridization data for CRH mRNA expression (www.gensat.org; for additional details see (Sarkar et al., 2011)), and our laboratory subsequently confirmed this at the protein level (Hooper and Maguire, 2014). CRH-Cre mice were genotyped using the following primers:
5': CTGTCTTGTCTGTGGGTGTCCGAT
3': CGGCAAACGGACAGAAGCATT

Gabrd/Pomc: Gabrd/Pomc mice were generated in-house by crossing Pomc-Cre and floxed Gabrd mice. Pomc-Cre mice were obtained from Jackson Laboratory (stock #0010714). Floxed Gabrd mice were generated by GenOway (Paris, France) as previously described (Lee and Maguire, 2013). Gabrd/Pomc mice were genotyped using the following primers:
floxed Gabrd 5': GACTCCAGTTGCCAAGCCTTTAATTCC
floxed Gabrd 3': CATCTGCCTGTACCTCCAATGCCTG
Pomc-Cre 5': GCATTACCGGTCGATGCAACGAGTGATGAG
Pomc-Cre 3': GAGTGAACGAACCTGGTCGAAATCAGTGCG

SST-Cre:$\gamma 2^{f/f}$:LSL-YFP: SST-Cre mice were obtained from JAX mice (Stock #013044, Jackson Laboratory, Bar Harbor, ME). $\gamma 2^{f/f}$ mice were generated by our collaborators (for details see (Schweizer et al., 2003)). The Cre-dependent reporter line LSL-YFP (also known as ROSA26-

EYFP) was obtained from JAX mice (Stock #006148). Our collaborators generated SST-Cre:$\gamma 2^{f/f}$:LSL-YFP mice and Cre-negative littermates in-house by crossing the above mouse lines.

CRH-KCC2: CRH-KCC2 mice were generated in-house by crossing $KCC2^{f/f}$ (Dr. Stephen Moss) and CRH-Cre mice (MMRC).

CRH-Ai9: CRH-Ai9 mice were generated in-house by crossing floxed Ai9 mice (Jackson Lab, Stock #007909) with CRH-Cre mice (MMRC).

ChR/Crh: ChR/Crh mice were generated in-house by crossing floxed Channelrhodopsin mice (Jackson Lab, Stock #017455) with CRH-Cre mice (MMRC).

2.3. Viruses

AAV-Flex-ChR2-tdTomato: Anterograde tract tracing was performed using a protocol adapted from (Atasoy et al., 2008). Adult (>8 week old) mice were anesthetized by intraperitoneal (i.p.) injection of a ketamine-xylazine mixture (160 mg/kg ketamine, 16 mg/kg xylazine), prepared for surgery, and stereotaxically injected with an adeno-associated virus encoding Channelrhodopsin and a red fluorescent protein in a Cre recombinase-dependent fashion (AAV-Flex-ChR2-tdTomato: Addgene plasmid #18917, produced by Dr. Scott Sternson; obtained from the Penn Vector Core). When an animal was no longer responsive to a firm foot pinch, an incision was made to open its scalp. The animal was placed in a stereotaxic apparatus and injection sites were marked on its skull. Coordinates for injection of area CA1 were: anterior-posterior (AP) -2.0 mm; medial-lateral (ML) ±1.5 mm; dorsal-ventral (DV) -1.0

mm. A needle tip or dental drill was used to bore holes through the skull at the marked injection sites. A 5 μL model 75 Hamilton syringe was then used to inject 1.5 μL of virus (500 nL per minute over 3 minutes) into each hemisphere. Following injection, the syringe was left in the injection site for 5 minutes before withdrawal, and the opposite hemisphere was then injected in the same manner. The scalp incision was closed using tissue adhesive, analgesic was administered by i.p. injection (Buprinex, 50 μL), and the animal was placed in a warm recovery chamber until alert and mobile before returning to group housing. Animals were sacrificed and their brains harvested at least 2 weeks after virus injection to allow maximal expression.

Pseudorabies: Monosynaptic retrograde tracing was performed using a protocol adapted from (Wall et al., 2010). Adult mice were stereotaxically injected with an adeno-associated virus encoding avian receptor protein TVA, rabies glycoprotein, and green fluorescent protein (AAV9-pEF1α-FLEX-GTB, hereinafter referred to as Helper virus) in a Cre recombinase-dependent fashion. Two weeks after Helper virus injection, animals were injected in the same site with an EnvA-pseudotyped, glycoprotein-deleted rabies virus encoding red fluorescent protein (pseudorabies virus, PRV). Stereotaxic virus injection surgery was performed exactly as described above, except that only 500 nL of each virus (~150 nL per minute over 3 minutes) was injected into each hemisphere. Animals were sacrificed and their brains harvested 3 weeks after PRV injection for optimal expression.

AAV-Cre-GFP: Site-specific expression of Cre recombinase was achieved by stereotaxic injection of an adeno-associated virus encoding Cre recombinase and enhanced green fluorescent protein, each driven by a separate CMV promoter (AAV2-Cre-GFP; Vector BioLabs #7016). Control mice were injected instead with an adenovirus encoding only GFP (AAV2-

GFP; Vector BioLabs #7004). Stereotaxic virus injection surgery was performed largely as described above, except that only 250 nL of virus was injected into each hemisphere. Coordinates for PVN injections were: AP -0.45mm; ML ±0.05mm; DV -5.0mm. Additionally, because the injection sites were so close together in the medial-lateral dimension, the empty syringe was first lowered 1.0mm into each hemisphere to puncture the dura before injecting virus into either site. This significantly improved accuracy, likely by preventing the syringe tip from following the path of least resistance and injecting the same site twice in a row. Mice were allowed to recover for 4 weeks after virus injection surgery before undergoing additional experiments, in order to allow maximal Cre recombinase-mediated gene excision.

Gq-DREADD: Cell type-selective chemogenetic stimulation was accomplished using a protocol adapted from (Krashes et al., 2011). Adult mice were stereotaxically injected with an adeno-associated virus encoding Cre recombinase-dependent stimulatory Designer Receptors Exclusively Activated by Designer Drugs (UNC Vector Core, AAV8-hM3Dq-DIO-mCherry). Stereotaxic virus injection surgery was performed as described above, with 500 nL of virus injected into each hemisphere. Control mice instead received AAV-GFP. Both experimental and control mice received i.p. injection of 0.3 mg/kg or 10 mg/kg of the designer drug for Gq-DREADD, clozapine N-oxide (CNO). CNO was prepared by dissolving 5 mg CNO in 50 µL of DMSO followed by 5 mL of injection saline. Mice were allowed to recover for 4 weeks after virus injection surgery before undergoing additional experiments, in order to allow maximal expression.

Gi-DREADD: Cell type-selective chemogenetic silencing was accomplished using a protocol adapted from (Krashes et al., 2011). Adult mice were stereotaxically injected with an adeno-

associated virus encoding Cre recombinase-dependent inhibitory Designer Receptors Exclusively Activated by Designer Drugs (UNC Vector Core, AAV8-hM4Di-DIO-mCherry). Stereotaxic virus injection surgery was performed as described above, with 500 nL of virus injected into each hemisphere. Control mice instead received AAV-GFP. Both experimental and control mice received i.p. injection of 0.3 mg/kg or 10 mg/kg of the designer drug for Gi-DREADD, clozapine N-oxide (CNO). CNO was prepared by dissolving 5 mg CNO in 50 µL of DMSO followed by 5 mL of injection saline. Mice were allowed to recover for 4 weeks after virus injection surgery before undergoing additional experiments, in order to allow maximal expression.

AAV-DTA: Cell type-selective ablation was accomplished with stereotaxic injection of an adeno-associated virus expressing the A subunit of diphtheria toxin (DTA) in a Cre recombinase-dependent fashion (AAV-Flex-DTA, a generous gift from Dr. Patrick Fuller at Harvard Medical School). Stereotaxic virus injection surgery was performed as described above, with 500 nL of virus injected into each hemisphere. Control mice instead received AAV-GFP. Mice were allowed to recover for 4 weeks after virus injection surgery before undergoing additional experiments, in order to allow maximal expression and DTA-mediated cell death.

2.4. Enzyme-Linked Immunosorbent Assay (ELISA)

Animals were deeply anesthetized by isoflurane inhalation, killed by decapitation, and their trunk blood was collected into clot activator blood collection tubes (Terumo). Serum was isolated from trunk blood by centrifugation (14,000 rpm for 5 min). ACTH was measured by enzyme immunoassay (Pheonix Pharmaceuticals) according to manufacturer's instructions. ACTH levels were measured in duplicate samples (25 µL) and compared to a standard curve of known ACTH

concentrations. Similarly, corticosterone levels were measured by enzyme immunoassay according to manufacturer's specifications. Corticosterone was measured using one of two kits (Assay Designs or Enzo Life Sciences) which have been shown to be successful in accurately determining plasma corticosterone levels in the mouse. Duplicate 5 μL serum samples were assayed and compared to a standard curve of absorbance at 415 nm wavelength using a spectrophotometer.

2.5. Western blot

Animals were deeply anesthetized by isoflurane inhalation, killed by decapitation, and their brains were dissected to isolate the PVN. The PVN was sonicated in homogenization buffer (10 mM NaPO4, 100 mM NaCl, 10 mM Na pyrophosphate, 25 mM NaF, 5 mM EDTA, 5 mM EGTA, 2% Triton X-100, 0.5% Deoxycholate, 1 mM Na vanadate, pH 7.4) with protease inhibitors (complete mini, Roche, with freshly prepared 100 mM phenylmethanesulfonyl fluoride dissolved in ethanol). The tissue lysate was incubated at 4°C for 30 min then centrifuged at 14,000 rpm for 5 min, and the resulting supernatant was collected. Protein concentration was determined using the DC Protein Assay (BioRad). 25 μg of total protein was loaded onto a 12% SDA-polyacrylamide gel, subjected to electrophoresis and transferred to a PVDF membrane (Immobilon P, Millipore). Membranes were blocked for 1 hr in 10% nonfat milk, then probed for 1 hr with a polyclonal antibody specific for KCC2 (1:1,000, Millipore), a polyclonal antibody specific for the phosphorylated Ser940 residue on KCC2 (1:1,000, gift from Dr. Stephen Moss), a polyclonal NKCC1 antibody (1:1,000, Millipore), a polyclonal antibody against the $GABA_AR$ γ2 (gamma2) subunit (1:1,000, AbCam), or a monoclonal beta-tubulin antibody (1:10,000, Sigma). Blots were then incubated for 1 hr with either peroxidase labeled anti-rabbit IgG (1:2,500, GE Healthcare) or peroxidase labeled anti-mouse IgG (1:2,500, GE Healthcare), and

finally immunoreactive proteins were visualized using enhanced chemiluminescence (Amersham). Optical density measurements were performed using NIH ImageJ software. Western blots for KCC2 produce two bands, one at approximately 140 kDa and one at 200 kDa. I only assessed the 140 kDa band because it corresponds to the predicted molecular weight of KCC2, whereas the physiological relevance of the 200 kDa band is not well-established (but see (Blaesse et al., 2006)).

2.6. Immunostaining

Animals were deeply anesthetized by isoflurane inhalation, killed by decapitation, and their brains were removed into ice-cold 4% paraformaldehyde (PFA) in phosphate-buffered saline (PBS) at pH 7.4. For CRH immunohistochemistry only, animals were instead killed by transcardial perfusion, using PBS for blood vessel clearance followed by 4% PFA for perfusion fixation. Brains were fixed overnight by immersion fixation in 4% PFA at 4°C, cryoprotected in 10% and 30% sucrose, rapidly frozen in isopentane, and stored at -80°C. Coronal sections were collected into PBS at 40 μm thickness using a Leica cryostat. Free-floating sections were then probed with antibodies for immunohistochemistry, rinsed briefly in deionized water, and mounted onto microscope slides (FisherBrand Superfrost Plus). After drying overnight, slides were coverslipped using mounting medium with DAPI (VectaShield Hard Mount) for visualization of cell nuclei. Coverslipped slides were then imaged on a Nikon A1R confocal microscope.

Parvalbumin: Sections were incubated in PBS with 0.3% Triton X-100 (PBS-T) and 10% bovine serum albumin (BSA) for 1 h to block nonspecific binding. Sections were then incubated in PBS-T with 10% BSA and 1:1,000 mouse anti-Parvalbumin (Sigma) at 4°C overnight.

Sections were washed in PBS (3x10 min), incubated in PBS-T with 10% BSA and 1:200 Alexa 488 anti-mouse secondary antibody (Molecular Probes) at 4°C for 2 h, and washed again in PBS (3x10 min). Sections were then rinsed and mounted as described above.

c-fos: Sections were incubated in PBS-T and 10% normal goat serum (NGS) for 1 h to block nonspecific binding. Sections were then incubated in PBS-T with 10% NGS and 1:10,000 rabbit anti-c-fos primary antibody (Calbiochem) at 4°C for 3 days. Sections were washed in PBS (3x10 min) and incubated in PBS-T with NGS and 1:200 biotinylated anti-rabbit secondary antibody (VectaStain Elite ABC Kit, Vector Labs) at 4°C for 2 h. Sections were then washed in PBS (3x10 min), incubated in PBS-T with 10% NGS and 1:1,000 Alexa Fluor 488 streptavidin (Molecular Probes) for 2 h, and washed again in PBS (3x10 min). Sections were then rinsed and mounted.

GAD67: Sections were incubated in PBS-T and 10% BSA for 1 h to block nonspecific binding. Sections were then incubated in PBS-T with 10% BSA and 1:1,000 mouse anti-GAD67 (Millipore) at 4°C overnight. Sections were washed in PBS (3x10 min), incubated in PBS-T with 10% BSA and 1:200 Alexa 488 anti-mouse secondary antibody at 4°C for 2 h, and washed again in PBS (3x10 min). Sections were then rinsed and mounted.

Somatostatin: Sections were incubated in PBS-T and 10% normal goat serum (NGS) for 1 h to block nonspecific binding. Sections were then incubated in PBS-T with 10% NGS and 1:1,000 rat anti-Somatostatin primary antibody (Millipore, MAB354) at 4°C overnight. Sections were washed in PBS (3x10 min) and incubated in PBS-T with NGS and 1:200 biotinylated anti-rat secondary antibody (VectaStain Elite ABC Kit, Vector Labs) at 4°C for 2 h. Sections were then

washed in PBS (3x10 min), incubated in PBS-T with 10% NGS and 1:1,000 Alexa Fluor 488 streptavidin (Molecular Probes) for 2 h, and washed again in PBS (3x10 min). Sections were then rinsed and mounted.

Calbindin: Sections were incubated in PBS-T and 10% BSA for 1 h to block nonspecific binding. Sections were then incubated in PBS-T with 10% BSA and 1:5,000 mouse anti-Calbindin (Cell Signaling) at 4°C overnight. Sections were washed in PBS (3x10 min), incubated in PBS-T with 10% BSA and 1:200 Alexa 488 anti-mouse secondary antibody (Molecular Probes) at 4°C for 2 h, and washed again in PBS (3x10 min). Sections were then rinsed and mounted as described above.

Calretinin: Sections were incubated in PBS-T and 10% BSA for 1 h to block nonspecific binding. Sections were then incubated in PBS-T with 10% BSA and 1:1,000 mouse anti-Calretinin (SWANT) at 4°C overnight. Sections were washed in PBS (3x10 min), incubated in PBS-T with 10% BSA and 1:200 Alexa 488 anti-mouse secondary antibody (Molecular Probes) at 4°C for 2 h, and washed again in PBS (3x10 min). Sections were then rinsed and mounted as described above.

KCC2: Sections were incubated in PBS-T with 10% NGS and 1% BSA for 2 h to block nonspecific binding. Sections were then incubated in PBS-T with 10% NGS, 1% BSA, and 1:1,000 rabbit anti-KCC2 (Millipore, 07-432) at 4°C overnight. Sections were washed in PBS (3x10 min), incubated in PBS-T with 10% NGS and 1:200 Alexa 568 anti-goat secondary antibody at 4°C for 2 h, and washed again in PBS (3x10 min). Sections were then rinsed and mounted.

CRH: Sections were incubated in PBS-T and 10% NGS for 1 h to block nonspecific binding. Sections were then incubated in PBS-T with 10% NGS and 1:10,000 rabbit anti-CRH primary antibody (Salk Institute) at 4°C for 5 days. Sections were washed in PBS (3x10 min) and incubated in PBS-T with NGS and 1:200 biotinylated anti-rabbit secondary antibody at 4°C for 2 h. Sections were then washed in PBS (3x10 min), incubated in PBS-T with 10% NGS and 1:1,000 Alexa Fluor 488 streptavidin for 2 h, and washed again in PBS (3x10 min). Sections were then rinsed and mounted.

2.7. Whole-cell patch clamp

All patch clamp experiments were conducted using methods similar to our previous publications (Sarkar et al., 2011;O'Toole et al., 2014;Lee et al., 2016;Hooper and Maguire, 2014). Briefly, 350 μm brain sections were collected into ice-cold cutting solution, which consisted of normal artificial cerebrospinal fluid (nACSF; 126 mM NaCl, 26 mM NaHCO3, 1.25 mM NaH2PO4, 2.5 mM KCL, 2 mM CaCl2, 2 mM MgCl2, and 10 mM dextrose at 300-310 mOsm) with 3 mM kynurenic acid, using a Leica vibratome. Slices were transferred to nACSF at 33°C for 1 hr prior to recording. Slices were then placed in a recording chamber where they were perfused with nACSF at 6 mL/min, bubbled with 95% O2/5% CO2 and maintained at 33°C.

2.8. Extracellular field recordings

Animals were deeply anesthetized by isoflurane inhalation, killed by decapitation, and 400 μm brain sections were collected into ice-cold sucrose cutting solution (87 mM NaCl, 3 mM KCl, 7 mM MgCl2, 1.25 mM NaH2PO4, 2.5 mM CaCl2, 40 mM sucrose, 20 mM glucose, and 20 mM

NaHCO3) using a Leica vibratome. Slices were transferred to nACSF (124 mM NaCl, 3 mM KCl, 2 mM MgSO4, 1.1 mM NaH2PO4, 2.0 mM CaCl2, 10 mM D-glucose, 25 mM NaHCO3) at 33°C for 1 hr prior to recording. Slices were then placed in an interface recording chamber where they were perfused with nACSF at 6 mL/min, bubbled with 95% O2/5% CO2 and maintained at 34°C. Recordings from the mossy fiber-CA3 pathway were obtained by placing a bipolar tungsten stimulating electrode over the mossy fiber bundle at the border between CA3 and the hilus, and a recording electrode in stratum radiatum of area CA3. The recording electrode was filled with nACSF and tethered to an optical fiber in order to optogenetically stimulate CRH neuron terminals in CA3. Laser illumination of 473 nm wavelength was delivered in 5 msec pulses at 20 Hz for all field recording experiments. Input-output curves were generated by delivering electrical stimuli of increasing width (20 to 240 μsec in 20 μsec steps, 4 times per stimulus width per input-output curve) at a fixed intensity (0.1 mA). Data was collected through a differential amplifier (Warner Instruments, DP311) connected via a switchboard (AD Instruments, PowerLab 4-30) to a desktop computer. LabChart 7 software was used for all data collection and analysis.

2.9. Electroencephalogram (EEG) recordings

Mice were anesthetized and prepared for EEG implant surgery as described above. A lengthwise incision was made along the scalp and a prefabricated headmount (Pinnacle Technology, part #8201) was fixed to the skull with four screws, which serve as two differential recording leads, a reference lead, and an animal ground. The headmount was fixed to the skull using dental cement and mice were allowed to recover for a minimum of 1 week prior to experimentation. Electroencephalogram recordings were collected using a 100x gain preamplifier high pass

filtered at 1.0 Hz (Pinnacle Technology, part #8202-SE) and tethered turnkey system (Pinnacle Technology, part #8200).

Seizure events were identified as previously described (Maguire and Mody, 2007) by the sudden onset of high amplitude activity, at least 2.5 times the standard deviation of the baseline, lasting longer than 5 s in duration. Seizure activity was also identified by consistent changes in the Power of the fast Fourier transform of the EEG, including a change in the Power and the frequency of activity over the course of the event. Abnormal periods of EEG activity which cannot be defined as a seizure, including periods of rhythmic spiking lasting longer than 30 s, along with ictal events were defined as "epileptiform activity". Seizure latency was defined as the time elapsed from the injection of kainic acid to the start of the first electrographic seizure. The fraction of total time exhibiting epileptiform activity and the average duration of each bout of epileptiform activity were calculated across the 120-min recording period. LabChart Pro software (ADInstruments) was used for data acquisition and analysis.

2.10. Behavior paradigms

Behavior experiments were conducted in the Behavior Core of the Tufts Center for Neuroscience Research (P30 NS047243 (PI: Jackson)). Without exception, mice were acclimated to the testing facility for at least 1 hour after transport from the animal colony in order to minimize confounding effects of stress. Additionally, for all behavior experiments where a drug was injected i.p., mice were acclimated to i.p. needle insertion for 3 consecutive days prior to the test day in order to minimize stressful effects of handling and needle insertion. All behavior tests were conducted during the light cycle as close as practically possible to 12:00 PM to minimize confounding effects of circadian arousal and stress hormone fluctuation.

2.11. Restraint stress

Mice were gently coaxed into modified 50 mL conical tubes, which were then capped to prevent escape. Each conical tube had a single hole (0.5 cm diameter) bored into the conical end to allow breathing. Each restraint session lasted 30 min: acute stress consisted of a single session, while chronic stress consisted of one session per day for 14 consecutive days. To assess the stress-induced increase in circulating CORT by ELISA, trunk blood was collected 30 min after the end of the restraint session.

2.12. Open field

Mice were individually placed in the center of a 40 cm x 40 cm open field apparatus with 16 x 16 equally spaced photocells (Hamilton-Kinder) and their activity recorded for a 10 min test period. The total number of beam breaks (basic movements), number of entries into the center, distance traveled through the center, and amount of time spent in the center were measured using automated MotorMonitor software (Hamilton-Kinder). The center of the open field is an aversive environment as it leaves the mouse more exposed; thus the time spent in the center is thought to be inversely proportional to the anxiety level of the mouse (Holter et al., 2015a).

2.13. Light-dark box

Mice were individually placed in a 22 cm x 43 cm light/dark box apparatus with 4 x 8 equally spaced photocells (Hamilton-Kinder) and their activity recorded for a 10 min test period. Each mouse began in the open compartment, which was illuminated by a high intensity light source (Fiber-Lite). The other half of the enclosure is an enclosed dark compartment of equal size. The

total number of beam breaks (basic movements), latency to enter the dark compartment, number of entries, distance traveled, and amount of time spent in the light compartment were measured using MotorMonitor software (Hamilton-Kinder). The brightness of the light compartment is aversive to the mouse, thus the time spent in the light compartment is thought to be inversely proportional to the anxiety level of the mouse (Holter et al., 2015a).

2.14. Elevated plus maze

Mice were individually placed in the center of a 50 cm x 50 cm plus maze elevated 55 cm from the floor with four 10 cm-wide alternating open and enclosed arms, and their activity was recorded for a 10 min test period. The total number of beam breaks (basic movements), number of entries, distance traveled, and amount of time spent in the open arms were measured using MotorMonitor software (Hamilton-Kinder). The exposure of the open arms is aversive to the mouse, thus the time spent in the open arms is thought to be inversely proportional to the anxiety level of the mouse (Holter et al., 2015a).

2.15. Forced swim test

Mice were placed into transparent plastic cylinders (21 cm diameter) containing 15 cm of room-temperature water and videotaped for a 6 min test period. The latency to immobility and total time spent immobile was measured by an investigator blind to experimental groups. The cylinder is inescapable and mice are capable of floating in place; however, the propensity to give up on escaping quickly and spend a greater proportion of time floating in place is thought to indicate depression-like behavior, particularly in light of the ability of antidepressant drugs to decrease immobility in this test (Borsini and Meli, 1988;Poleszak et al., 2014;Yan et al., 2010).

2.16. Tail suspension test

Mice were suspended by the tip of their tail from a bar at a height of 36 cm above a table top and videotaped for a 6 min test period. The latency to immobility and total time spent immobile was measured by an investigator blind to experimental groups. Like the forced swim, this test is a model of learned helplessness, so the propensity to give up quickly is taken for a measure of depression-like behavior (Cryan et al., 2005;Yan et al., 2010).

2.17. Fear conditioning

Fear conditioning was performed over the course of two days in a rectangular box with a steel grid floor (Coulbourn Instruments; H10-11R-TC, 12"W x 10"D x 12" H). On the first day (acquisition), mice were placed in the center of the arena, allowed to acclimate for 3 min, then presented with two 20 sec tones (2,800 Hz at 80 dB) which ended concurrently with 2 sec foot shocks (0.7 mA), each separated by a 1 min interval. Mice were then returned to their home cage. The following day (retrieval), mice were placed in the same arena for 3 min (context) then returned to their home cage. After a 3 hour interval, the mice were then placed in a novel context, a rectangular plastic container with black and white vertical stripes on the walls and bedding scented with 1% acetic acid. In this context, the mice were presented with the same tones they heard during acquisition, this time in the absence of foot shocks (cued). Freezing behavior was measured for all three phases of testing using Actimetrics FreezeFrame software (Coulbourn Instruments; bout length 1 sec). Contextual fear memory retrieval is thought to be primarily hippocampal-dependent, while cued fear memory is considered hippocampal-independent as it relies primarily on the amygdala. Thus a reduction of freezing behavior in

experimental mice relative to controls is taken as a measure of impaired learning and memory, either hippocampal-dependent or −independent depending on the retrieval task exhibiting reduced freezing (LeDoux, 1992;Fanselow and Kim, 1992;Bergstrom, 2016).

2.18. Object recognition memory

The object recognition memory test was adapted from (Holter et al., 2015b). Object recognition memory testing was performed over the course of two days in 15 cm x 26 cm rectangular plastic home cages empty of bedding. On the first day, mice were placed in a cage where two identical objects (stainless steel hex bolts; familiar) were affixed to the floor at opposite ends of the cage. Mice were allowed to explore the objects for three 5 min sessions spaced 15 min apart. After a 3 hr retention interval, mice were then placed in a cage where one familiar object and a novel object (white nylon washer; novel A) were affixed to the floor at opposite ends of the cage. Mice were allowed to explore the objects for a 5 min session and then returned to their home cage. Finally, after a 24 hr retention interval, mice were placed in a cage where one familiar object and a second novel object (white-and-green plastic rectangle; novel B) were affixed to the floor at opposite ends of the cage. All sessions were videotaped and exploration of each object was measured by an investigator blind to experimental groups. Total explorations were assessed as a measure of locomotor activity, and relative exploration of the left vs right familiar object was assessed to rule out a confounding preference for one side of the arena. A novel:familiar preference ratio was calculated for both the 3 hr and the 24 hr retention trials. The novel object in each retention trial is a more salient feature of the arena than the familiar object; thus a reduction of the novel:familiar ratio in experimental mice relative to controls is taken as a measure of impaired spatial learning and memory (Holter et al., 2015b).

2.19. Statistical analysis

Data are presented as "mean ± standard error of the mean", and unpaired Student's *t* tests were used to determine statistically significant differences between experimental groups, except where otherwise noted. In cases where more than two groups were compared, analysis of variance (ANOVA) was used along with *post hoc* Tukey's test. Where normal distribution of data was in question, normality was assessed by the Kolmogorov-Smirnov one-sample test (Ghasemi and Zahediasl, 2012). In cases where data were non-normal, non-parametric Mann-Whitney *U* tests were instead used to determine statistical significance.

Results

The following sections contain figures and figure legends reproduced from three copyrighted publications (O'Toole et al., 2014;Lee et al., 2016;Hooper and Maguire, 2014) and one forthcoming publication (Fuchs et al., 2016). I have obtained written permission from the respective rights holders to reproduce these copyrighted materials in my dissertation.

3. Hypothalamic CRH neurons: Stress and seizures alter chloride homeostasis and $GABA_AR$ expression

Stress is the most commonly reported trigger for seizures, and stress-related disorders frequently co-occur with epilepsy, strongly suggesting common mechanisms. Our laboratory recently demonstrated that stress activates CRH neurons in the PVN by rapidly downregulating GABAergic inhibition. We therefore set out to test the hypothesis that seizures share this cellular mechanism of HPA axis activation, in order to shed light on stress-seizure pathophysiology. This section contains data and figures from (O'Toole et al., 2014) on which I was a contributing author.

Rationale

Our laboratory previously showed that, following stress, rapid breakdown of the chloride gradient erodes GABAergic inhibitory efficacy to mediate PVN CRH neurons' switch from inactive to active (Sarkar et al., 2011). Considering the abundance of clinical evidence for HPA axis dysregulation in epilepsy (Tellez-Zenteno et al., 2007) and significant anecdotal evidence for the ability of stress to trigger seizures (Balamurugan et al., 2013;Sperling et al., 2008), it stands to reason that stress and seizures activate overlapping circuits, but the cellular mechanism underlying seizure-induced HPA axis activation remains unknown. We hypothesized that seizures hijack the same chloride plasticity mechanism normally utilized by the adaptive stress response to rapidly erode inhibitory efficacy in the PVN. In parallel, we hypothesized that this seizure-induced HPA axis activation exacerbates susceptibility to future seizures, forming a vicious cycle by which "seizures beget stress begets seizures".

Does seizure induction mobilize the HPA axis?

We first induced acute seizures with either kainic acid (KA) (20 mg/kg, i.p.) or pilocarpine (340 mg/kg, i.p.) to assess activation of the HPA axis following seizures. In both seizure models, electroencephalogram (EEG) recordings were performed to assess seizure severity. Seizures were induced for 2 hours, then mice were sacrificed and their trunk blood and brains collected. Serum samples were assayed by ELISA for ACTH and CORT by other members of the laboratory. Both KA and pilocarpine produced elevations in ACTH (KA: 265.6±40.3 pg/mL; pilocarpine: 223.0±16.7 pg/mL) compared to saline-injected control littermates (138.9±7.6 pg/mL) (n=7–13 mice per experimental group) (Figure 3.1a). Corticosterone levels were also increased following KA (169.8±19.2 ng/mL) and pilocarpine (153.2±13.7 ng/mL) compared to controls (48.0±6.2 ng/mL) (n=7–28 mice per experimental group) (Figure 3.1b). The effect of KA seizures on CORT was dose-dependent, as 10 mg/kg produced a significant but smaller increase (111.3±17.7 ng/mL) over controls (n=22–28 mice per experimental group) (Figure 3.1c). The increase in CORT also positively correlated with the severity of seizures as measured by the proportion of the 2-hour recording window exhibiting epileptiform activity (r=0.819) (n=10 mice per experimental group) (Figure 3.1d). Additionally, the number of neurons expressing the immediate early gene c-fos, which is induced by periods of high activity, was increased in the PVN following seizures induced with either kainic acid or pilocarpine (193.2±31.7 and 242.4±33.0 respectively) compared to saline-injected control littermates (147±2.6) (n=18 sections, 3 mice per experimental group) (Figure 3.2). Finally, 400 μm slices containing the PVN were collected for patch clamp electrophysiology following seizures, and the spontaneous firing rates of PVN neurons were measured. The firing rates were significantly increased by both KA (7.5±0.9 Hz) and pilocarpine (7.0±0.9 Hz) compared to saline-injected controls (3.8±0.5 Hz) (n=15–16 cells, 3–4 mice per experimental group) (Figure 3.3). Together,

these data demonstrated that seizures induced in two separate models of temporal lobe epilepsy activated the HPA axis by increasing the excitability of PVN CRH neurons to a similar extent.

Does exogenous stress hormone administration exacerbate seizure severity?

Since the stress and seizures appear to be mutually reinforcing, we asked the converse question by administering a slow-release CORT pellet and assessing the severity of KA seizures (20 mg/kg, i.p.). Mice were implanted with a 10 mg, slow-release CORT pellet. After 7 days, there was a significant elevation of CORT (192.2±17.1 ng/mL) similar to that produced by the seizure models above, in contrast to sham (scalp incision-only) or vehicle-implanted mice (sham: 57.9±13.7 ng/mL; vehicle: 47.2±6.9 ng/mL) (n=6–9 mice per experimental group). Measurement of KA seizure severity by EEG revealed that CORT administration decreased the latency to the first seizure (239.0±35.0 sec) and increased the percent time exhibiting epileptiform activity (89.8±1.6%) compared to sham-implanted control littermates (451.4±85.2 sec latency, 74.5±6.5% epileptiform activity) (n=6–9 mice per experimental group) (Figure 3.4). These data demonstrate that high levels of stress hormones exacerbate seizure severity, reinforcing the notion that stress can trigger seizures.

What is the synaptic mechanism of seizure-induced HPA axis mobilization?

Based on our previous findings regarding changes in GABAergic signaling in stress-induced activation of the HPA axis, we assessed inhibitory currents in PVN CRH neurons following KA seizures. Electrophysiological recordings were performed on CRH neurons in the PVN 2 hours after seizures were induced with KA. Seizures had no effect on the frequency or amplitude of spontaneous excitatory postsynaptic currents (sEPSCs) (1.1±0.3 Hz; 21.7±2.3 pA) compared to saline-injected controls (1.0±0.1 Hz; 18.4±1.0 pA) (Figure 3.5b). However, there was an increase

in both the frequency and amplitude of spontaneous inhibitory postsynaptic currents (sIPSCs) (5.1±0.7 Hz; 45.8±3.8 pA) compared to controls (2.7±0.5 Hz; 26.6±3.3 pA) (n=14 cells, 4–5 mice per experimental group) (Figure 3.5a, c).

In light of the seizure-induced increase in HPA axis output associated with an increase in the firing rate of CRH neurons in the PVN, the observed increase in phasic inhibition was counterintuitive. Therefore, we also assessed tonic inhibition, and found that seizures induced by KA injection caused a significant decrease in PVN CRH neurons' Gabazine-sensitive tonic current (4.6±1.2 pA) compared to saline-injected controls (10.5±2.6 pA) (n=15–17 cells, 5 mice per experimental group) (Figure 3.6a, b). In turn we hypothesized that potentiating the tonic current with a $GABA_AR$ δ (delta) subunit-preferring agonist, THIP, should reduce seizure-induced activation of the HPA axis. Instead, we found the opposite: injection of a non-sedative dose (10 mg/kg) of THIP 30 min before seizure induction strongly potentiated the seizure-induced elevation of CORT (THIP+KA: 1093.6±259.8 ng/mL; KA alone: 169.8±19.2 ng/mL) (n=6 mice per experimental group) (Figure 3.6c). These otherwise contradictory results could be reconciled by a mechanism in which seizure-induced collapse of the chloride gradient gives rise to depolarizing or excitatory actions of GABA.

Do seizures alter $GABA_AR$ subunit expression and chloride homeostasis in the PVN?

I probed PVN tissue extracts for seizure-induced alterations in the expression of both $GABA_AR$ subunits and the chloride exporter KCC2. Consistent with the observed increase in phasic inhibition, expression of the γ2 subunit of the $GABA_AR$ was increased in the PVN following KA seizures (60.2±3.0 OD units/25 μg total protein) compared to saline-injected controls (41.6±6.1 OD units/25 μg total protein) (Figure 3.7). Critically, the phosphorylation of KCC2

on residue Ser940 – thought to be involved in stabilizing KCC2 at the cell surface by impeding endocytosis and increasing transport function – was downregulated following seizures (27.6±2.6 OD units/25 μg total protein) compared to controls (42.8±3.0 OD units/25 μg total protein) (Figure 3.7), as was total expression of KCC2 (57.0±1.8 vs 72.9±2.5 OD units/25 μg total protein) (Figure 3.7). Conversely, expression of the chloride-importing protein NKCC1 was slightly elevated following seizures (32.8±2.0 OD units/25 μg total protein) compared to controls (27. 9±0.7 OD units/25 μg total protein) (n=8–15 mice per experimental group) (Figure 3.7). Together these data indicate that erosion of inhibition in the PVN may underlie the seizure-induced activation of the HPA axis.

We next set out to functionally assay chloride homeostasis in the PVN, employing perforated patch clamp electrophysiology to maintain PVN CRH neurons' native ionic gradients. Following KA seizures, a higher proportion of PVN CRH neurons exhibited depolarizing spontaneous inhibitory postsynaptic potentials (sIPSPs) (40.7±9.6%) compared to vehicle-injected controls (7.1±5.0%) (Figure 3.8a, b). Additionally, the amplitude of hyperpolarizing sIPSPs was lower following KA seizures (2.6±0.2 mV) compared to controls (3.9±0.4 mV) (n=17–28 cells, 6–8 mice per experimental group) (Figure 3.8a, c). These data complement the biochemical evidence above implicating chloride homeostasis as the mechanism for seizure-induced activation of the HPA axis.

Does HPA axis activation contribute to the seizure-induced increase in future seizure susceptibility?

In order to test the notion that "seizures beget seizures", seizures were induced with 10 mg/kg KA and 7 days later the same mice received a second dose of 10 mg/kg KA. As demonstrated

above, the initial dose of KA increased CORT levels (100.5±20.1 ng/mL) compared to saline-injected controls (47.2±6.9 ng/mL) (Figure 3.9; "+Antalarmin" and "+bumetanide" conditions are discussed below). Importantly, the second dose of KA produced significantly more severe electrographic seizures as measured by the latency to first seizure (330.8±186.3 sec) and percent time exhibiting epileptiform activity (81.8±10.4%) compared to the first dose (1117.7±520.1 sec latency; 44.4±13.6% epileptiform activity) (n=6 mice per experimental group) (Figure 3.10b, c). As previously noted, systemic KA does not lead to the development of spontaneous seizures; accordingly, we observed no epileptiform activity beyond 10 hours after the initial dose of KA (0–2 h: 54.9±8.4%; 2–4 h: 46.9±13.4%; 4–6 h: 9.2±4.8%; 6–8 h: 11.3±8.6%; 8–10 h: 5.9±5.6%; 10–12 h:0.0±0.0%; 12–14 h: 0.0±0.0%; 14–16 h: 0.0±0.0%; 16–18 h: 0.0±0.0%; 18–20 h: 0.0±0.0%; 20–22 h: 0.0±0.0%; 22–24 h: 0.0±0.0%) (n=5 mice) (Figure 3.11).

We then tested the hypothesis that preventing seizure-induced activation of the HPA axis could attenuate the increase in seizure susceptibility in response to a second challenge of KA. Following the initial dose of 10 mg/kg KA, drinking water administration of 10 mg/kg daily Antalarmin, a CRHR1 antagonist, blocked the seizure-induced increase in CORT (48.4±7.7 ng/mL) (n=17–20 mice per experimental group), maintaining CORT at a level similar to that of saline-injected, seizure-free controls (Figure 3.9). Antalarmin also reduced the severity of seizures induced by the second dose of KA (3082.5±552.4 sec latency; 25.3±6.6% epileptiform activity) (n=6–10 mice per experimental group) (Figure 3.10b, c). This was unlikely to be a result of direct anticonvulsant actions of Antalarmin, as it was ineffective in reducing the severity of seizures to an initial dose of 20 mg/kg KA (74.0±9.5% epileptiform activity) compared to controls receiving KA without Antalarmin (76.7±5.9%) (n=6–7 mice per experimental group).

Finally, having previously shown that HPA axis activation depends on collapsing the chloride gradient, we tested the hypothesis that pharmacologically rescuing chloride plasticity could similarly block seizure-induced vulnerability to future seizures. Daily administration of 0.2 mg/kg bumetanide, an NKCC1 antagonist, for 7 days following the initial 10 mg/kg KA dose restored the serum CORT level (56.2±10.0 ng/mL) to a level similar to that of controls (47.2±6.9 ng/mL) and well below that of animals treated with KA alone (100.5±20.1 ng/mL) (n=17–20 mice per experimental group) (Figure 3.9). Additionally, treatment with bumetanide reduced the severity of seizures induced by the second dose of KA (3458.0±1585.8 sec latency; 5.3±4.9% epileptiform activity) compared to animals that did not receive bumetanide (330.8±186.3 sec latency; 81.8±10.4% epileptiform activity) (n=6 mice per experimental group) (Figure 3.10b, c). These data demonstrate that seizure-induced susceptibility to future seizures relies significantly on seizure-induced mobilization of the HPA axis.

Significance

A wealth of clinical and anecdotal evidence describes a mutually-reinforcing pathological relationship between stress and seizures. Here we have shown that seizures mobilize the HPA axis by the same mechanism as that of a typical psychogenic stressor like restraint stress: reducing the driving force of chloride to rapidly, transiently liberate PVN CRH neurons from GABAergic inhibitory constraint. Indeed, the ability of an extrasynaptic $GABA_AR$ agonist, THIP, to exacerbate seizure-induced HPA axis activation suggests that this constraint reverses completely during seizures, rendering GABA depolarizing or excitatory in the PVN. The resulting seizure-induced elevation of serum CORT renders mice more susceptible to future seizures, which in turn we would expect to mobilize the HPA axis once again, and so on in a vicious cycle. In the KA model of seizures, the vicious cycle can be broken by preventing

seizure-induced HPA axis activation with either Antalarmin (presumably at the level of the pituitary corticotroph CRH receptor) or bumetanide (presumably at the level of GABAergic inhibitory efficacy in PVN CRH neurons). Of course, we cannot rule out the possibility that Antalarmin and bumetanide impact seizure-induced HPA axis activation indirectly through actions at brain regions outside of the PVN (discussed in greater detail in Section 9). However, despite this uncertainty about the cellular mechanism, we have demonstrated that interventions targeting stress signaling hold great promise as strategies for reducing seizure burden.

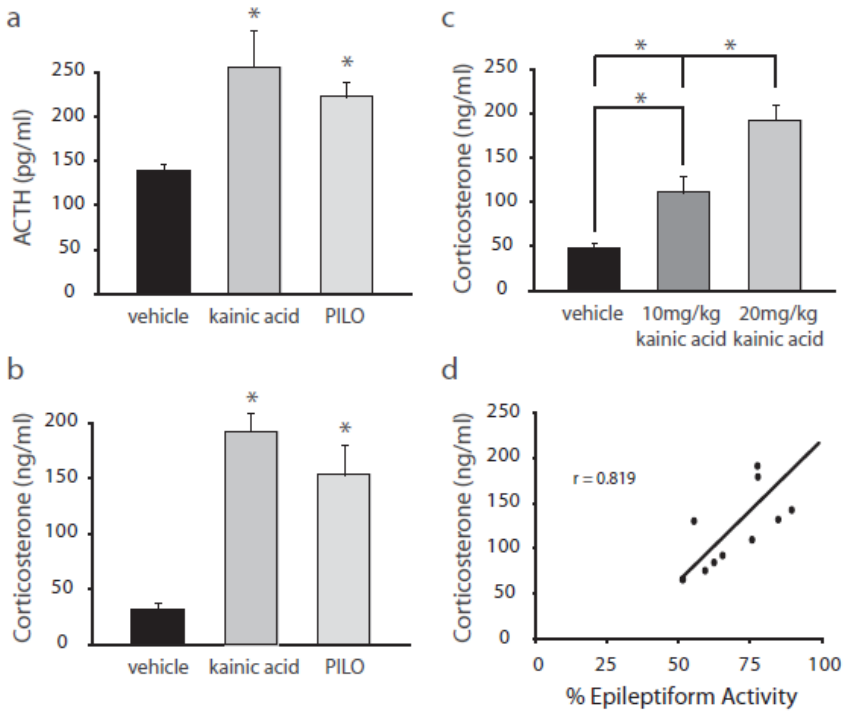

Reproduced from (O'Toole et al., 2014)

Figure 3.1. Seizure-induced elevations in ACTH and corticosterone. (a) Average circulating ACTH levels 2 h following treatment with vehicle, kainic acid (20 mg/kg), or pilocarpine (340 mg/kg). n=7-13 mice per experimental group. (b) Average corticosterone levels measured 2 h following treatment with vehicle, 20 mg/kg kainic acid, or pilocarpine (340 mg/kg). n=7-28 mice per experimental group. (c) Average circulating corticosterone levels measured 2 h following vehicle, 10 mg/kg kainic acid, or 20 mg/kg kainic acid treatment. n=22-28 mice per experimental group. (d) The correlation calculation between the percent electrographic epileptiform activity and circulating corticosterone levels (r=0.819). n=10 mice per experimental group. * denotes significance ($p<0.05$) compared to control using a one-way ANOVA with Tukey's test for multiple comparisons.

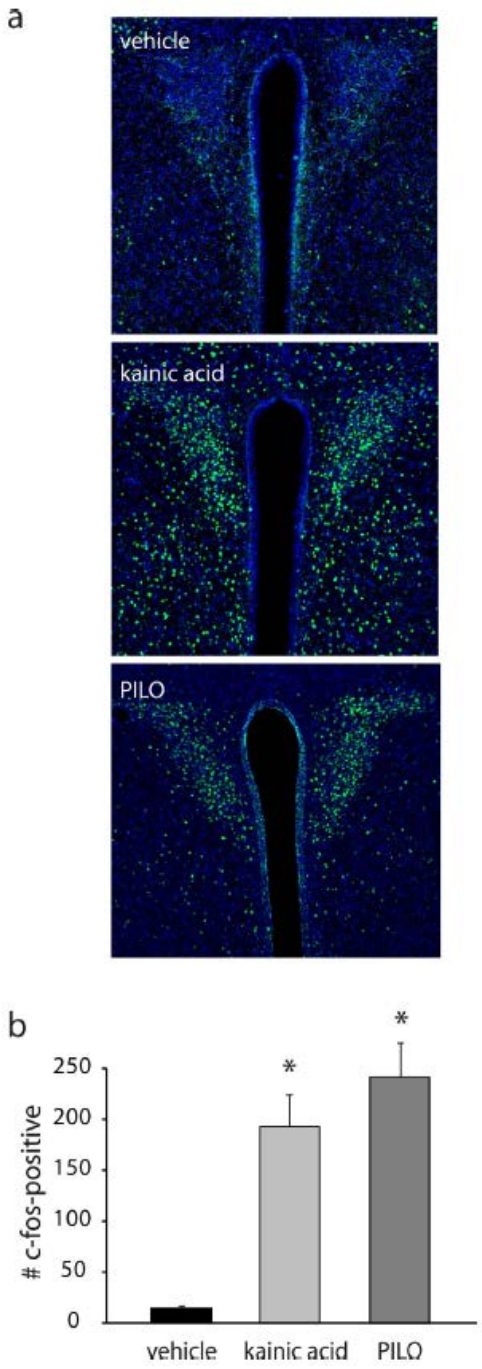

Reproduced from (O'Toole et al., 2014)

Figure 3.2. Seizure-induced activation of c-fos in PVN neurons. (a) Representative images of c-fos immunoreactivity in the PVN of vehicle, kainic acid (20 mg/kg), and pilocarpine (340 mg/kg) treated mice. (b) The average number of c-fos-positive neurons in the PVN of vehicle, kainic acid, and pilocarpine-treated mice. n=18 sections, 3 mice per experimental group. * denotes significance ($p<0.05$) compared to control using a one-way ANOVA with Tukey's test for multiple comparisons.

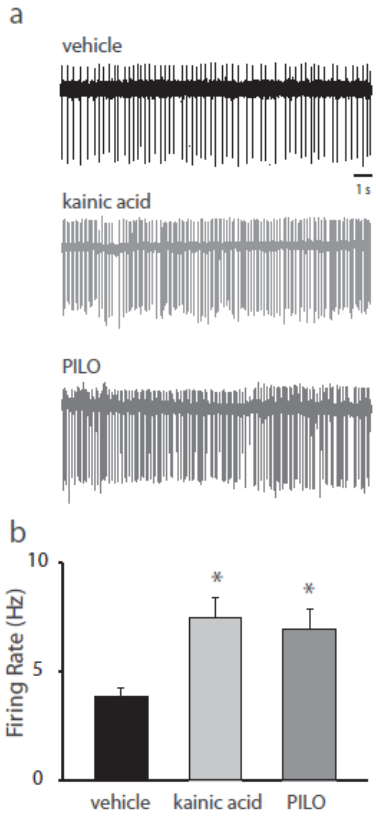

Reproduced from (O'Toole et al., 2014)

Figure 3.3. Seizure-induced increase in the activity of CRH neurons. (a) Representative traces of the spontaneous firing rate of CRH neurons in vehicle, kainic acid (20 mg/kg), and pilocarpine (340 mg/kg) treated mice. (b) The average firing rate of CRH neurons in the PVN in vehicle, kainic acid, and pilocarpine treated mice. n=15-16 cells, 3-4 mice per experimental group. * denotes significance ($p<0.05$) compared to control using a one-way ANOVA with Tukey's test for multiple comparisons.

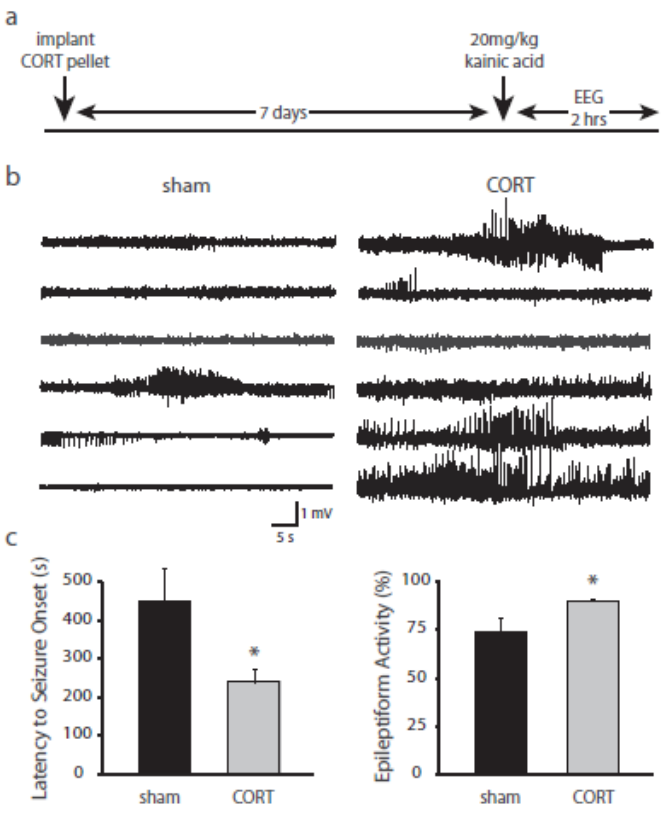

Reproduced from (O'Toole et al., 2014)

Figure 3.4. Increased seizure susceptibility in corticosterone treated mice. (a) Timeline of corticosterone and kainic acid treatment prior to in vivo EEG recording. (b) Representative traces of epileptiform activity in sham and corticosterone implanted mice at the same time post kainic acid administration (approximately 10 min post-KA administration). Each line is 1 min of EEG activity for a total of 6 min in each experimental group. (c) The average latency to the first seizure episode in sham and corticosterone-implanted mice following 20 mg/kg kainic acid administration. (d) The percent time exhibiting epileptiform activity for the 2 h post kainic acid administration in sham and corticosterone-implanted mice. n=6-9 mice per experimental group. * denotes significance ($p<0.05$) compared to sham using a Student's *t*-test.

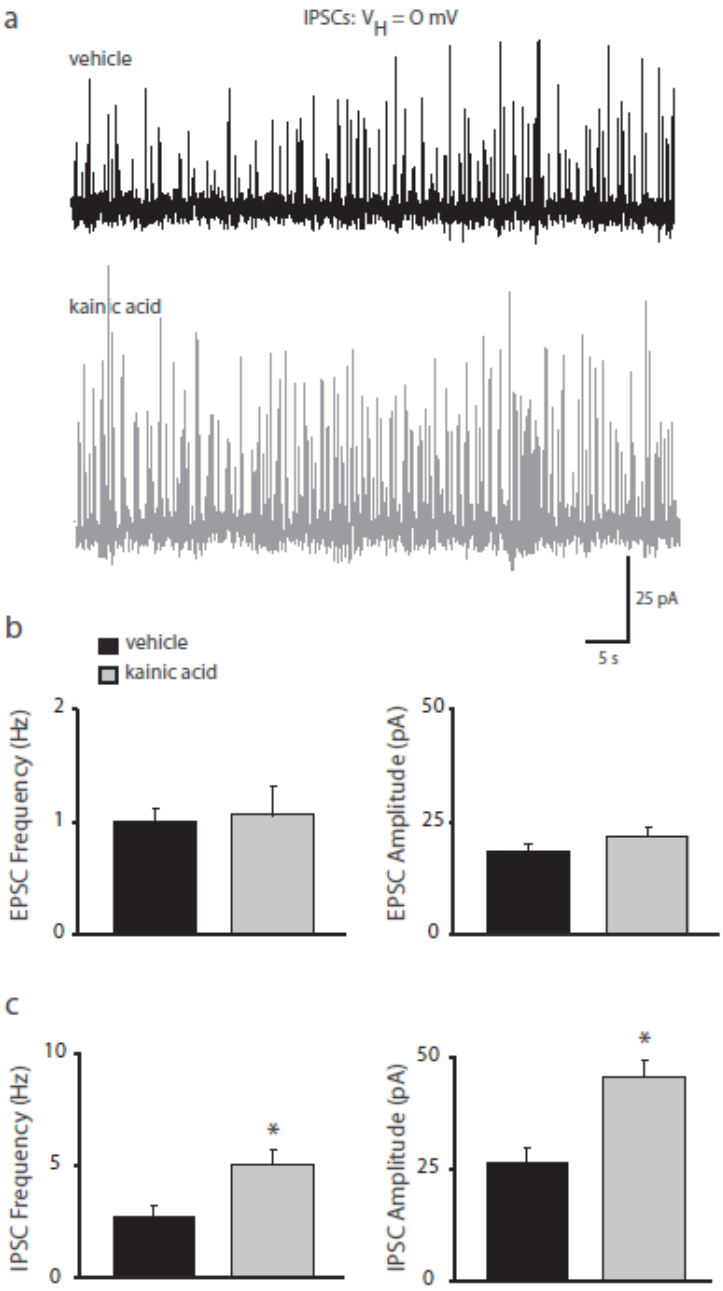

Reproduced from (O'Toole et al., 2014)

Figure 3.5. Increased phasic GABAergic inhibition following seizures. (a) Representative traces of sIPSCs (V_H=0 mV) recorded in CRH neurons 2 h following administration of either vehicle (black) or 20 mg/kg kainic acid (gray). (b) The average frequency and peak amplitude of sEPSCs in CRH neurons from vehicle and kainic acid-treated mice. (c) The average frequency and peak amplitude of sIPSCs in CRH neurons from vehicle and kainic acid-treated mice. n=14 cells, 4-5 mice per experimental group. * denotes significance ($p<0.05$) compared to vehicle using a Student's *t*-test.

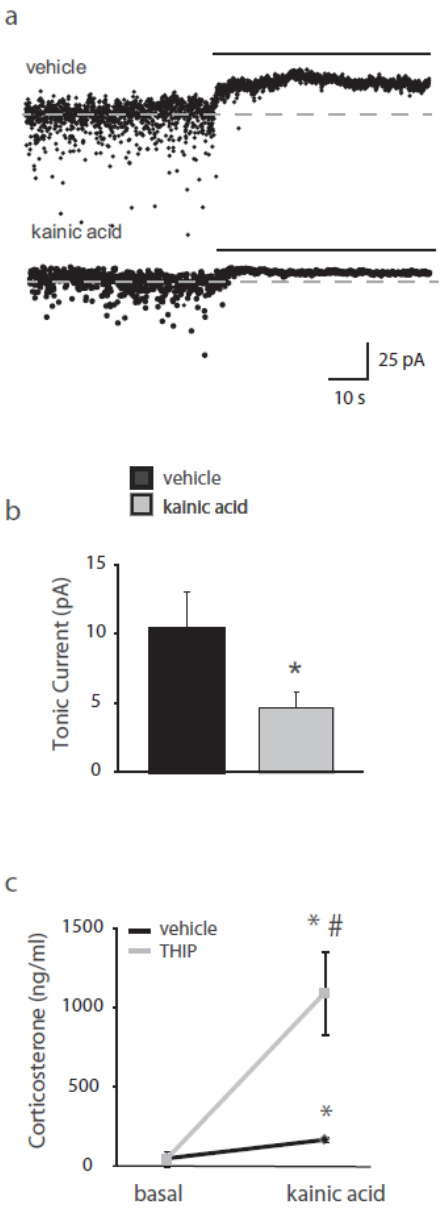

Reproduced from (O'Toole et al., 2014)

Figure 3.6. Decreased tonic GABAergic inhibition in CRH neurons following kainic acid-induced seizures. (a) Representative graphs of the tonic GABAergic current on CRH neurons from vehicle and kainic acid-treated mice. Each dot represents the average holding current every 100 ms before and after the addition of SR95531 (black line). (b) The average tonic GABAergic inhibition in CRH neurons recorded in CRH neurons in vehicle and kainic acid-treated mice. n=15-17 cells, 5 mice per experimental group. * denotes significance ($p<0.05$) compared to vehicle using a Student's *t*-test. (c) The average corticosterone levels before and after kainic acid-induced seizures in vehicle and THIP-treated mice. n=6 mice per experimental group. * denotes significance ($p<0.05$) compared to vehicle using a paired *t*-test.

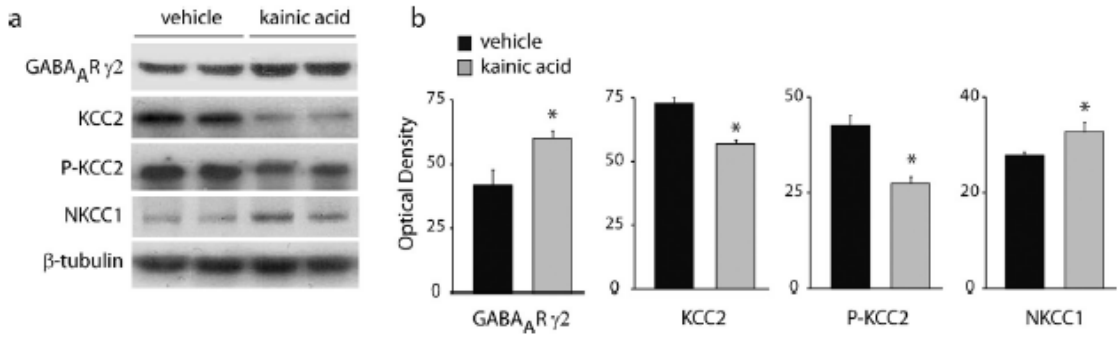

Reproduced from (O'Toole et al., 2014)

Figure 3.7. Alterations in GABA-relevant proteins following seizures. (a) Representative Western blots of the total protein isolated from the PVN of vehicle and kainic acid-treated mice in two independent samples per experimental group probed with antibodies against KCC2, a phosphospecific antibody for KCC2 residue Ser 940 (P-KCC2), NKCC1, the $GABA_AR$ γ2 subunit, and beta-tubulin. (b) The average optical density measurements for KCC2, P-KCC2, NKCC1, and the $GABA_AR$ γ2 subunit in the PVN of vehicle and kainic acid-treated mice. n=8–15 mice per experimental group. * denotes significance ($p<0.05$) compared to vehicle using a Student's *t*-test.

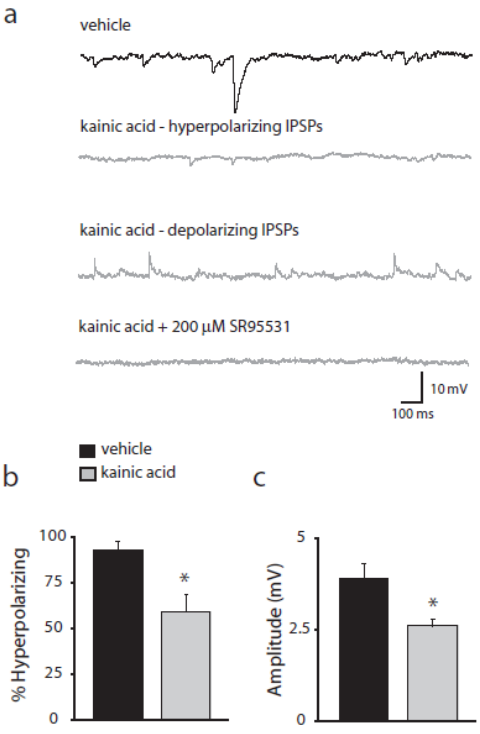

Reproduced from (O'Toole et al., 2014)

Figure 3.8. Compromised GABAergic inhibition of CRH neurons following seizures. (a) Representative perforated patch clamp traces of sIPSPs recorded in CRH neurons from vehicle and kainic acid-treated mice. The majority of sIPSPs in CRH neurons from vehicle-treated mice are hyperpolarizing (control). Spontaneous IPSPs recorded in CRH neurons from kainic acid-treated mice are either hyperpolarizing with a decreased amplitude (kainic acid - hyperpolarizing IPSPs) or depolarizing (kainic acid - depolarizing IPSPs) compared to those recorded in vehicle treated mice. All sIPSPs were blocked with SR95531. (b) The percentage of hyperpolarizing sIPSPs recorded in CRH neurons from vehicle- and kainic acid-treated mice. (c) The average peak amplitude of hyperpolarizing sIPSPs recorded in CRH neurons from vehicle- and kainic acid-treated mice. n=17–28 cells, 6–8 mice per experimental group. * denotes significance ($p<0.05$) compared to vehicle using a Student's *t*-test.

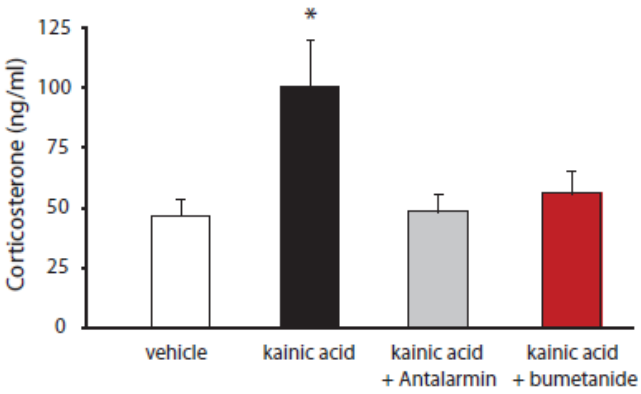

Reproduced from (O'Toole et al., 2014)

Figure 3.9. Prevention of seizure-induced elevations in corticosterone. The average corticosterone levels 7 days following kainic acid treatment in vehicle–, Antalarmin–, or bumetanide-treated mice compared to controls (no kainic acid). n=17–20 mice per experimental group. * denotes significance ($p<0.05$) compared to vehicle using a one-way ANOVA with Tukey's test for multiple comparisons.

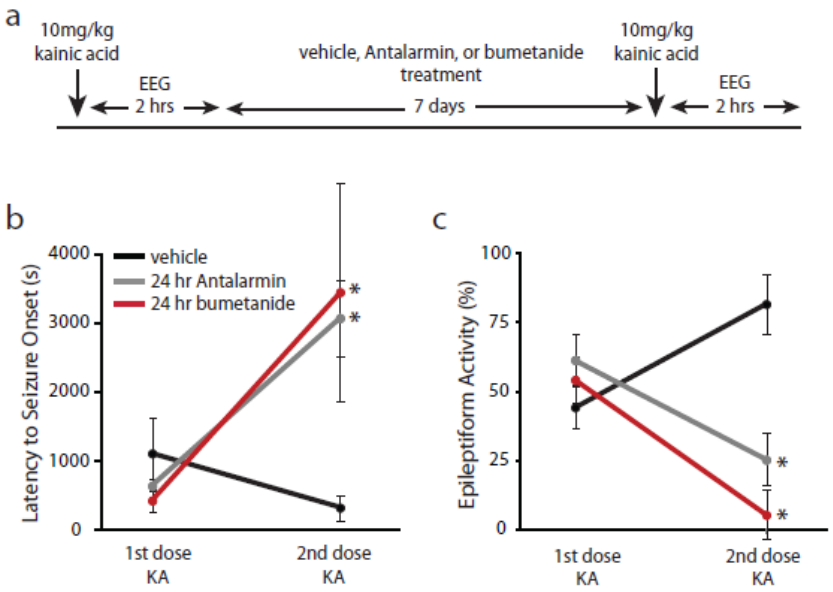

Reproduced from (O'Toole et al., 2014)

Figure 3.10. Blocking seizure-induced corticosterone elevations prevents future seizure susceptibility. (a) Timeline of drug treatments and EEG recording. The average latency to the first seizure detected (b) and percent time exhibiting epileptiform activity (c) in response to a second 10 mg/kg dose of kainic acid 7 days following initial kainic acid treatment. n=6–10 mice per experimental group. * denotes significance ($p<0.05$) compared to vehicle using a one-way ANOVA with Tukey's test for multiple comparisons.

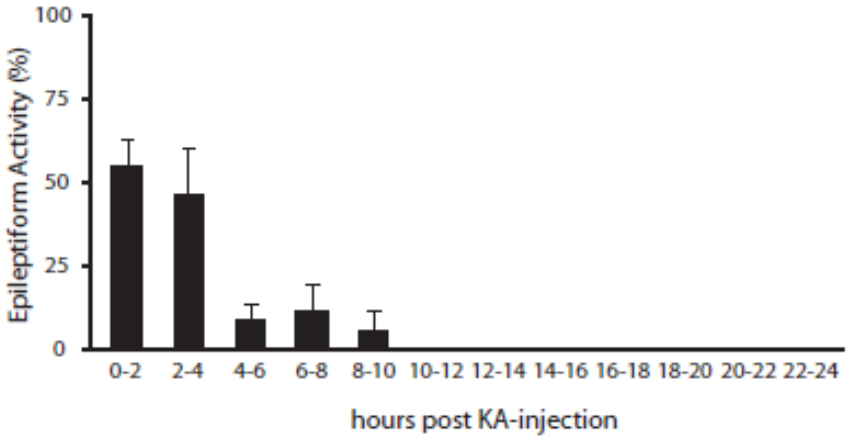

Reproduced from (O'Toole et al., 2014)

Figure 3.11. Time course of kainic acid-induced seizures. The average percent time exhibiting epileptiform activity in 2 h blocks following treatment with 10 mg/kg kainic acid. n=5 mice.

4. KCC2 in the PVN: Chloride homeostasis disruption as a model of hypothalamic-pituitary-adrenal axis dysfunction

One of the hallmark features and principle underlying mechanisms of stress-related disorders such as MDD is HPA axis dysregulation. Our laboratory previously demonstrated that GABAergic inhibition in the PVN, the pinnacle of HPA axis control, is rapidly and transiently eroded by stress. Here I test the hypothesis that selectively knocking out the chloride-exporting function of KCC2 from PVN CRH neurons can disrupt the adaptive stress response and produce features of stress-related disorders. This section contains unpublished data that I generated, analyzed, and interpreted.

Rationale

It is well-established that normal KCC2 function is necessary for maintaining low neuronal intracellular [Cl^-] and thus preserving efficacy of inhibitory synaptic transmission. We previously showed that stress mobilizes the HPA axis by transiently inhibiting KCC2 function to collapse the chloride gradient in PVN CRH neurons (Sarkar et al., 2011). Thus, we hypothesized that there is a direct mechanistic link between dysregulation of KCC2's transport function and pathological HPA axis activation. This would give KCC2 unique placement as a novel target of pharmacological intervention in stress syndromes – by far the most common co-occurring class of neuropsychiatric conditions (Duric et al., 2016). In this study I investigated the role of KCC2 in stress reactivity by selectively knocking out its transport function from the PVN and assessing the effects of KCC2 dysregulation on stress anatomy and physiology, as well as stress-reactive behavior.

Transgenic knockout: Is total KCC2 expression altered by CRH neuron-selective deletion of KCC2's transporter domain?

In order to selectively dysregulate KCC2 in PVN CRH neurons, we utilized the $KCC2^{f/f}$ mouse line, in which exons 22-25 of the SLC12A5 (KCC2) gene, encompassing KCC2's transporter domain (Mercado et al., 2006), is flanked by loxP sites. Thus, in cells expressing Cre recombinase, these exons are excised and KCC2 is unable to extrude chloride. By crossing $KCC2^{f/f}$ mice with the CRH-Cre line, we expected to selectively impair chloride homeostasis – and thus GABAergic inhibitory efficacy – in PVN CRH neurons. Although this manipulation should also eliminate chloride extrusion capacity in other CRH neuron populations throughout the brain, we anticipated that any systemic functional changes should be mediated by the PVN population in light of the considerable inhibitory input this region receives compared to other CRH-expressing brain regions (Miklos and Kovacs, 2002). I assessed whether this transgenic approach results in changes in KCC2 expression or post-translational modifications by probing PVN protein for both KCC2 and S940 phospho-KCC2. Surprisingly, protein from the PVN of CRH-KCC2 mice displayed no change in total KCC2 expression (0.71±0.08 OD units/25 μg protein) or phosphorylation at S940 (0.78±0.12 OD units/25 μg protein) compared to Cre-negative control littermates (KCC2: 0.73±0.15 OD units/25 μg protein; phospho-KCC2: 0.96±0.46 OD units/25 μg protein) (n=2-4 mice per genotype) (Figure 4.1a). I also applied immunostaining of PVN brain sections, and similarly found no difference in KCC2 immunoreactivity between CRH-KCC2 (19.63±4.14 OD units) and control mice (19.14±1.94 OD units) (n=3-6 mice per genotype) (Figure 4.1b). In common with most available antibodies against KCC2, the antibodies I used bind to the C-terminal intracellular domain of KCC2 ((Chamma et al., 2012) and Dr. Stephen Moss, personal communication). Since a large portion of the C-terminal domain of KCC2 should be excised in the CRH neurons of CRH-KCC2 mice,

we expected to see a significant decrease in both total expression and S940 phosphorylation in the PVN. Thus my results above indicate that either (1) Western blot and immunostaining lack sufficient sensitivity to detect KCC2 expression changes in transgenic mice, (2) our transgenic approach fails to truncate KCC2 in a significant portion of PVN CRH neurons, or (3) knocking KCC2 out of CRH neurons throughout development gives rise to a compensatory reorganization of the PVN – for example, a reduction in the number of CRH neurons and an increase in the number of AVP neurons. However, a more definitive demonstration of KCC2 transport function knockout in the PVN is needed to distinguish between these possible explanations; I will discuss alternative strategies to assess KCC2 function in Section 9.

Transgenic knockout: Does CRH-selective KCC2 transport knockout alter stress-related anatomy and physiology?

Chloride plasticity is a critical cellular mechanism underlying the adaptive stress response, so we hypothesized that persistently impaired chloride plasticity in the PVN would give rise to structural and functional abnormalities in the systemic stress signaling pathway. I first isolated and weighed the adrenal glands, but found no obvious difference in the adrenal gland-to-body weight ratio between CRH-KCC2 mice ($1.30x10^{-4}\pm2.17x10^{-5}$) and wild-type controls ($9.98x10^{-5}\pm1.71x10^{-6}$) (n=2-4 mice per genotype). Next I assessed basal serum CORT levels, but again found no change in resting stress hormone levels in mutant mice (9.31±4.55 ng/mL) compared to controls (9.17±2.92 ng/mL). These data suggested that the HPA axis is able to compensate for the persistent lack of chloride plasticity in the PVN and maintain low basal activity; however, we hypothesized that the effects of the KCC2 transport knockout might be unmasked by challenging the system with an acute stress. Surprisingly, restraint stress also failed to reveal any effect of the CRH-KCC2 mutation on circulating CORT (47.96±4.79 ng/mL) compared to

controls (65.47±16.58 ng/mL) (n=2-6 mice per experimental group) (Figure 4.2). Together these results point to two possible explanations: either our transgenic model fails to significantly perturb PVN CRH neurons' ability to export chloride, or the collective stress signaling pathway is able to compensate for a persistent lack of chloride plasticity in the PVN by as-yet unidentified adaptations – such as synaptic scaling or structural rewiring of connectivity – throughout the pathway.

Transgenic knockout: How does CRH-selective KCC2 transport knockout impact stress-reactive behaviors?

Despite the lack of a significant effect on the neuroendocrine output of the HPA axis, we hypothesized that perturbing inhibitory constraint on PVN CRH neurons might nevertheless have consequences for stress-reactive emotional behavior through upstream, compensatory changes in limbic forebrain structures. Therefore I assessed anxiety-like behavior in the open field and light-dark box paradigms (Holter et al., 2015a). Mutants lacking KCC2 transport function in CRH neurons exhibited no changes in locomotor activity (2172±147 basic movements) or anxiety-like behavior (14.63±2.78% time in center) in the open field test compared to wild-type control littermates (2188±86 basic movements; 10.75±1.09% time in center) (n=8-21 mice per genotype) (Figure 4.3a). Similarly, the light-dark box revealed no significant differences between CRH-KCC2 mice (33.10±4.35% time in light compartment) compared to controls (25.36±1.95% time in light compartment) (n=7-11 mice per genotype) (Figure 4.3b). Thus, our transgenic approach to persistently impairing chloride plasticity in CRH neurons throughout the brain did not significantly impact anxiety-like behavior.

A highly relevant consequence of chronic stress and related animals models of HPA axis dysregulation is an increase in depression-like behavior, which is generally reversible by antidepressant medication. Thus, I probed depression-like behavior in our transgenic model by assessing immobility in the forced swim test (Yan et al., 2010). Once again, CRH-specific KCC2 transport-deficient mutants showed no alterations of depression-like behavior in terms of latency to immobility (73.1±9.0 sec) or total immobility (219.1±19.5 sec) compared to wild-type controls (77.7±5.9 sec latency; 227.3±8.6 sec total immobility) (n=8-21 mice per genotype) (Figure 4.3c).

Together our results from transgenic knockout of KCC2 transport function indicate that the persistent, developmental impairment of chloride export from CRH neurons was insufficient to modify basal stress anatomy or physiology, stress-induced mobilization of the neuroendocrine stress response, or stress-reactive emotional behavior – or alternatively, that our transgenic approach was ineffective at functionally knocking out KCC2 (see Section 9 for further discussion). The importance of PVN CRH neurons in the HPA axis is well-established, there is ample evidence for erosion of inhibition as a critical mechanism underlying neuroendocrine stress signaling, and we previously demonstrated that our CRH-Cre line expresses Cre recombinase in the PVN (Sarkar et al., 2011). Thus, we tentatively concluded that our transgenic model fails to perturb the systemic stress signaling pathway because the persistent loss of KCC2 from CRH neurons through development enables adaptive compensatory changes – for example, a reduction in the number of CRH neurons and corresponding increase in AVP neurons in the PVN, and/or increased KCC2 expression in AVP neurons – leading to normalized stress signaling in the adult brain. This observation raises interesting questions about the anatomical and cellular substrates of such developmental circuit plasticity. However,

focusing on the original goals of our investigation, we transitioned to an alternative model for manipulating KCC2 activity in the PVN that improves spatial specificity and avoids the complications of persistent, developmental knockout of chloride extrusion: stereotaxic injection of viral Cre recombinase into the PVN of $KCC2^{f/f}$ adults.

Viral knockout: Is total KCC2 expression altered by PVN-specific deletion of KCC2's transporter domain?

I first assessed whether the viral approach to KCC2 transport knockout influenced KCC2 expression in the PVN by applying immunostaining to PVN brain sections. In contrast to the transgenic knockout of KCC2 transporter function, I found a moderate but non-significant reduction of KCC2 immunoreactivity in the PVN of $KCC2^{f/f}$ mice injected with AAV-Cre-eGFP (16.08±1.59 OD units) compared to AAV-eGFP-injected controls (20.06±1.57) (n=4-6 mice per experimental group) (Figure 4.4c). This indicates that selective excision of the KCC2 transporter domain from the adult PVN reduces total KCC2 expression, possibly mediated by the removal of stabilizing protein-protein interactions within the excised portion of the cytosolic C-terminal domain. Alternatively, it is possible that the reduced KCC2 expression simply reflects excision of the portion of the C-terminal domain recognized by the KCC2 antibody. This finding potentially lends support to the notion that persistent, developmental knockout permits compensatory mechanisms, while the viral, adult knockout more efficiently impairs functional expression of KCC2. As noted above, a more conclusive demonstration of KCC2 transport function knockout in the PVN is still needed (discussed further in Section 9).

Viral knockout: Does PVN-specific KCC2 transport knockout alter stress hormone levels?

Given my finding of reduced expression of KCC2 in the PVN following viral knockout of the transporter domain, I anticipated corresponding changes in the neuroendocrine stress response. I assessed serum CORT in unstressed animals but, similar to the transgenic approach, found no changes in Cre-injected KCC2$^{f/f}$ mice (18.36±2.83 ng/mL) compared to GFP-injected controls (29.72±3.43) (n=2 mice per experimental group) (Figure 4.5a). While my results are still preliminary and this experiment must be repeated, these data at least suggest the absence of a dramatic effect of viral KCC2 knockout on basal CORT levels. However, I did identify a trend toward exacerbation of the acute stress-induced elevation of serum CORT in viral knockout mice (AAV-Cre: 151.10±66.23 ng/mL; AAV-GFP: 86.66±21.70 ng/mL) (Figure 4.5b). Furthermore, animals that received accurate injections of Cre to both hemispheres showed a greater elevation of CORT, while those exhibiting only unilateral AAV-Cre expression presented intermediate levels (107.37±12.42 ng/mL) (n=4-15 mice per experimental group) (Figure 4.5b). The small size of the injection target and substantial variability of serum CORT concentrations across groups urge caution in drawing conclusions from these data. Nevertheless, these findings suggest that, unexpectedly, intact KCC2 function in the PVN is dispensable for maintaining low levels of CORT in the absence of stress, yet critical for terminating HPA axis activity to prevent excessive increases in stress hormone levels.

Viral knockout: How does PVN-specific KCC2 transport knockout impact stress-reactive behaviors?

We next asked whether the viral knockout approach sufficiently perturbed stress signaling to produce significant changes in stress-reactive emotional behavior. I first applied the open field paradigm to assess anxiety-like behavior. While I did not observe any significant changes in anxiety-like behavior between viral knockout (14.04±1.78% time in center) and control mice

(19.10±2.84% time in center), I did observe a striking increase in locomotor activity among the viral knockouts (AAV-Cre: 3596±329 basic movements; AAV-GFP: 2694±72 basic movements) (n=3-10 mice per experimental group) (Figure 4.6a). In the light-dark box paradigm, viral knockout similarly increased locomotor activity (2478±228 basic movements) compared to controls (1856±74 basic movements), but importantly, this test further revealed a significant reduction in anxiety-like behavior among viral knockout mice (AAV-Cre: 46.18±1.89% time in light compartment; AAV-GFP: 27.09±3.19% time in light compartment) (n=3-10 mice per experimental group) (Figure 4.6b). The light-dark box may be a more stressful test of anxiety-like behavior, as the brightly-illuminated light compartment is more aversive than the center of an open field enclosure (Hart et al., 2010). This in turn could make the light-dark box more sensitive to stress signaling effects on state anxiety, which may explain the discrepancy we observed between the two tests.

Considering the observed anxiolytic effect of viral KCC2 transporter knockout, we anticipated a potential effect on depression-like behavior as well, so next I employed the forced swim test. Similar to the transgenic knockout, I found no effect of viral KCC2 transporter knockout on latency to immobility (98.0±36.1 sec) or total time immobile (208.7±36.1 sec) compared to GFP-injected controls (93.7±8.9 sec latency; 207.1±9.6 sec total immobility) (n=3-9 mice per experimental group) (Figure 4.6c). However, considering the striking locomotor hyperactivity phenotype produced by the viral knockout, we cannot rule out the possibility that impairing KCC2 function in the PVN does influence depression-like behavior but that this influence is masked by hyperactivity. Apart from this caveat, our data indicates that reducing KCC2 function and expression in the PVN causes modest reduction in anxiety-like behavior with no significant effect on depression-like behavior.

Activation of the HPA axis also impacts spatial learning and memory through ascending projections to the limbic forebrain as well as glucocorticoid receptor (GR) actions. Thus I also performed fear conditioning on Cre- and GFP-injected KCC2$^{f/f}$ mice. Viral KCC2 transporter knockout did not have a significant impact on either contextual (31.40±8.77% freezing) or cued (44.47±9.98% freezing) fear memory retrieval compared to controls (context: 54.92±5.47% freezing; cued: 39.98±3.94% freezing) (n=3-10 mice per experimental group.) (Figure 4.6d). In the contextual retrieval task there was a non-significant trend toward lower freezing among Cre-injected mice; this apparent learning and memory effect may be confounded by the substantial increase in locomotor activity, but merits follow-up investigation.

Viral knockout: Does PVN-specific KCC2 transport knockout influence metabolic homeostasis?

The apparent functional relevance of PVN CRH neurons to locomotor activity was surprising, and this finding prompted us to further investigate the physiological consequences and potential circuit-level mechanism underlying the viral knockout mice's hyperactivity. First I asked whether there was a corresponding change in body weight among viral KCC2 transporter domain knockout mice, and in fact I did observe a trend toward a reduction in body weight gain among Cre-injected KCC2$^{f/f}$ mice (105.2±2.8% of initial weight after 8 weeks) following virus injection surgery, compared to GFP-injected littermates (113.1±5.5% of initial weight after 8 weeks) (n=6 mice per experimental group) (Figure 4.7a). I next asked whether this attenuated weight gain resulted purely from hyperactivity, or if PVN KCC2 dysfunction also impacted metabolic homeostasis. Thus, I placed mice in an indirect calorimetry chamber that tracks locomotor activity, food and water consumption, energy expenditure, and respiration, and analyzed these

parameters from two 3-day recording epochs: once before virus injection surgery (baseline), and once after recovery from surgery. Interestingly, I found that food consumption was increased following surgery (AAV-Cre: 101.01% of baseline consumption; AAV-GFP: 65.08% of baseline consumption) while locomotor activity was unchanged (AAV-Cre: 92.89% of baseline activity; AAV-GFP: 100.74% of baseline activity) in Cre-injected mice relative to a GFP-injected control (Figure 4.7b, c). On the other hand, water consumption was unchanged (AAV-Cre: 96.63% of baseline consumption; AAV-GFP: 85.39% of baseline consumption) while both energy expenditure (AAV-Cre: 124.59; AAV-GFP: 98.94) and respiration quotient (AAV-Cre: -0.66; AAV-GFP: -1.51) were elevated in Cre-injected mice compared to the GFP-injected control (n=1-2 mice per experimental group) (Figure 4.7d-f). The discrepancy between the locomotor activity result here and those above might be explained by the comparative lengths of recording periods: the open field and light-dark box are novel environments that mice actively explore for just 10 minutes, whereas in indirect calorimetry, mice presumably habituate to the novelty of the chambers by the end of trial day zero, before activity recording even begins. Therefore, collectively my findings from indirect calorimetry indicate that the PVN is functionally relevant to food consumption and energy metabolism, and thus disrupting inhibitory constraint of the PVN gives rise to abnormalities in body weight homeostasis. One obvious caveat to these findings on energy homeostasis is the very small sample size, so additional experiments will be needed to confirm the effects observed above.

The effect of our PVN-specific manipulation on body weight homeostasis could be explained by increased activity of afferents from the PVN to neighboring nuclei involved in modulating food intake and energy metabolism, such as the arcuate nucleus and lateral hypothalamus (Krashes et al., 2011;Burdakov et al., 2013). The hypothalamic nuclei are known

to be extensively interconnected (Bernardis and Bellinger, 1993). However, the specific synaptic connectivity of distinct cell types within the PVN has not yet been assessed, and we had recently obtained a Cre recombinase-dependent anterograde tract tracing virus (AAV-Flex-ChR2-tdTomato) with which to address precisely this question. Therefore I injected AAV-Flex-ChR2-tdTomato into the PVN of CRH-Cre mice and examined brain sections containing transduced PVN CRH cells and fibers via confocal microscopy to determine their connectivity. I observed extensive labeling of fibers in the external layer of the median eminence, the well-established destination of CRH-releasing fibers from the PVN (Swanson et al., 1983), thus confirming the validity of the tract tracing approach (Figure 4.8a, b). Additionally, I observed extensive labeled arborizations originating from the PVN but coursing along a trajectory distinct from that of the median eminence fibers. Interestingly, this second set of arborizations terminated in the tuberal nucleus of the lateral hypothalamus (Figure 4.8c). Though it has so far been sparsely investigated, the tuberal nucleus is reported to be important for interactions between stress and feeding (Kremer, 1992;Swaab et al., 1993). Thus, our circuit-mapping experiment identified a novel downstream target of synaptic innervation by PVN CRH neurons, which also happens to be a highly promising candidate for explaining how liberating the PVN from inhibitory constraint through selective knockout of KCC2's transporter function results in dysregulation of body weight and energy homeostasis.

Significance

Several unexpected and interesting findings emerged from our experimental manipulation of chloride plasticity in the PVN. We observed that cell type-specific, persistent, developmental knockout of KCC2's transporter domain (CRH-KCC2) has a negligible impact on systemic stress signaling and stress-reactive behavior, perhaps because of circuit rearrangement and other

compensatory changes through development that ultimately permit adaptive stress signaling in the mature animal. On the other hand, spatially-specific, adult knockout of KCC2 transporter function (AAV-Cre) gives rise to an exaggerated neuroendocrine response to acute stress, while sparing the ability of the HPA axis to maintain low basal CORT secretion in the absence of stress. Additionally, impaired PVN KCC2 function is associated with alteration of emotional behavior, disruption of body weight homeostasis, and a locomotor hyperactivity phenotype that seems to manifest specifically in novel contexts. Finally, a potential circuit-level explanation for the observed body weight homeostasis phenotype is provided by the novel finding of afferents from PVN CRH neurons to the tuberal nucleus, a sparsely-characterized region with functional relevance to stress effects on feeding. Though I have not yet experimentally assessed the effects of viral KCC2 knockout on GR signaling (namely, regional changes in the expression of GR-response element-containing genes), in Section 9 I will discuss possible CORT-mediated mechanisms for the effects we observed on stress-reactive physiology and behavior.

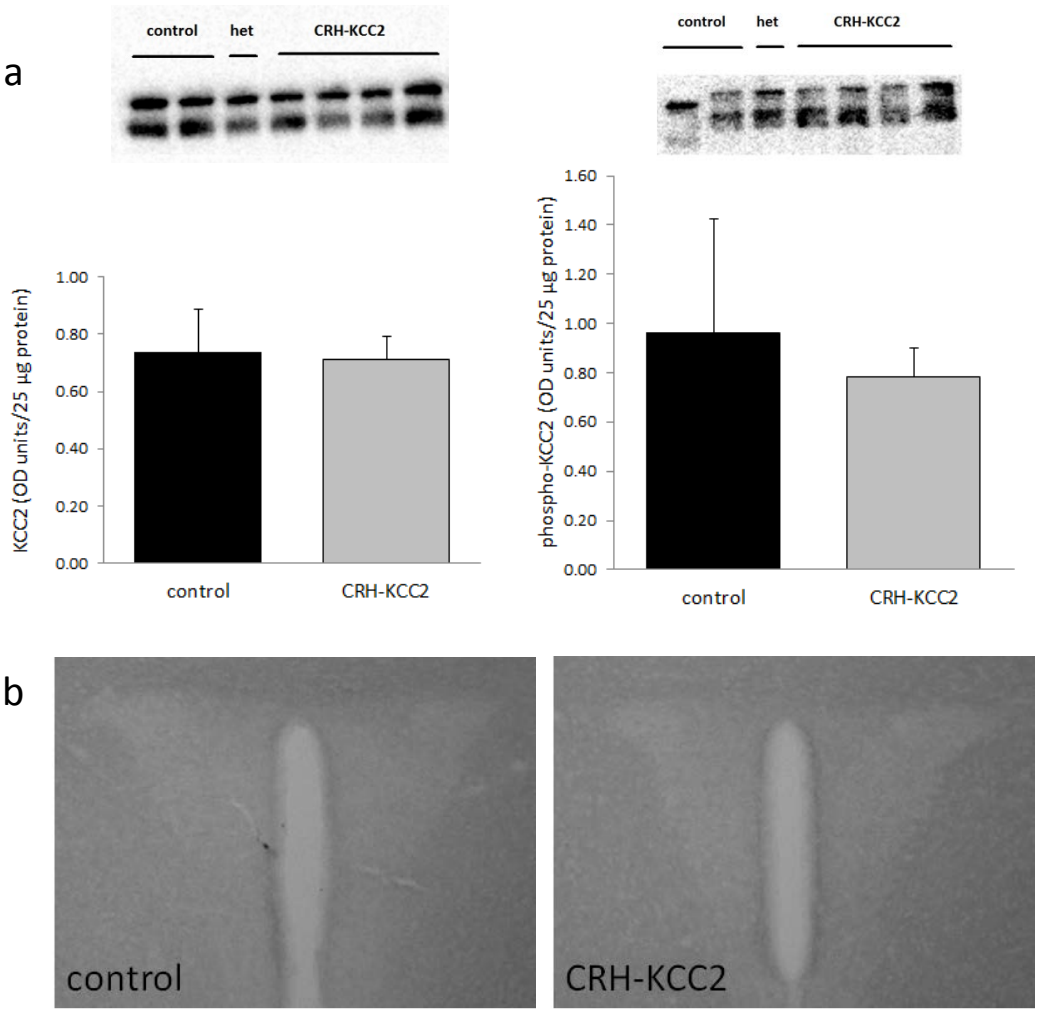

Figure 4.1. Transgenic KCC2 transporter domain knockout does not alter KCC2 expression or S940 phosphorylation in the PVN. (a) Representative Western blots of KCC2 (left) and S940 phospho-KCC2 (right). CRH-KCC2 mice demonstrated no differences in KCC2 or phosphor-KCC2 expression in the hypothalamus compared to Cre-negative controls (n=2-4 mice per genotype). (b) Representative images showing DAB staining of KCC2 in the PVN. CRH-KCC2 mice showed no difference in KCC2 immunoreactivity compared to Cre-negative controls (n=3-6 mice per genotype).

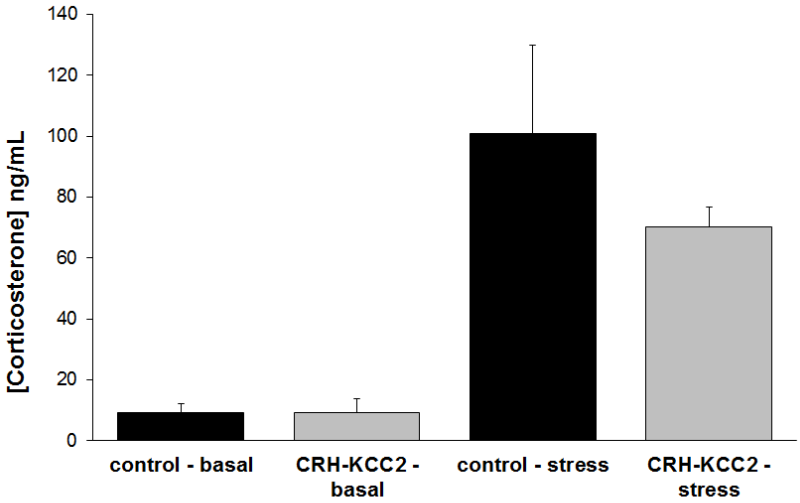

Figure 4.2. Transgenic KCC2 transporter domain knockout does not alter basal or stress levels of CORT. CORT ELISA results from serum collected from minimally-handled mice (basal), or collected 30 minutes after a 30-minute acute restraint stress (stress), revealed no significant differences between CRH-KCC2 mice and Cre-negative controls (n=2-6 mice per experimental group).

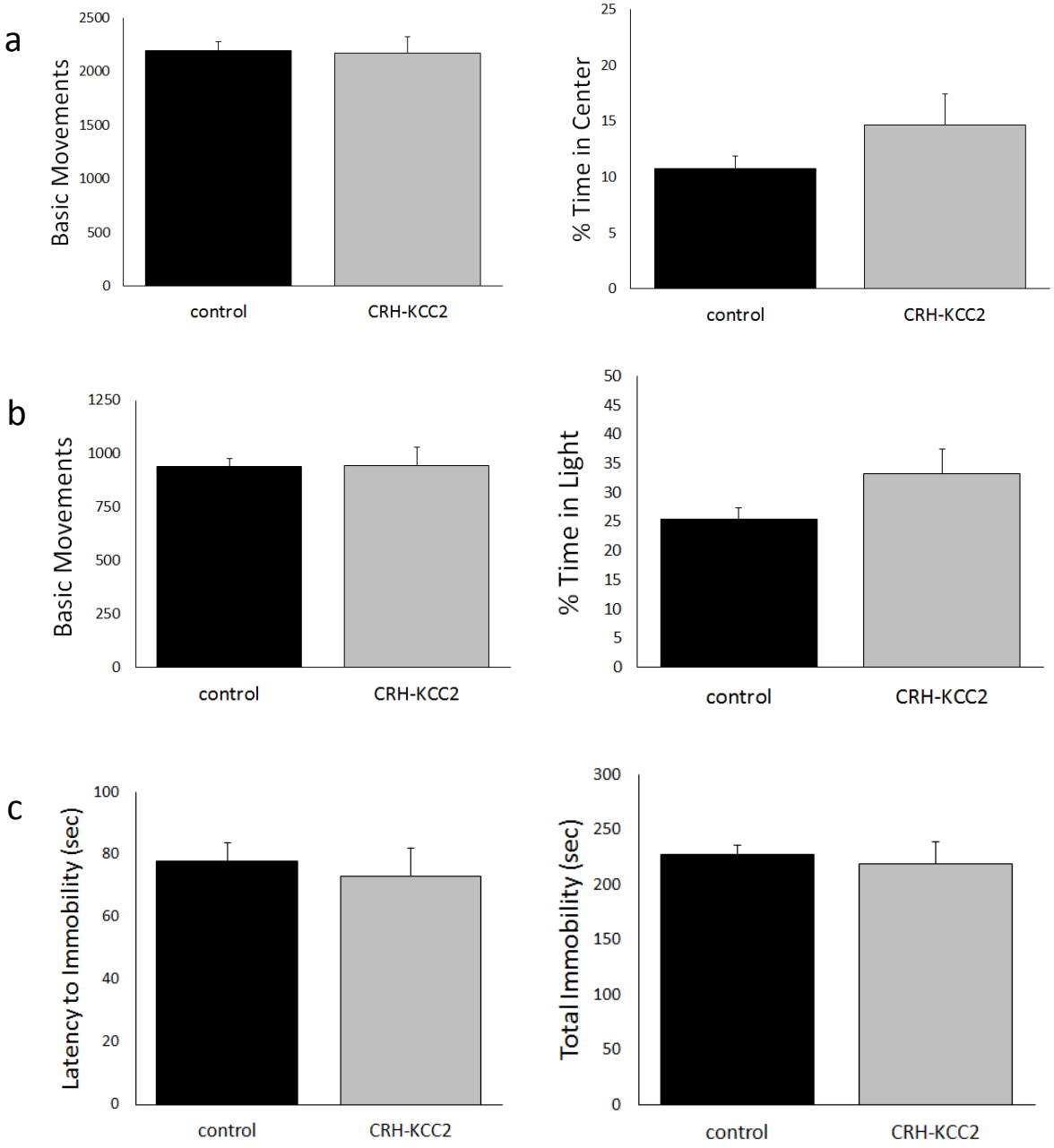

Figure 4.3. Transgenic KCC2 transporter domain knockout has no impact on emotional behavior. (a) Results from the open field paradigm reveal no difference in locomotor activity (left) or anxiety-like behavior (right; p=0.41) between CRH-KCC2 mice and Cre-negative controls (n=8-21 mice per genotype). (b) Results from the light-dark box paradigm reveal no difference in locomotor activity (left) or anxiety-like behavior (right; p=0.20) between CRH-KCC2 mice and Cre-negative controls (n=7-11 mice per genotype). (c) Results from the forced swim test reveal no difference in latency to immobility (left) or total immobility (right) between CRH-KCC2 mice and Cre-negative controls (n=8-21 mice per genotype).

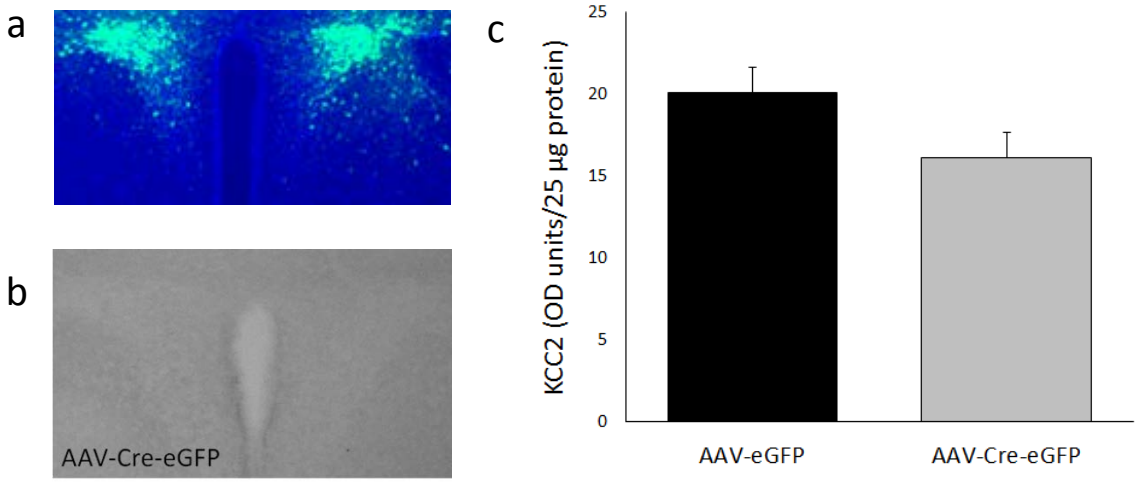

Figure 4.4. Viral KCC2 transporter domain excision reduces KCC2 expression in the PVN. (a) Representative image of bilateral AAV-Cre-GFP expression (green) in PVN of KCC2$^{f/f}$ mouse (blue=DAPI). (b) Representative image showing DAB immunostaining of KCC2 in the PVN of an AAV-Cre-GFP-injected KCC2$^{f/f}$ mouse. (c) Quantification of KCC2 immunoreactivity in PVN demonstrates a promising but preliminary trend toward reduced KCC2 expression in AAV-Cre mice compared to AAV-GFP controls (n=4-6 mice per experimental group) (p=0.13; power=0.42).

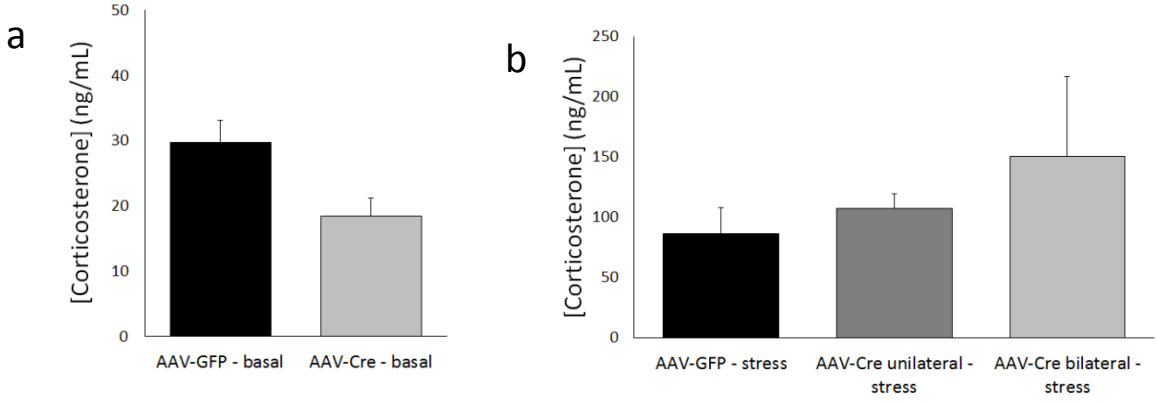

Figure 4.5. Viral KCC2 transporter domain excision enhances stress-induced CORT release. (a) CORT ELISA results from serum of minimally-handled (basal) mice revealed no significant difference between AAV-Cre KCC2$^{f/f}$ mice and AAV-GFP-injected control littermates (n=2 mice per experimental group) (p=0.12). (b) CORT ELISA results from serum of acute restraint stress-exposed mice reveals a non-significant trend toward increased stress CORT levels in AAV-Cre KCC2$^{f/f}$ mice compared to AAV-GFP-injected controls (n=4-15 mice per experimental group).

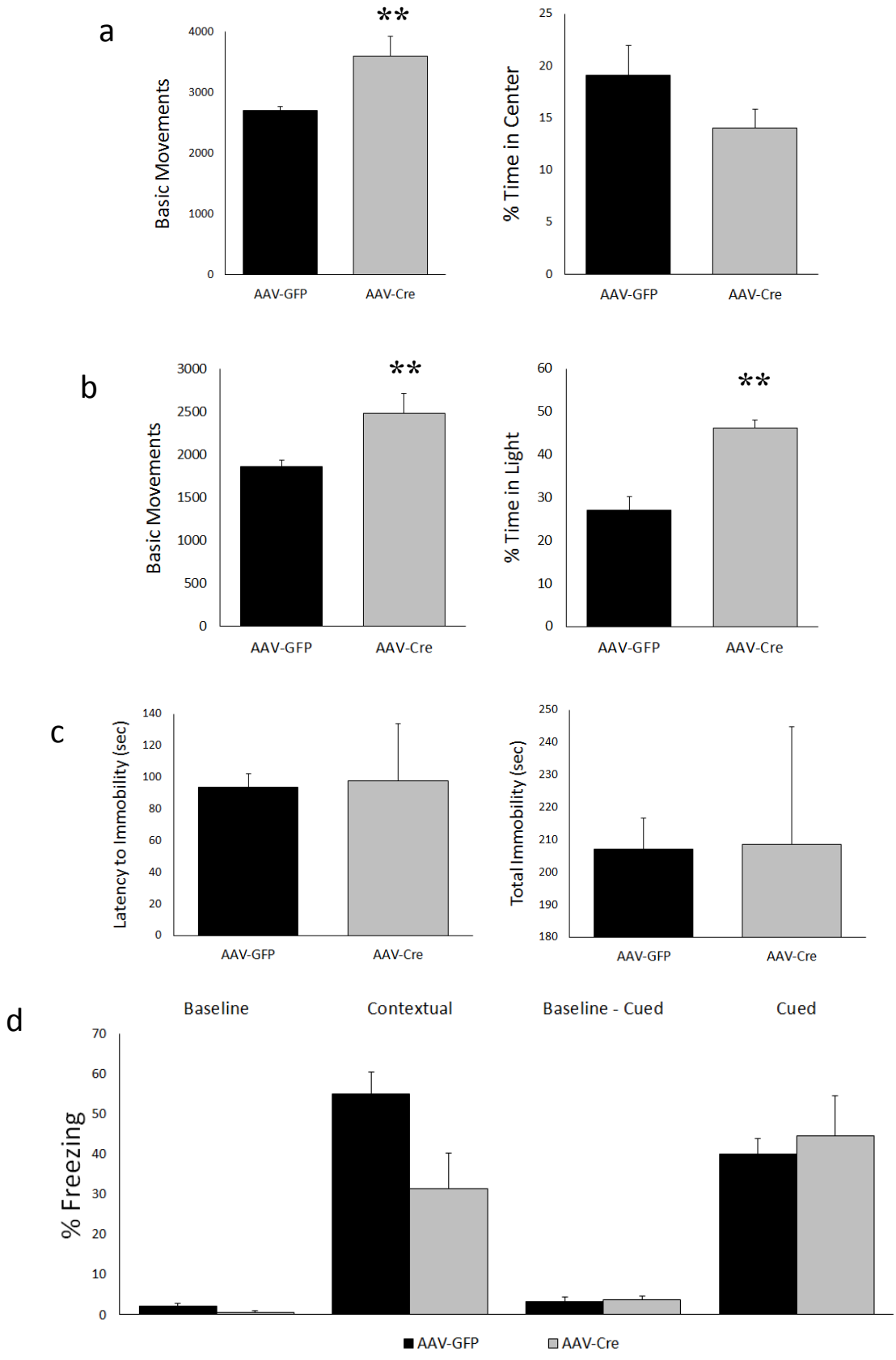
a
**
Basic Movements
4000
3000
2000
1000
0
AAV-GFP
AAV-Cre
% Time in Center
25
20
15
10
5
0
AAV-GFP
AAV-Cre
b
**
Basic Movements
3000
2500
2000
1500
1000
500
0
AAV-GFP
AAV-Cre
**
% Time in Light
60
50
40
30
20
10
0
AAV-GFP
AAV-Cre
c
Latency to Immobility (sec)
140
120
100
80
60
40
20
0
AAV-GFP
AAV-Cre
Total Immobility (sec)
250
240
230
220
210
200
190
180
AAV-GFP
AAV-Cre
d
Baseline
Contextual
Baseline - Cued
Cued
% Freezing
70
60
50
40
30
20
10
0
AAV-GFP
AAV-Cre

Figure 4.6. Viral KCC2 transporter domain knockout effects on locomotor activity, emotional behavior, and memory. (a) Open field paradigm results showed a significant increase in locomotor activity in AAV-Cre-injected $KCC2^{f/f}$ mice compared to AAV-GFP controls (n=3-10 mice per experimental group). (b) Light-dark box results reveal a similar increase in locomotor activity as well as a significant reduction in anxiety-like behavior among $KCC2^{f/f}$ mice that received AAV-Cre injections in the PVN, compared to AAV-GFP-injected controls (n=3-10 mice per experimental group). (c) Forced swim test results show no difference in depression-like behavior between AAV-Cre mice and AAV-GFP controls (n=3-9 mice per experimental group). (d) Fear conditioning results reveal no impact of PVN injection of AAV-Cre in cued memory retrieval, and a non-significant trend toward impaired contextual memory ($p=0.059$), compared to AAV-GFP-injected controls (n=3-10 mice per experimental group). ** denotes significance at $p<0.01$.

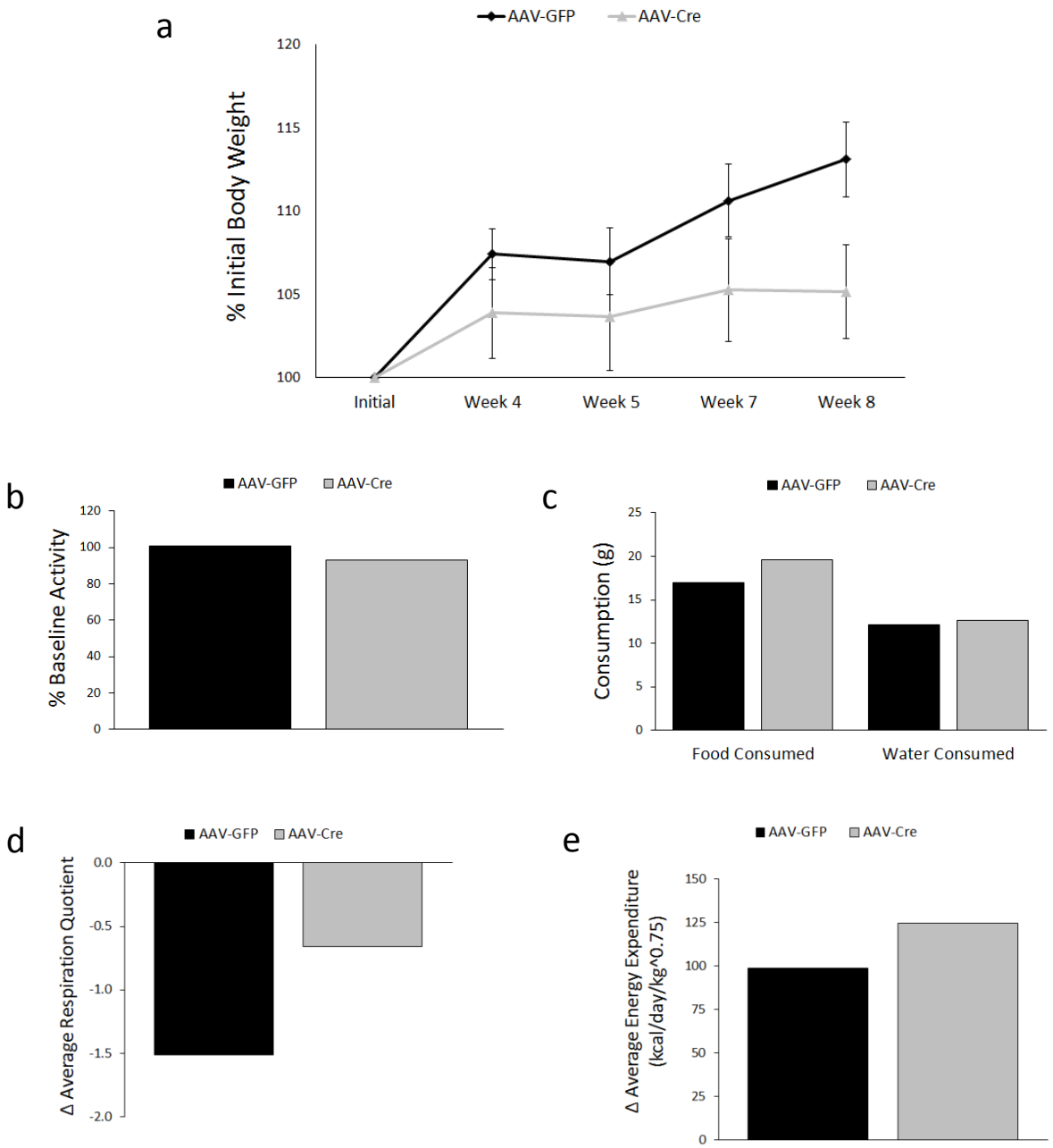
a
AAV-GFP
AAV-Cre
% Initial Body Weight
120
115
110
105
100
Initial
Week 4
Week 5
Week 7
Week 8
b
AAV-GFP
AAV-Cre
% Baseline Activity
120
100
80
60
40
20
0
c
AAV-GFP
AAV-Cre
Consumption (g)
25
20
15
10
5
0
Food Consumed
Water Consumed
d
AAV-GFP
AAV-Cre
Δ Average Respiration Quotient
0.0
-0.5
-1.0
-1.5
-2.0
e
AAV-GFP
AAV-Cre
Δ Average Energy Expenditure (kcal/day/kg^0.75)
150
125
100
75
50
25
0

Figure 4.7. Viral KCC2 transporter domain knockout in the PVN perturbs body weight homeostasis. (a) Results from weekly measurement of body weight beginning at virus injection surgery (Initial). AAV-Cre-injected $KCC2^{f/f}$ mice appeared to gain less weight than AAV-GFP-injected littermates though this difference was not statistically significant at any time point measured (n=6 mice per experimental group). (b) Ratio of post-surgery to pre-surgery locomotor activity, each measured across 3 days in indirect calorimetry chambers. AAV-Cre-injected $KCC2^{f/f}$ mice (n=2) exhibited slightly less activity than an AAV-GFP control mouse (n=1). (c) Summary of post-surgery food and water consumption across 3 days in indirect calorimetry chambers. AAV-Cre-injected mice consumed more food than the AAV-GFP control. (d) Difference between pre-surgery and post-surgery respiration quotient, each measured across 3 days in indirect calorimetry chambers. AAV-Cre-injected mice showed a higher respiration quotient than the AAV-GFP control. (e) Difference between pre-surgery and post-surgery respiration quotient, each measured across 3 days in indirect calorimetry chambers. AAV-Cre-injected mice showed an increase in energy expenditure compared to AAV-GFP control. Statistical analysis of indirect calorimetry results is not yet possible given the small sample sizes.

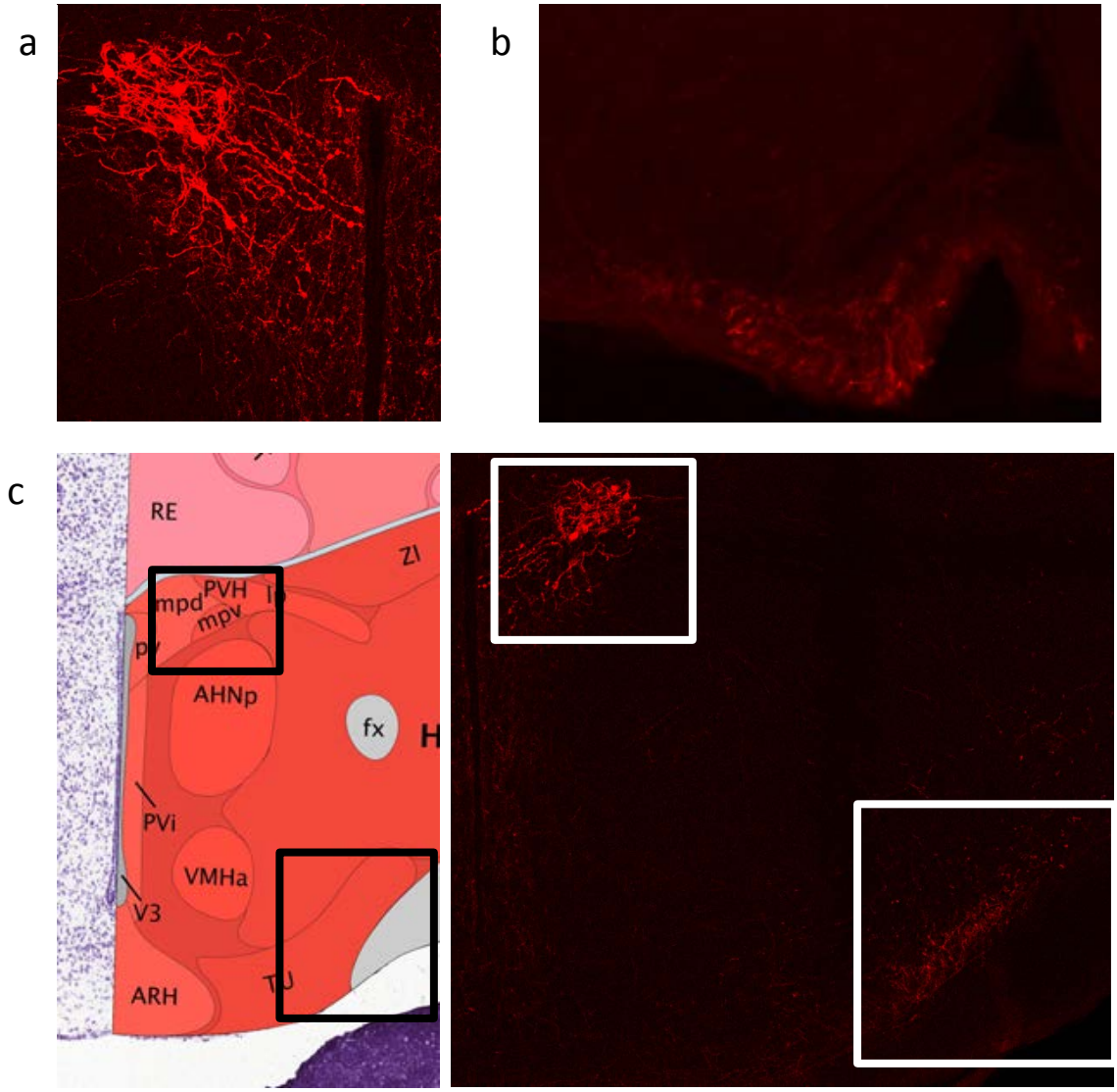

Figure 4.8. Novel projections from PVN CRH neurons to the tuberal nucleus of the lateral hypothalamus. (a) Representative image of anterograde tracer virus-transduced CRH neurons in the PVN of a CRH-Cre mouse. (b) Projections in the median eminence from the same mouse as (a), indicating well-established connection of CRH neurons and validating anterograde tracing approach. (c) Right, anterograde tracer virus expression in PVN CRH neuron somata gives rise to fibers in the tuberal nucleus of the lateral hypothalamus, indicating a novel projection target of PVN CRH neurons. Left, corresponding plate from Allen Mouse Brain Atlas for orientation.

5. Hippocampal dentate granule cells: Tonic inhibition mediates chronic stress effects on behavior

Chronic stress has long been known to adversely affect learning and memory. Little is known about the specific stress-induced changes in synaptic transmission that contribute to learning and memory deficits, but tonic GABAergic inhibition in the hippocampus has been implicated. Here we set out to test the hypothesis that alteration of tonic inhibition in the dentate gyrus of the hippocampus is an important mechanism by which chronic stress impacts learning and memory. This section contains data and figures from (Lee et al., 2016) on which I was a middle author.

Rationale

Previous studies have demonstrated widespread effects of chronic CORT elevation on dendrite morphology, neurogenesis, and inhibitory neurotransmission in the hippocampus (McEwen and Sapolsky, 1995). Additionally, long-term potentiation (LTP), the cellular correlate of learning and memory, is deficient in animal models of chronic stress (Howland and Wang, 2008). We have recently shown that GABAergic signaling in the hippocampus is compromised following stress (Mody and Maguire, 2011), and modulation of tonic inhibition has been shown to impact learning and memory (Cushman et al., 2014;Whissell et al., 2013). However, it is unknown whether the effects of stress on learning and memory are mediated by changes in hippocampal tonic inhibition. In this study, we investigated alteration of tonic GABAergic inhibition in the dentate gyrus of the hippocampus as a potential cellular mechanism of chronic stress-associated deficits in learning and memory.

Does chronic stress produce elevations in CORT and impairment of learning and memory?

In order to validate our model of chronic stress, we assessed stress hormone levels and cognition in mice following 14 consecutive days of daily restraint stress (30 min). As expected, chronic stress caused an increase in serum CORT (97.78±26.46 ng/mL) compared to unstressed controls (20.23±3.01 ng/mL) (n=4-5 mice per experimental group; $p<0.05$ using a Student's unpaired *t*-test). In classical fear conditioning experiments, mice subjected to chronic stress showed an impairment in both contextual (21.52±4.20% freezing) and cued (11.81±2.22% freezing) fear memory retrieval compared to unstressed controls (contextual: 50.61±4.48% freezing; cued: 29.45±2.22% freezing) (n=12-22 mice per experimental group) (Figure 5.1c, d). Thus, our restraint model of chronic stress was able to mobilize the HPA axis and produce learning and memory deficits.

How does chronic stress affect tonic and phasic GABAergic currents on dentate gyrus granule cells?

The dentate gyrus is the point of entry for most neocortical input into the hippocampus and plays a vital pattern separation role in learning and memory. Therefore, we hypothesized that chronic stress might impair this node of the hippocampal network through alterations of its inhibitory afferent inputs. Electrophysiological recordings were performed on dentate gyrus granule cells (DGGCs), and their spontaneous postsynaptic responses were recorded (Figure 5.2a). Chronic stress produced no difference in the frequency (2.70±0.21 Hz) or decay kinetics (4.61±0.31 msec) of DGGCs' spontaneous inhibitory postsynaptic currents (IPSCs) compared to unstressed controls (frequency: 3.03±0.39 Hz; decay: 4.86±0.26 msec) (Figure 5.2b, c). However, chronic stress did lead to an increase in sIPSC amplitude (34.23±2.63 pA) over that of controls (27.32±1.98 pA) (n=18-27 cells, 10-11 mice per experimental group) (Figure 5.2c). Chronic stress also gave rise to a reduction in the Gabazine- and picrotoxin-sensitive tonic

inhibitory current (Gabazine: 7.06±0.94 pA; picrotoxin: 4.88±1.33 pA) compared to unstressed controls (Gabazine: 12.70±1.97 pA; picrotoxin: 13.04±2.08 pA) (n=13-27 cells, 7-11 mice per experimental group) (Figure 5.2d-f). These data implicate alterations in both phasic and tonic GABAergic signaling on DGGCs as potential mechanisms of chronic stress effects on learning and memory.

How does chronic stress impact $GABA_A$R subunit expression in the hippocampus?

Phasic GABAergic currents are primarily carried by γ2 subunit-containing $GABA_A$ receptors at the synapse, whereas tonic currents are primarily carried by δ subunit-containing, extrasynaptic receptors. We therefore investigated whether alterations in subunit expression could provide a biochemical explanation for the observed changes in DGGC phasic and tonic GABAergic currents. Following chronic stress, total protein was isolated from the hippocampus and probed with $GABA_A$R subunit antibodies via Western blot. Chronic stress gave rise to an increase in γ2 subunit expression (69.79±17.08 OD units/25 μg total protein) and a decrease in δ subunit expression (9.48±3.41 OD units/25 μg total protein) compared to unstressed controls (γ2: 39.18±4.53 OD units/25 μg total protein; δ: 39.18±4.53 OD units/25 μg total protein) (n=8-19 mice per experimental group) (Figure 5.3). Together these data demonstrate that chronic stress alters the expression of $GABA_A$R subunits in the dentate gyrus, corresponding with its effects on phasic and tonic GABAergic currents described above.

Does chronic stress impact GABAergic efficacy in dentate gyrus granule cells?

Previous work from our laboratory has shown that stress causes a depolarizing shift in the reversal potential for chloride (E_{GABA}) in CA1 pyramidal neurons via downregulation of KCC2 expression (Mackenzie and Maguire, 2014). Thus we hypothesized that chronic stress may cause

similar alterations in inhibitory efficacy in the dentate gyrus, which we assessed using gramicidin perforated patch recordings of DGGCs following chronic stress. No alterations of E_{GABA} were observed in DGGCs following chronic stress (-72.79±1.63 mV) compared to unstressed controls (-75.36±2.21 mV) (n=8-9 cells, 6-9 mice per experimental group) (Figure 5.4c). This indicates that, in contrast to area CA1, principal cells in the dentate gyrus do not undergo erosion of inhibition following chronic stress.

Does selective knockout of the $GABA_AR$ δ subunit from the dentate gyrus replicate the effect of chronic stress on learning and memory?

Our electrophysiological and biochemical evidence suggested that reduction of tonic inhibition underlies chronic stress-induced deficits in learning and memory. Therefore, we next asked whether selectively manipulating tonic GABA in the dentate gyrus could replicate the effects of chronic stress. In order to selectively knock the $GABA_AR$ δ subunit out of DGGCs, we crossed a Cre recombinase-dependent δ knockout mouse line (Gabrd) with a Pomc-Cre line for cell specificity (Figure 5.5c) to produce Pomc/Gabrd mice. To assess the validity of this transgenic approach, Western blot analysis was performed and we found that δ subunit expression was dramatically reduced in the hippocampus of Pomc/Gabrd mice (9.93±3.26 OD units/25 μg protein) compared to Cre-negative littermates (44.08±2.93 OD units/25 μg protein) (n=6 mice per experimental group) (Figure 5.5e, f). The reduction of δ subunit expression was less obvious, but still significant, when assessed by immunohistochemistry (Pomc/Gabrd: 49.98±1.91 OD; Cre-negative: 55.24±1.68 OD) (n=3 mice per experimental group) (Figure 5.5a, b, d). We also assessed functional expression of extrasynaptic $GABA_ARs$ by patch clamp electrophysiology, and found that the Gabzine-sensitive tonic current was decreased in Pomc/Gabrd DGGCs (3.28±1.01 pA) compared to Cre-negative control DGGCs (13.92±1.75 pA) (n=12-25 cells, 3-8

mice per experimental group) (Figure 5.6d, e). Assessment of phasic inhibition, on the other hand, revealed no compensatory change in either the frequency (Pomc/Gabrd: 4.03±0.27 Hz; Cre-negative: 3.80±0.40 Hz) or amplitude (Pomc/Gabrd: 36.50±3.26 pA; Cre-negative: 38.93±2.30 pA) of sIPSCs (n=12-13 cells, 3-8 mice per experimental group) (Figure 5.6a-c). These biochemical and electrophysiological data convincingly demonstrate that our transgenic approach to selective reduction of tonic inhibition in DGGCs is effective.

Finally we performed behavioral experiments using Pomc/Gabrd mice to assess the effect of selectively reducing tonic inhibition on learning and memory. Other members of the laboratory performed fear conditioning and found that Pomc/Gabrd mice displayed impaired contextual (47.06±5.90% freezing) and cued (34.53±5.14% freezing) fear memory retrieval compared to Cre-negative controls (contextual: 61.86±3.23% freezing; cued: 53.95±4.93% freezing) (n=19-20 mice per experimental group) (Figure 5.7c, d), reminiscent of the memory impairment brought on by chronic stress. In order to verify that this deficit was specific to learning and memory and not the result of general abnormalities in behavior brought on by the manipulation of δ subunit expression, we also assessed locomotor, anxiety-like, and depression-like behavior. In the open field test, Pomc/Gabrd mice did not demonstrate significant alterations in either locomotor activity (2231.26±132.24 beam breaks) or anxiety-like behavior (111.84±10.12 sec in center) compared to Cre-negative controls (1972.55±154.16 beam breaks; 109.50±14.92 sec in center) (n=19-20 mice per experimental group) (Figure 5.8b). Similarly, the light-dark box revealed no changes in locomotor activity (Pomc/Gabrd: 1101.64±65.58 beam breaks; Cre-negative: 964.11±39.49 beam breaks) or anxiety-like behavior (Pomc/Gabrd: 199.22±18.92 sec in light; Cre-negative: 172.56±21.11 sec in light) (n=19-20 mice per experimental group) (Figure 5.8d). Depression-like behavior as measured by immobility in the

forced swim and tail suspension tests was also unchanged in Pomc/Gabrd mice (forced swim: 19.78±2.81% time immobile; tail suspension: 35.09±3.22% time immobile) compared to Cre-negative controls (forced swim: 20.78±4.68% time immobile; tail suspension: 39.58±2.65% time immobile) (n=19-20 mice per experimental group) (Figure 5.9b, d). Together, our behavioral data implicate modulation of tonic GABA in the dentate gyrus as a key mediator of chronic stress effects specifically on learning and memory.

Significance

It is well-established that chronic elevation of CORT gives rise to structural and functional changes throughout the hippocampus, as well as deficits in learning and memory. However, the specific cellular mechanisms underlying stress-induced changes in synaptic physiology remain sparsely characterized. In this study, we identified one such mechanism: alterations in tonic GABAergic inhibitory constraint of DGGCs. The importance of this mechanism is underscored by the observation that selectively reducing tonic GABA in the dentate gyrus is, by itself, sufficient to reproduce the chronic stress phenotype of learning and memory impairment. Although POMC is also expressed in the arcuate nucleus of the hypothalamus (McHugh et al., 2007), the δ subunit of the $GABA_AR$ is not (Pirker et al., 2000), so the observed behavioral effects of our manipulation most likely arise specifically from the dentate gyrus. Additionally, although cued fear conditioning memory is generally considered hippocampal-independent, and certainly does depend on intact amygdala function, limbic cortical regions are also involved in cued retrieval (Burgos-Robles et al., 2009;Arruda-Carvalho and Clem, 2014;Bergstrom, 2016). The extensive connections directly coupling the hippocampus to both the amygdala and limbic cortex may therefore account for the observed influence of hippocampal tonic GABA on cued fear memory (Thierry et al., 2000;Vertes, 2006;Cenquizca and Swanson, 2007). Thus, our

findings highlight the importance of hippocampal tonic GABA in learning and memory generally, and in pathological effects of stress in particular.

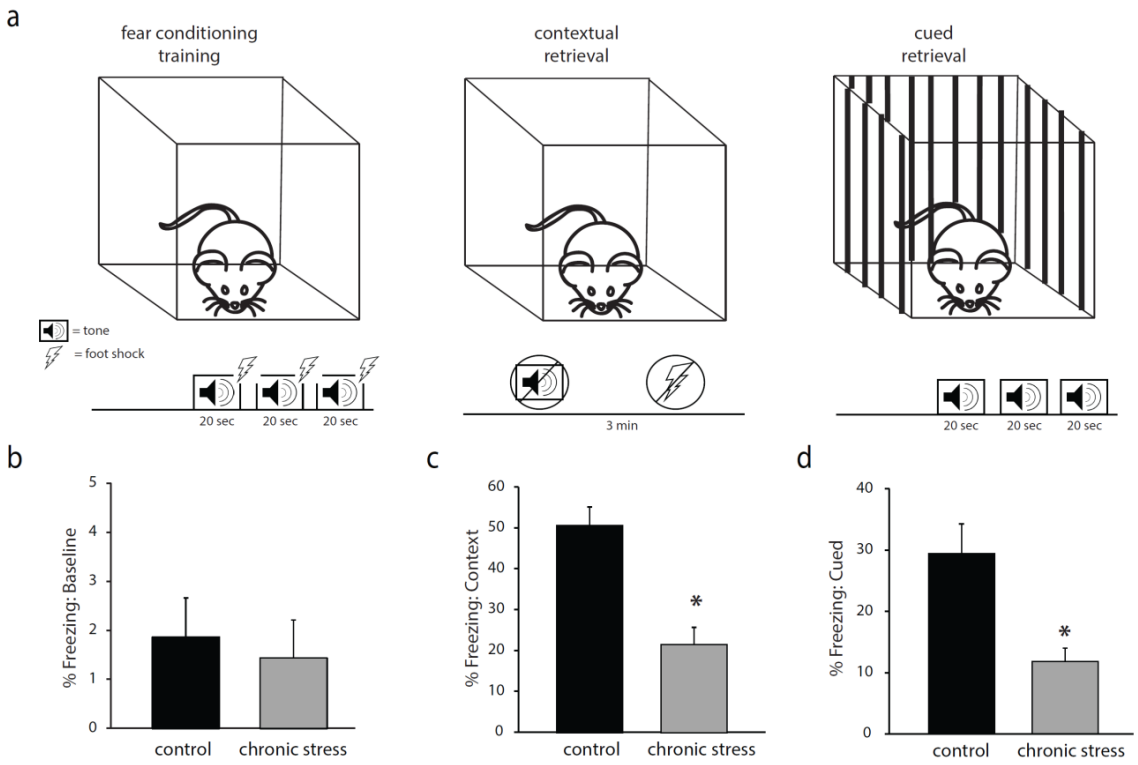

Reproduced from (Lee et al., 2016)

Figure 5.1. Chronic restraint stress impairs learning and memory. (a) A diagram of the experimental design of the fear conditioning paradigm. Minimally handled controls or mice subjected to chronic stress underwent fear conditioning training in which they were exposed to three separate 20 s tones paired with a foot shock. Twenty-four hours later, the percent time freezing as a measure of fear learning was measured in the context in which the foot shocks occurred or in response to the tone cue presented in a novel environment. (b) There was no baseline difference in freezing behavior pre-tone during the training session. However, mice subjected to chronic stress exhibit impairments in both contextual and cued memory, evident by a decrease in the percent time freezing in the same context in which the foot shock occurred (c) or in response to the auditory cue (d) n=12–22 mice per experimental group. * denotes significance of $p<0.01$ using a Student's *t*-test.

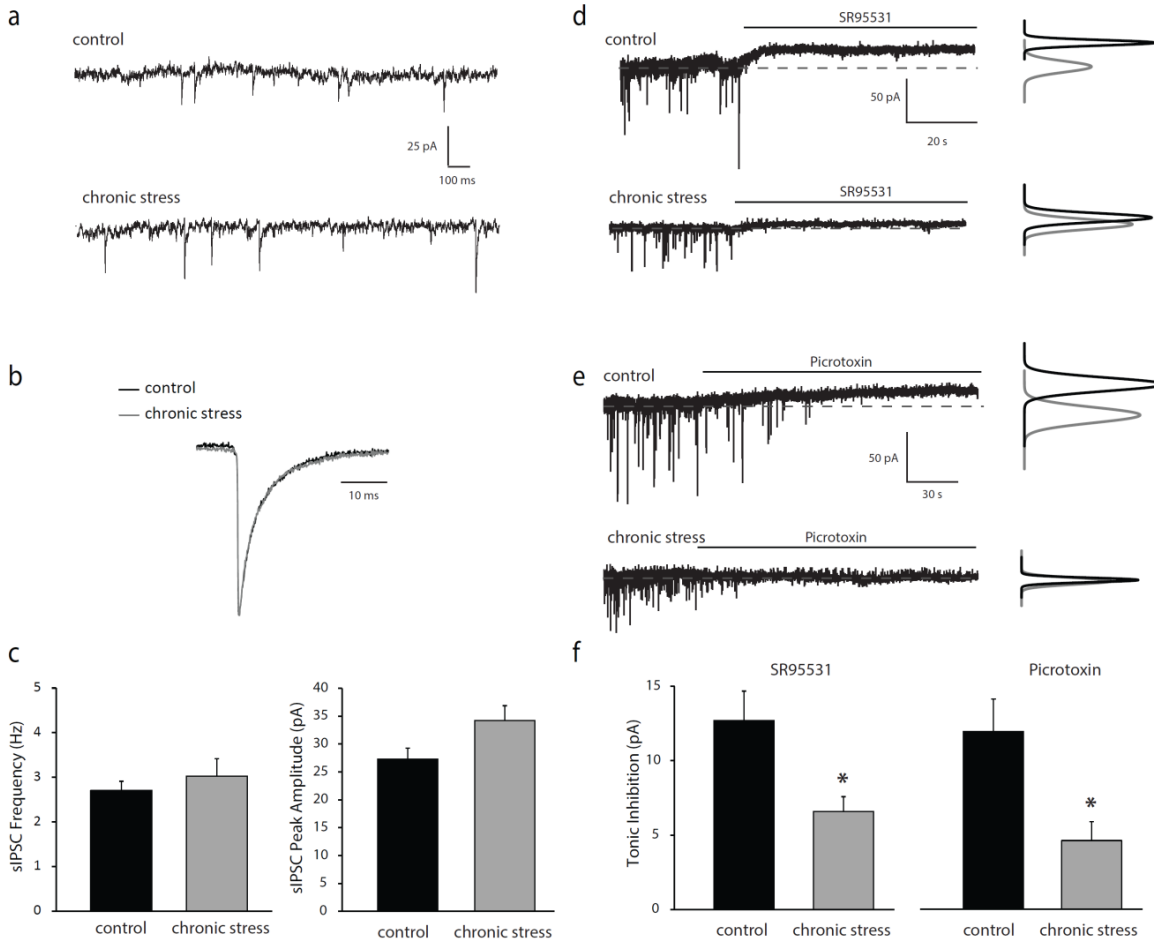

Reproduced from (Lee et al., 2016)

Figure 5.2. Alterations in GABAergic inhibition in dentate gyrus granule cells following chronic stress. (a) Representative traces of sIPSCs in dentate gyrus granule cells from minimally handled controls or mice subjected to chronic restraint stress. (b) Superimposed traces of average sIPSCs normalized to the peak amplitude from control and chronic stress mice showing no change in the decay time constant. (c) There is no difference in the frequency of sIPSCs between controls and mice subjected to chronic stress. The average peak amplitude of sIPSCs recorded in dentate gyrus granule cells is increased in chronic stress mice compared to controls. (d–e) Representative traces of tonic currents in dentate gyrus granule cells from minimally handled controls or mice subjected to chronic restraint stress recorded by blocking $GABA_A$Rs with either SR95531 (d) or picrotoxin (e). (f) Tonic inhibition measured using either SR95531 or picrotoxin is decreased in dentate gyrus granule cells in slices from mice subjected to chronic stress compared to minimally handled controls. n=13–27 cells, 7–11 mice per experimental group. * denotes significance of $p<0.05$ using a Student's *t*-test.

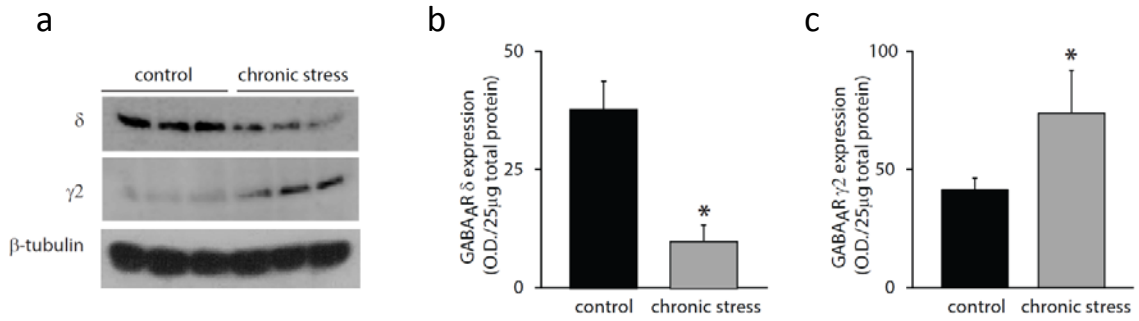

Reproduced from (Lee et al., 2016)

Figure 5.3. Chronic stress-induced decrease in the expression of the $GABA_AR$ δ subunit in the dentate gyrus. (a) Representative Western blots of $GABA_AR$ δ and γ2 subunit expression in minimally handled controls and mice subjected to chronic restraint stress. (b) The average optical density of $GABA_AR$ δ subunit expression is decreased in mice subjected to chronic stress compared to controls. n=8 mice per experimental group; $P < 0.01$ using a Student's unpaired *t*-test. (c) The average optical density of $GABA_AR$ γ2 subunit expression is increased in mice subjected to chronic stress compared to controls. n=11–19 mice per experimental group; * denotes significance of $p<0.05$ using an unpaired Student's *t*-test.

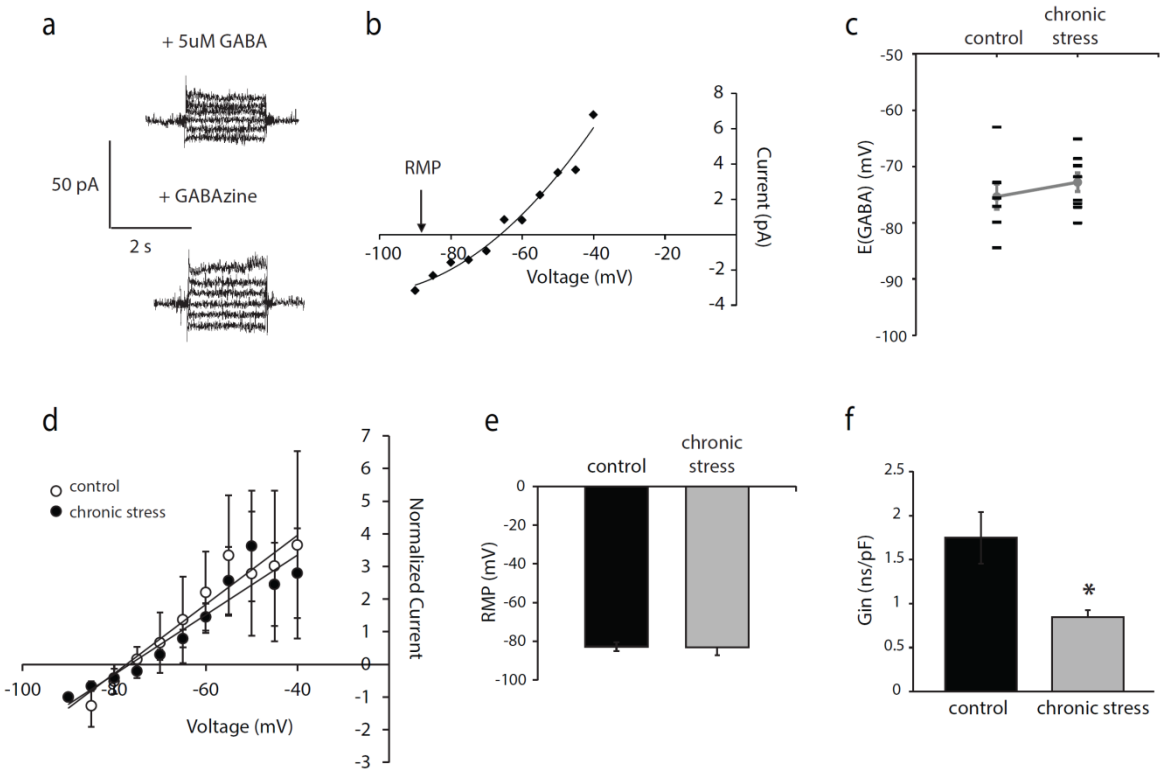

Reproduced from (Lee et al., 2016)

Figure 5.4. No shift in EGABA in dentate gyrus granule cells following chronic stress. (a) Representative current traces at different voltages in the presence of 5 mM GABA, with or without SR95531. The voltage–current relationships generated were subtracted and plotted to measure EGABA. A representative example is shown (b). No difference in the average EGABA values (c,d) or resting membrane potential (e) were observed in dentate gyrus granule cells from minimally-handled controls or mice subjected to chronic restraint stress. (d) Normalized, averaged voltage–current relationships in dentate gyrus granule cells from control and chronic stress mice demonstrate equivalent E_{GABA} values. n=8–9 cells, 6–9 mice per experimental group; * denotes significance of $p<0.05$ using a Student's *t*-test.

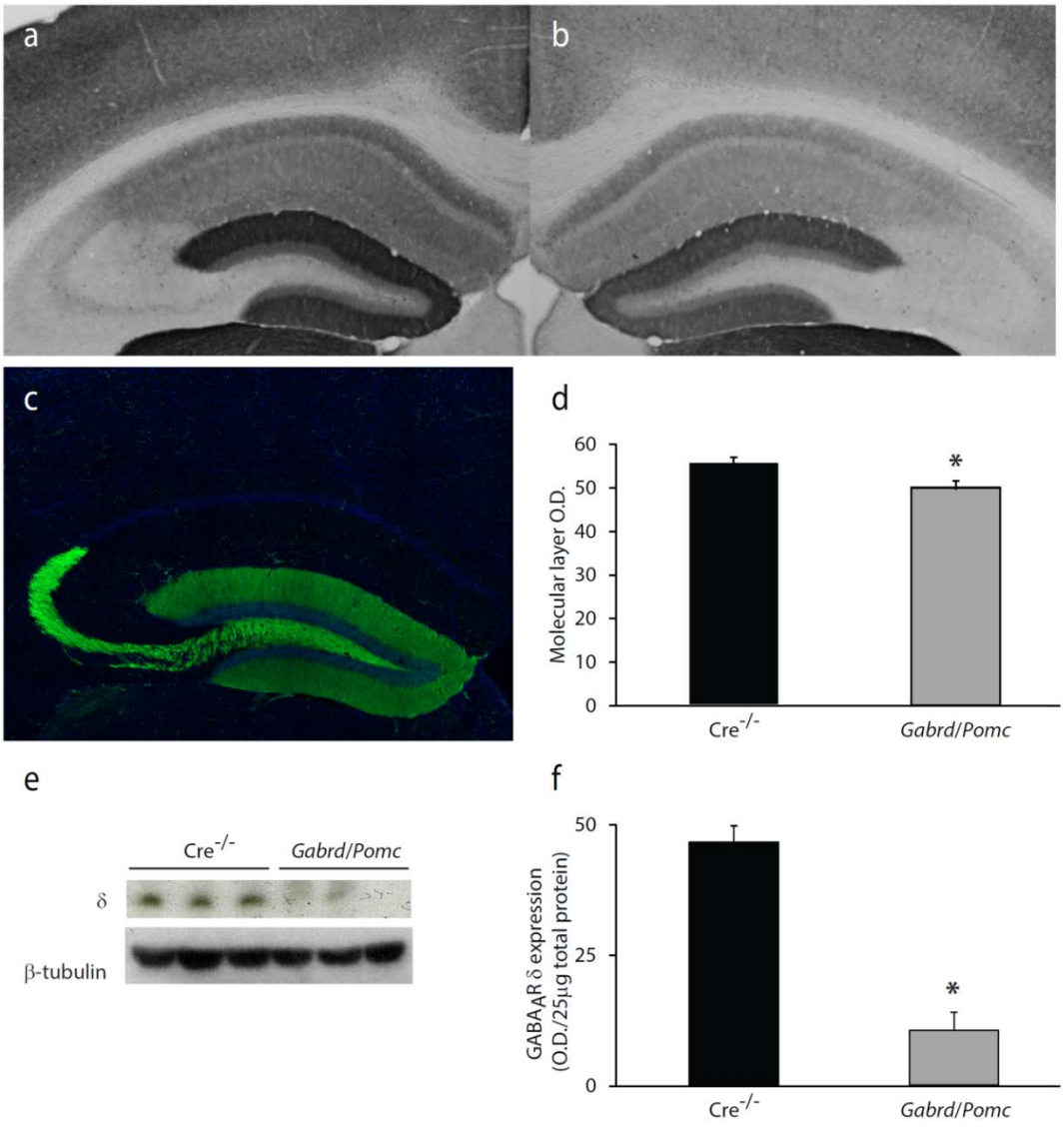

Reproduced from (Lee et al., 2016)

Figure 5.5. Reduced expression of the $GABA_AR$ δ subunit in the dentate gyrus of Gabrd/Pomc mice. Representative images of immunoreactivity for the $GABA_AR$ d subunit in Cre-/- littermates (a) and Gabrd/Pomc mice (b). (c) Representative image of GFP reporter expression in Pomc-GFP mice, demonstrating the specificity of Cre expression in dentate gyrus granule cells. (d) The average optical density of $GABA_AR$ δ subunit immunoreactivity is decreased in Gabrd/Pomc mice compared to Cre-/- littermates. n=3 mice per experimental group. (e) Representative Western blot of $GABA_AR$ δ subunit expression in Gabrd/Pomc mice and Cre-/- littermates. (f) The average optical density of $GABA_AR$ δ subunit expression, quantified using Western blot analysis, is decreased in Gabrd/Pomc mice Gabrd/Pomc mice compared to Cre-/- littermates. n=6 mice per experimental group; * denotes significance of $p<0.05$ using a Student's *t*-test.

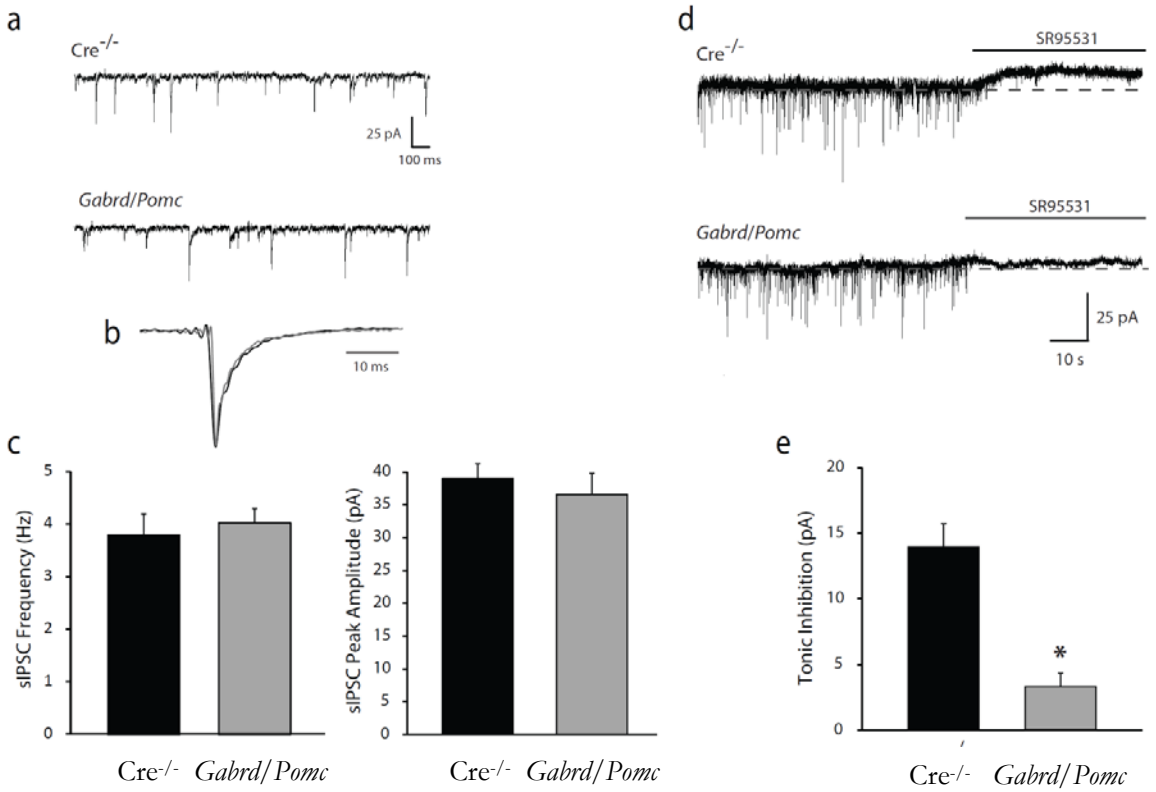

Reproduced from (Lee et al., 2016)

Figure 5.6. Decreased tonic inhibition of dentate gyrus granule cells in Gabrd/Pomc mice. (a) Representative traces of sIPSCs in dentate gyrus granule cells from Gabrd/Pomc mice and Cre-/- littermates. (b) Superimposed traces of average sIPSCs normalized to the peak amplitude from Gabrd/Pomc mice and Cre-/- littermates showing no change in the decay time constant. (c) There is no difference in the frequency or peak amplitude of sIPSCs between in Gabrd/Pomc mice or Cre-/- littermates. (d) Representative traces of tonic currents in dentate gyrus granule cells from Gabrd/Pomc mice and Cre-/- littermates. (e) The average tonic current is decreased in dentate gyrus granule cells from Gabrd/ Pomc mice compared to Cre-/- littermates. n=12–25 slices, 3–8 mice per experimental group. * denotes significance of $p<0.05$ using a Student's *t*-test.

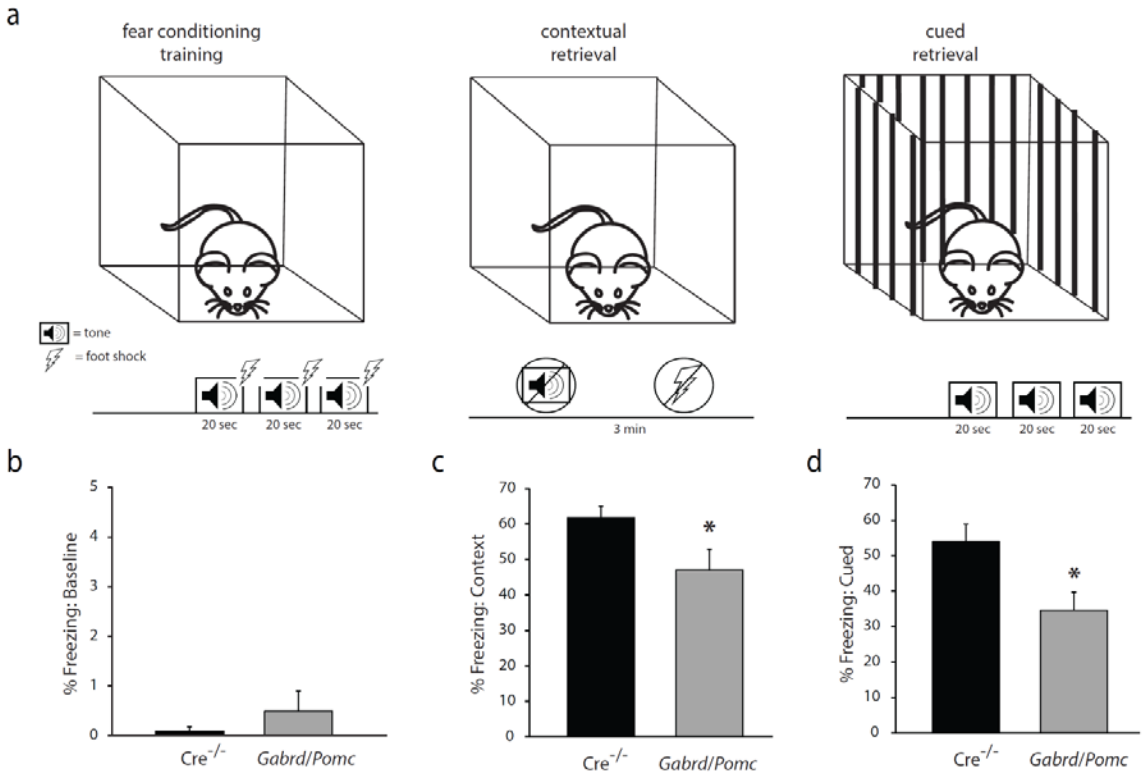

Reproduced from (Lee et al., 2016)

Figure 5.7. Impairments in learning and memory in Gabrd/Pomc mice. (a) A diagram of the experimental design of the fear conditioning paradigm. Minimally handled controls or mice subjected to chronic stress underwent fear conditioning training in which they were exposed to three separate 20 s tones paired with a foot shock. Twenty-four hours later, the percent time freezing as a measure of fear learning was measured in the context in which the foot shocks occurred or in response to the tone cue presented in a novel environment. (b) There was no baseline difference in freezing behavior pre-tone during the training session. However, Gabrd/Pomc mice exhibit impairments in both contextual and cued memory, evident by a decrease in the percent time freezing in the same context in which the foot shock occurred (c) or in response to the auditory cue (d). n=19–20 mice per experimental group. * denotes significance of $p<0.05$ using a Student's *t*-test.

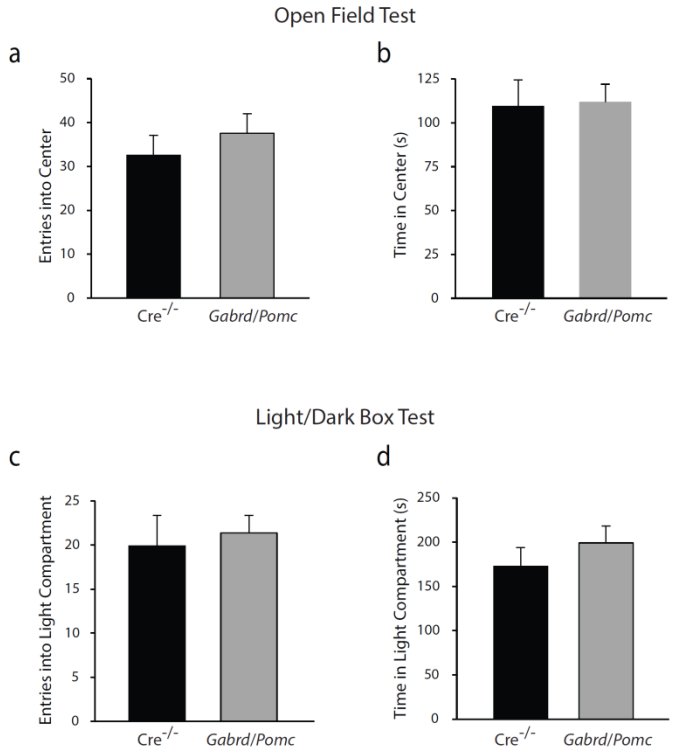

Reproduced from (Lee et al., 2016)

Figure 5.8. No difference in anxiety-like behaviors in Gabrd/Pomc mice. There is no difference in the number of entries (a) or the amount of time spent (b) in the center of open field in Gabrd/Pomc mice compared to Cre-/- littermates. Similarly, there is no difference in the number of entries (c) or the amount of time (d) that Gabrd/Pomc mice spend in the light compartment of thelight/dark box compared to Cre-/- littermates. n=19–20 mice per experimental group. * denotes significance of $p<0.05$ using a Student's *t*-test.

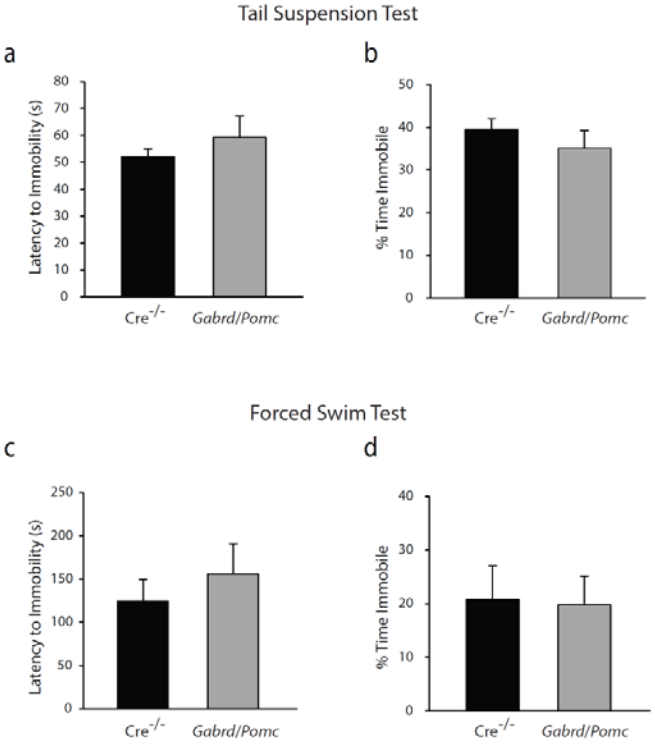

Reproduced from (Lee et al., 2016)

Figure 5.9. No difference in depression-like behaviors in Gabrd/Pomc mice. There is no difference in the latency (a) or total time spent immobile (b) during the tail suspension test between Gabrd/Pomc mice and Cre-/- littermates. Similarly, Gabrd/Pomc mice and Cre-/- littermates exhibit an equivalent latency to immobility (c) and total time spent immobile (d) in the forced swim test. N=19–20 mice per experimental group. * denotes significance of $p<0.05$ using a Student's *t*-test.

6. Somatostatin interneurons: Functional relevance to anxiolytic and antidepressant states

Major depressive disorder (MDD) is associated with deficits in neocortical and hippocampal GABAergic signaling (Ren et al., 2015;Pytka et al., 2016), particularly among somatostatin (SST) interneurons (Lin and Sibille, 2013) . Accordingly, antidepressant medications are thought to act in part by restoring GABAergic signaling (Luscher and Fuchs, 2015). However, it is not yet understood how specific interneuron types mediate the beneficial effects of antidepressant therapy. Using a transgenic approach, we selectively and persistently increased the activity of SST interneurons in order to assess this population's role in behaviors associated with depression. This section contains data and figures from (Fuchs et al., 2016) which has been accepted for publication as of the date of this writing, and on which I was a middle author. This study was conducted in collaboration with Dr. Bernhard Luscher's laboratory at Pennsylvania State University.

Rationale

The depressive brain state is complex, yet recent evidence suggests that downregulation of $GABA_A$Rs and altered inhibition throughout the cortex may be an important and straightforward common pathogenic mechanism. We have recently demonstrated that stress, a key precipitating factor in major depressive disorder, can alter inhibitory neurotransmission in multiple brain regions (Sarkar et al., 2011;Lee et al., 2014), while other groups have shown that SST interneurons in particular are vulnerable to the adverse effects of stress and may be critically involved in the pathophysiology of mood disorders (Czeh et al., 2015;Lin and Sibille, 2013). Normalization of GABAergic signaling is thought to be one important mechanism of effective

antidepressants, but the specific cellular mechanisms linking antidepressants' effects on inhibitory drive to their effects on behavior have yet to be delineated (Vollenweider et al., 2011;Earnheart et al., 2007). In this study we set out to test the hypothesis that enhancing inhibitory neurotransmission from SST interneurons can reproduce the behavioral effects of antidepressants, and to compare the cellular mechanism of this manipulation with that of the novel rapidly-acting antidepressant ketamine.

Does conditional knockout of the $GABA_AR$ γ2 subunit give rise to fewer inhibitory synapses and reduced inhibitory currents on SST neurons?

In order to selectively, persistently enhance SST interneuron activity, we generated a conditional knockout mouse line in which the $GABA_AR$ γ2 subunit was knocked out from SST neurons throughout the brain (SST-Cre:$\gamma2^{f/f}$:LSL-YFP) (Figure 6.1b). We anticipated that this would result in a reduction of phasic inhibitory input to SST interneurons, increasing their spontaneous activity (Figure 6.1a). Other members of the collaboration validated the mouse line first by staining brain sections for the γ2 subunit and gephyrin, then counting puncta on YFP-labeled hippocampal SST interneurons (Figure 6.1c). We found that γ2 puncta were greatly reduced in both stratum pyramidale and stratum radiatum of conditional knockout animals compared to $\gamma2^{f/+}$ controls (Figure 6.1d, e) (n=30-40 cells, 2 mice per genotype). Similarly, knockout animals exhibited far fewer gephryin puncta in stratum pyramidale and stratum radiatum compared to $\gamma2^{f/+}$ controls (Figure 6.1d, e).

Functional validation of the conditional knockout was conducted by performing electrophysiological recordings from SST interneurons to assess inhibitory postsynaptic currents (IPSCs) and excitability. In agreement with the histological results, we found that both the

frequency and amplitude of spontaneous IPSCs (sIPSCs) were significantly reduced in SST interneurons in area CA1 of the hippocampus (Figure 6.2a) and layer 2/3 of the cingulate cortex (Figure 6.2d) compared to controls (n=6-8 cells, 3 mice per experimental group). Miniature IPSCs (mIPSCs), recorded in the presence of the sodium channel blocker tetrodotoxin to block action potentials, were similarly reduced in knockout SST interneurons of both regions in frequency and amplitude (Figure 6.2b, e). At the same time, the conditional knockout had no effect on spontaneous excitatory postsynaptic currents (sEPSCs) in either brain region (Figure 6.2c, f). Finally, while there was no alteration in the resting membrane potential of knockout SST interneurons compared to controls (Figure 6.2j, n), their input resistance (Figure 6.2i, m) and firing rate (Figure 6.2h, l) were significantly increased in the knockout compared to controls, consistent with the expected effects of reducing inhibitory constraint on SST interneurons (n=9-10 cells, 3 mice per experimental group). Together these data affirm that our conditional knockout approach was effective at reducing phasic inhibitory input on hippocampal and neocortical SST interneurons, thereby increasing their excitability.

How does disinhibition of SST interneurons influence pyramidal neurons' postsynaptic currents?

One predicted effect of disinhibiting SST interneurons is an increase in inhibitory currents on downstream pyramidal neurons. To test this prediction, electrophysiological recordings were performed on pyramidal neurons in area CA1 of the hippocampus and layer 2/3 of the cingulate cortex to measure their postsynaptic responses. In the hippocampus, as expected, sIPSC frequency and amplitude were significantly increased in knockout SST interneurons compared to controls (Figure 6.3a, e) (n=8-15 cells, 4 mice per experimental group). Interestingly, mIPSC amplitude was also increased in knockout hippocampus compared to controls (Figure 6.3b, f), possibly reflecting a presynaptic activity-dependent influence on the number of postsynaptic

receptors. The frequency of mIPSCs was unchanged between knockout and control hippocampal SST interneurons (Figure 6.3b, f), as were the Gabazine-sensitive tonic current (Figure 6.3c, g) (n=8-11 cells, 3 mice per experimental group) and sEPSCs (Figure 6.3d, h) (n=8-15 cells, 4 mice per experimental group). A nearly identical pattern of alterations was seen in layer 2/3 cingulate cortical SST interneurons, except that mIPSC amplitude was unaffected by γ2 subunit knockout. Together these data indicate that disinhibiting SST interneurons was sufficient to significantly increase inhibitory currents on local pyramidal neurons.

How does disinhibition of SST interneurons affect basal anxiety-like and depression-like behavior?

Given the association between deficient GABAergic signaling and stress-related disorders – particularly the link between SST interneuron dysregulation in MDD – we next investigated whether disinhibiting hippocampal and neocortical SST interneurons has an impact on anxiety-like and depression-like behavior. Our collaborators employed the elevated plus maze (EPM) and novelty-suppressed feeding test (NSFT) to probe for changes in anxiety-like behavior. In the EPM, knockout mice demonstrated a decrease in anxiety-like behavior as measured by the time spent in the open arm compared to controls (Figure 6.4a) (n=29-35 mice per experimental group). Similarly, knockout mice in the NSFT exhibited a shorter latency to feed compared to controls (Figure 6.4b) (n=31-35 mice per experimental group), providing additional evidence for an anxiolytic effect of SST interneuron disinhibition. Knockout mice also demonstrated decreased depression-like behavior, manifested as reduced time spent immobile in the forced swim test compared to control mice (Figure 6.4c) (n=31-35 mice per experimental group). This antidepressant-like effect was corroborated by similar findings in the learned helplessness task, where knockout male mice demonstrated fewer failures to escape compared to control males

(Figure 6.4d) (n=17-19 mice per experimental group). A spatial learning and memory paradigm, the Morris water maze, was also conducted to assess the specificity of the anxiolytic and antidepressive effects of SST interneuron disinhibition. No difference was found between the performance of SST-Cre:$\gamma 2^{f/f}$:LSL-YFP knockout mice and $\gamma 2^{f/+}$ controls, supporting the notion that SST interneuron disinhibition specifically influences emotional behavior.

Does SST interneuron disinhibition produce changes in protein translation signaling cascades similar to those of antidepressant medications?

The anxiolytic and antidepressive effects of disinhibiting SST interneurons mimic those of fast-acting antidepressants such as ketamine and 5-HT2C receptor antagonists. We next examined whether the similarity of these effects on behavior extended to the biochemical level of protein translation regulatory cascades. Other members of the collaboration analyzed protein from hippocampal and medial prefrontal cortical tissue extracts via Western blot. The SST-Cre:$\gamma 2^{f/f}$:LSL-YFP mutants showed a reduction in phosphorylation at T56 of eEF2 compared to controls in both brain regions(Figure 6.5a) (n=10-11 mice per experimental group), indicating an increase in eEF2 mRNA translation activity in mutants. The kinase targeting eEF2, eEF2K, showed a reduction in phosphorylation at its CaM-dependent autophosphorylation site, T348 compared to controls (Figure 6.5d) (n=5-8 mice per experimental group), a finding consistent with the reduced phosphorylation of eEF2 at T56. Phosphorylation of another site on eEF2K that is targeted by PKA and thus independent of intracellular [Ca^{2+}], S500, was unchanged between SST interneuron-disinhibited mutants and controls (Figure 6.5d) (n=5-8 mice per experimental group). Importantly, the specific, activity-dependent phosphorylation of eEF2K at T348 is distinct from the pathway recruited by fast-acting antidepressants, as mTOR and S6K phosphorylation were unchanged in mutants compared to controls in both brain regions

analyzed (Figure 6.5b, c) (n=6-7 mice per experimental group). Together these data demonstrate that SST disinhibition throughout hippocampus and neocortex give rise to a significant, widespread decrease in synaptic excitation and hence reduced pyramidal neuron calcium influx, in turn broadly increasing mRNA translation via reduced inhibitory phosphorylation of eEF2 by eEF2K. This reveals that enhancing GABAergic signaling by cortical SST interneurons exerts antidepressant-mimetic effects via biochemical pathways parallel to those of fast-acting antidepressants that ultimately converge on the same target, to similar effect: reduced mRNA translation mediated by eEF2.

Significance

The mechanisms of antidepressant medication represent a long-standing puzzle, because monoamine-acting drugs show significant efficacy in human patients but only after a delay of weeks, whereas in animal models of depression-like behavior, they act on the order of hours to days (Artigas, 2001). The noncompetitive NMDA receptor antagonist ketamine, by contrast, exerts antidepressant effects on a much shorter time scale (Ionescu et al., 2014). Counterintuitively, ketamine appears to function as an antidepressant by enhancing glutamatergic transmission through activation of the mammalian target of rapamycin (mTOR) pathway, leading to increased expression of neuroligin 1 and NMDAR subunits as well as an increase in the number of glutamatergic synapses (Ren et al., 2016;Li et al., 2010). Ketamine's efficacy as an antidepressant, and its mechanism of action at sub-anesthetic doses, remain highly controversial due to the widespread expression of NMDAR throughout the brain. However, collectively, these prior studies indicate that monoamine modulation may not be the end-mechanism of antidepressant effects, but rather an intermediary to the true mechanism of correcting the depression-associated imbalance between excitatory and inhibitory activity in the

hippocampus, anterior cingulate gyrus, and prefrontal cortex (Cai et al., 2013;Ren et al., 2016;Li et al., 2010). Our work here shows that selectively enhancing SST interneuron output is sufficient to produce anxiolytic-like and anti-depressive-like effects, via a biochemical pathway that converges with that of ketamine's putative mechanism of action. This lends compelling support to the notion that disruption of hippocampal and neocortical GABAergic inhibition is a critical component of the pathophysiology of major depressive disorder. Furthermore, our results provide a potential unifying mechanism for the glutamatergic and GABAergic deficiency models of depression: enhancing glutamatergic input specifically to SST interneurons may account for the antidepressant actions of ketamine, since selectively disinhibiting SST interneurons has the same impact on behavior.

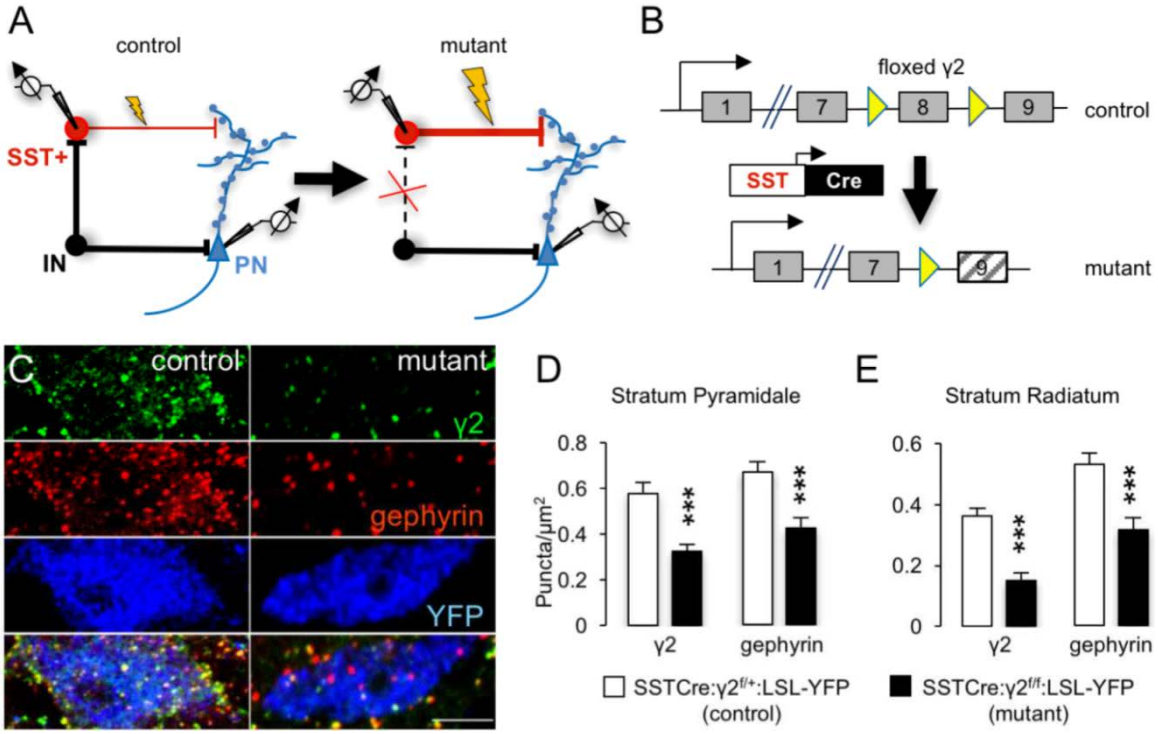

Reproduced from from (Fuchs et al., 2016)

Figure 6.1. Deletion of postsynaptic $GABA_A$Rs and gephyrin from SST+ neurons of SSTCre:$\gamma2^{f/f}$ mice. (A) Strategy for γ2 subunit KO-mediated disinhibition of SST+ interneurons. Loss of synaptic $GABA_A$Rs removes inhibitory input (IN) to SST+ neurons and increases excitability of these neurons. Increased excitability of SST+ neurons strengthens inhibitory synaptic inputs to apical dendrites and spines of pyramidal cells (PN). (B) Schematic of Cre mediated inactivation of the 'floxed' γ2 locus. (C) Representative micrographs of the soma of an SST+ neuron from a SSTCre: $\gamma2^{f/+}$:LSL–YFP control mouse (left column) compared to a SST+ neuron from a SSTCre:$\gamma2^{f/f}$:LSL–YFP mutant animal, immunostained for the γ2 subunit (top row, green), gephyrin (second row; red) and YFP (third row; blue) with merged images showing colocalization of γ2 and gephyrin in yellow in the bottom row. Note the drastic reduction in punctate staining for both the γ2 subunit and gephyrin, indicative of loss of functional synapses. Residual staining for γ2 is likely attributable to dendrites of Cre-lacking neighboring neurons. (D) Quantification of puncta densities overlapping with YFP+ cell somata (puncta/μm^2) in S. pyramidale and S. radiatum of the hippocampus. Densities for both proteins were significantly reduced in both areas ($p<0.001$, respectively). *** $p<0.001$, Mann-Whitney, n=30-40 cells, 2 mice per genotype.

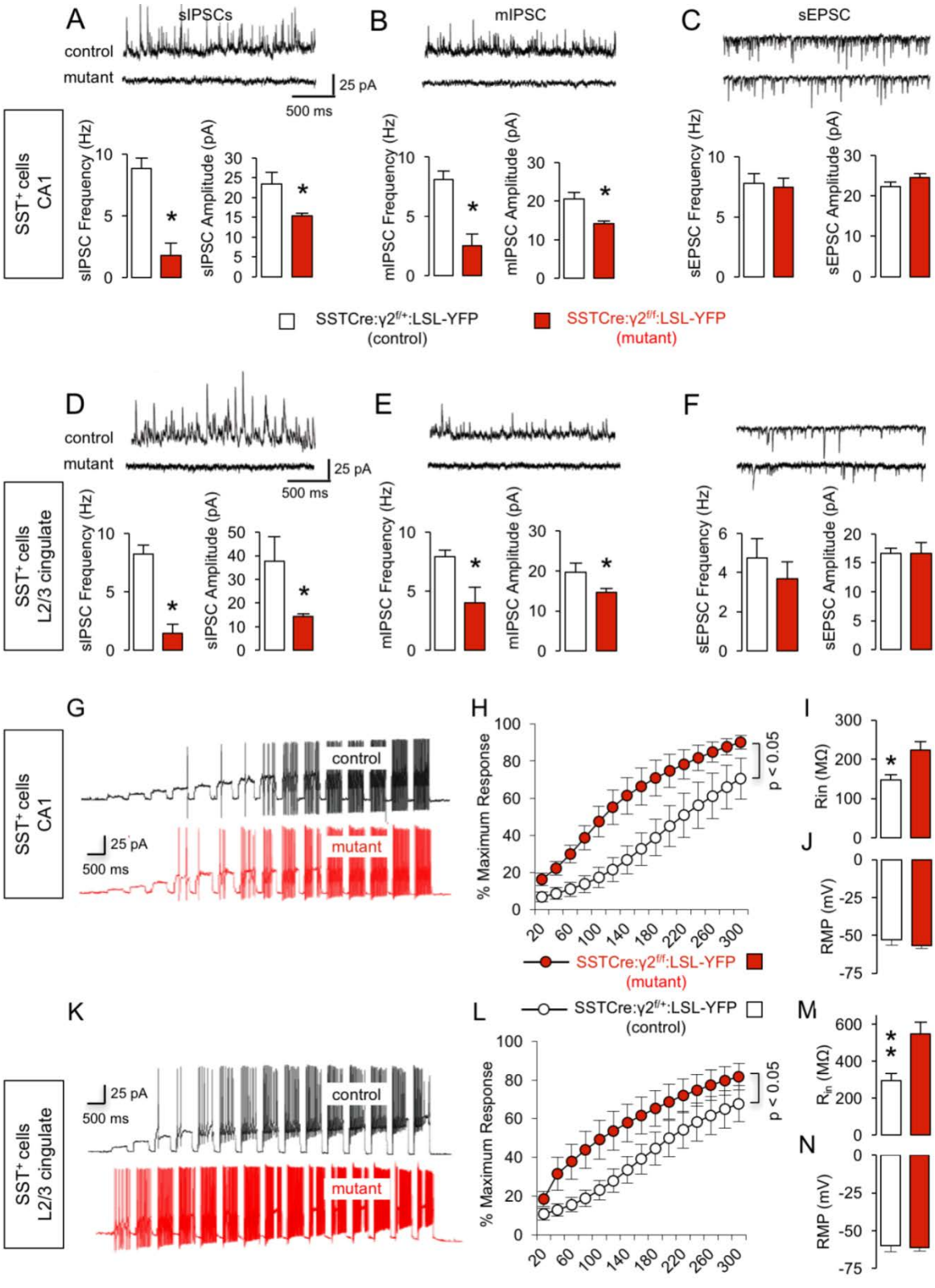
A
sIPSCs
control
mutant
25 pA
500 ms
B
mIPSC
C
sEPSC
SST+ cells CA1
sIPSC Frequency (Hz)
sIPSC Amplitude (pA)
mIPSC Frequency (Hz)
mIPSC Amplitude (pA)
sEPSC Frequency (Hz)
sEPSC Amplitude (pA)
SSTCre:γ2f/+:LSL-YFP (control)
SSTCre:γ2f/f:LSL-YFP (mutant)
D
E
F
SST+ cells L2/3 cingulate
G
H
I
J
K
L
M
N
control
mutant
% Maximum Response
p < 0.05
Rin (MΩ)
RMP (mV)

Reproduced from from (Fuchs et al., 2016)

Figure 6.2. Recordings from SST+ neurons. (A–F) sIPSC, mIPSC and sEPSC recordings from SST+ neurons of SSTCre:$\gamma 2^{f/f}$:LSL-YFP mutants and SSTCre:$\gamma 2^{f/+}$:LSL-YFP control mice, in hippocampus CA1 (A–C) and L2/3 cingulate cortex (D–F). Representative traces are shown on top of summary statistics. Note the significant reductions in both sIPSC and mIPSC frequencies and amplitudes recorded from CA1 (A, B) and L2/3 (D, E) SST+ neurons of mutant vs. control mice ($p<0.05$ for all eight measures, n= 6-8 cells, 3 mice per experimental group). sEPSCs recorded from SST+ neurons were unaffected by genotype independent of brain area (C, F, CA1, L2/3 frequency, p, n.s., amplitude, p, n.s., n=6-8 cells , 3 mice per experimental group). (G–N) Current injection data from SST+ neurons in CA1 and L2/3 cingulate cortex of SSTCre:$\gamma 2^{f/f}$:LSL-YFP mutants and controls. Representative traces are shown in (G) (CA1) and (K) (L2/3) with summary data in (H–J) (CA1) and (L–N) (L2/3). Note the increased number of action potentials recorded from SST+ neurons in mutant vs. control mice in both CA1 and L2/3 (H, L. $p<0.05$ for both comparisons, Boltzmann fit, W50, *t*-tests). The input resistance (R_{in}; J, N) was significantly reduced in SSTCre:$\gamma 2^{f/f}$:LSL–YFP mutant vs. control mice in both brain areas (R_{in}, CA1, $p<0.05$; L2/3, $p<0.01$, n=9-10 cells), while the resting membrane potentials (RMP; J, N) of SST+ cells were unaffected by genotype independent of brain area (RMP, p, n.s.). Data represent means ± SE. * $p<0.05$, ** $p<0.01$, *t*-tests.

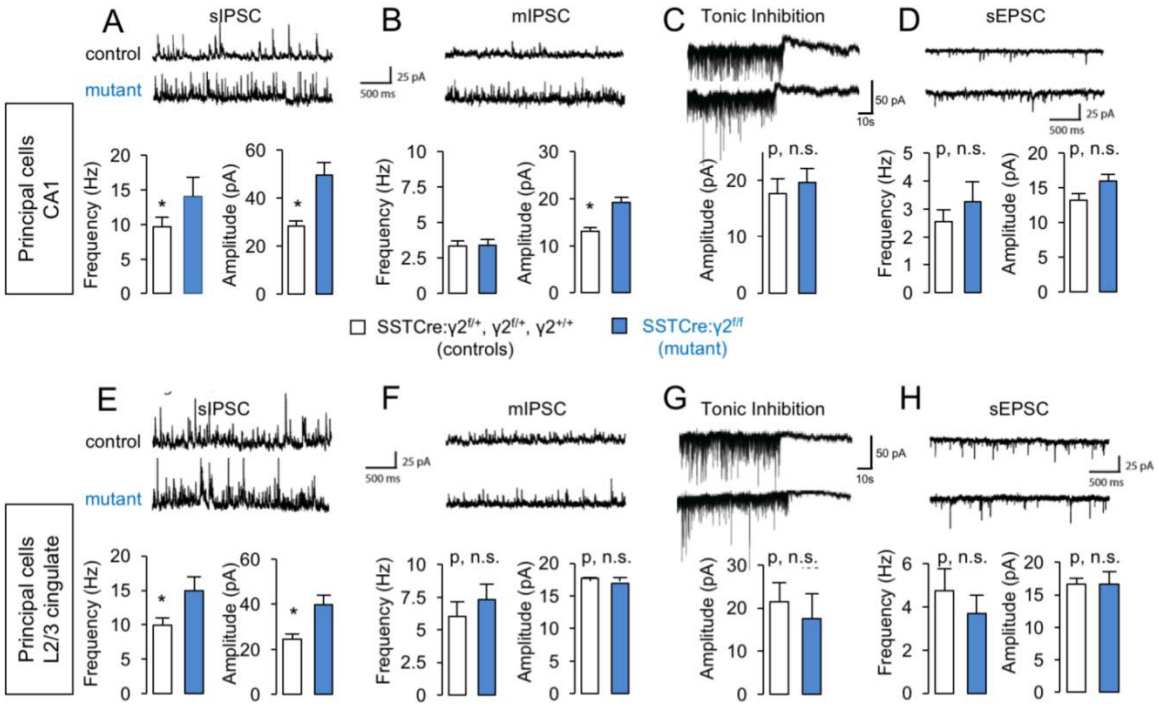

Reproduced from from (Fuchs et al., 2016)

Figure 6.3. Recordings from pyramidal cells. (A–H) sIPSC, mIPSC, tonic inhibition and sEPSC recordings from pyramidal neurons of SSTCre:$\gamma2^{f/f}$ compared to control mice (SSTCre:$\gamma2^{f/+}$, $\gamma2^{f/f}$ and $\gamma2^{+/+}$) in CA1 hippocampus (A–D) and L2/3 cingulate cortex (E–H). Representative traces are shown on top of bar graph summary statistics. Note the significant increases in sIPSC frequency and amplitude recorded from neurons of SSTCre:$\gamma2^{f/f}$ mice in both brain areas (A, E, $p<0.05$ for all four measures; n=8-15 cells, 4 mice per experimental group). By contrast, mIPSCs showed a moderate increase in amplitude for SSTCre:$\gamma2^{f/f}$ mice in CA1 only (B, F) (CA1 amplitude, $p<0.05$, frequency, p, n.s. for CA1 frequency, L2/3 amplitude and L2/3 frequency). Tonic inhibition (C, G) was unaffected by genotype (p, n.s. for all comparisons, n=8-11 cells, 3 mice per experimental group). Similarly, the sEPSCs (D, H) did not differ between genotypes independent of brain area (p, n.s., all comparisons, n=8-15 cells, 4 mice per experimental group). Data represent means ± SE. * $p<0.05$, *t*-tests.

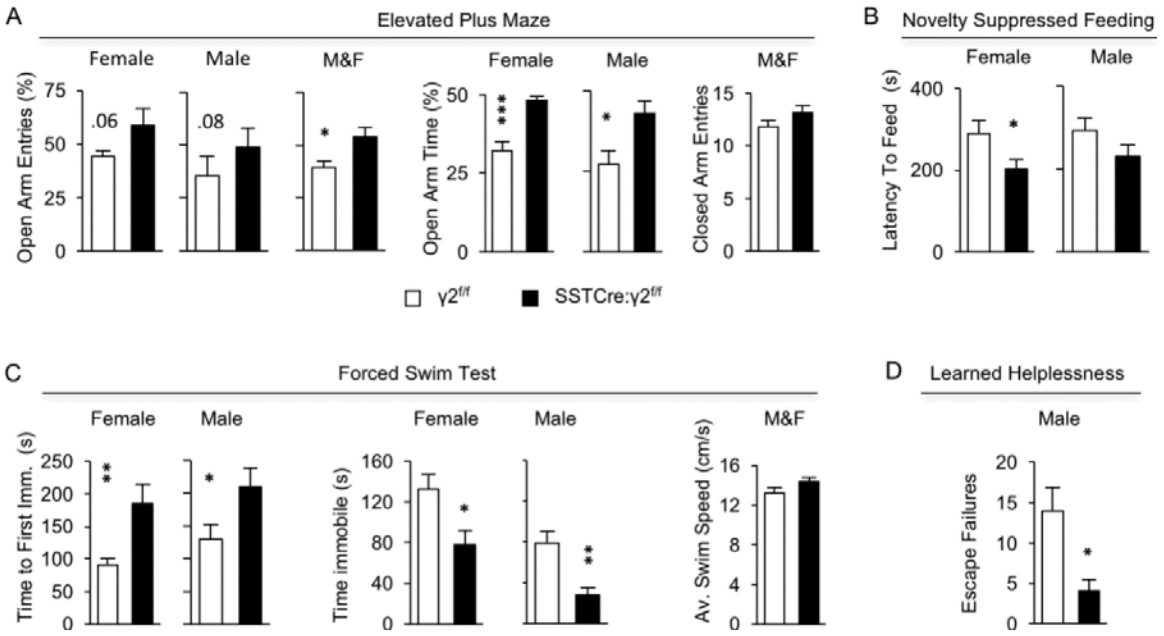

Reproduced from from (Fuchs et al., 2016)

Figure 6.4. SSTCre:$\gamma2^{f/f}$ mice show an anxiolytic- and antidepressant-like behavioral phenotype. (A) EPM: Percentage of open arm entries of SSTCre:$\gamma2^{f/f}$ mutants was increased compared to $\gamma2^{f/f}$ controls [sexes combined (M&F), $F(1, 60)=6.34$, $p<0.05$, n=29-35] with similar trends in females ($p=0.06$, n=14-16) and males ($p=0.08$, n=15-19). The percent time spent in open arms was increased in mutants vs. controls in both sexes ($F(1, 57)=19.16$, $p<0.001$; male: $p<0.05$, n=14-19; female: $p<0.001$, n=12-16). The number of closed arm entries did not differ between genotypes ($p>0.05$, n.s., t -test). (B) NSFT: SSTCre:$\gamma2^{f/f}$ mutants showed a reduced latency to feed vs. controls ($F(1, 62)=6.4$, $p=0.014$), with significant effects in females ($p<0.05$, n=16) and a tendency in the same direction in males (p, n.s., n=15-19). (C) FST: SSTCre:$\gamma2^{f/f}$ mice of both sexes showed increased latencies to their first bout of immobility ($F(1, 62)=15.41$, $p=0.0002$; female: $p<0.01$, n=16; male: $p<0.05$, n=15-19) and a reduced total time immobile vs. controls ($F(1, 62)=15.98$, $p<0.0001$; female: $p<0.05$; male: $p<0.01$). The average swim speed during the first minute did not differ between genotypes (M&F: p, n.s., n=32-34, *t*-test). (D) LHT: Male SSTCre:$\gamma2^{f/f}$ mice showed fewer escape failures than controls ($p<0.05$, n=17-19, Mann-Whitney). Data represent means ±SE. * $p<0.05$, ** $p<0.01$, *** $p<0.001$, ANOVAs and post hoc *t*-tests, *t*-tests or Mann-Whitney.

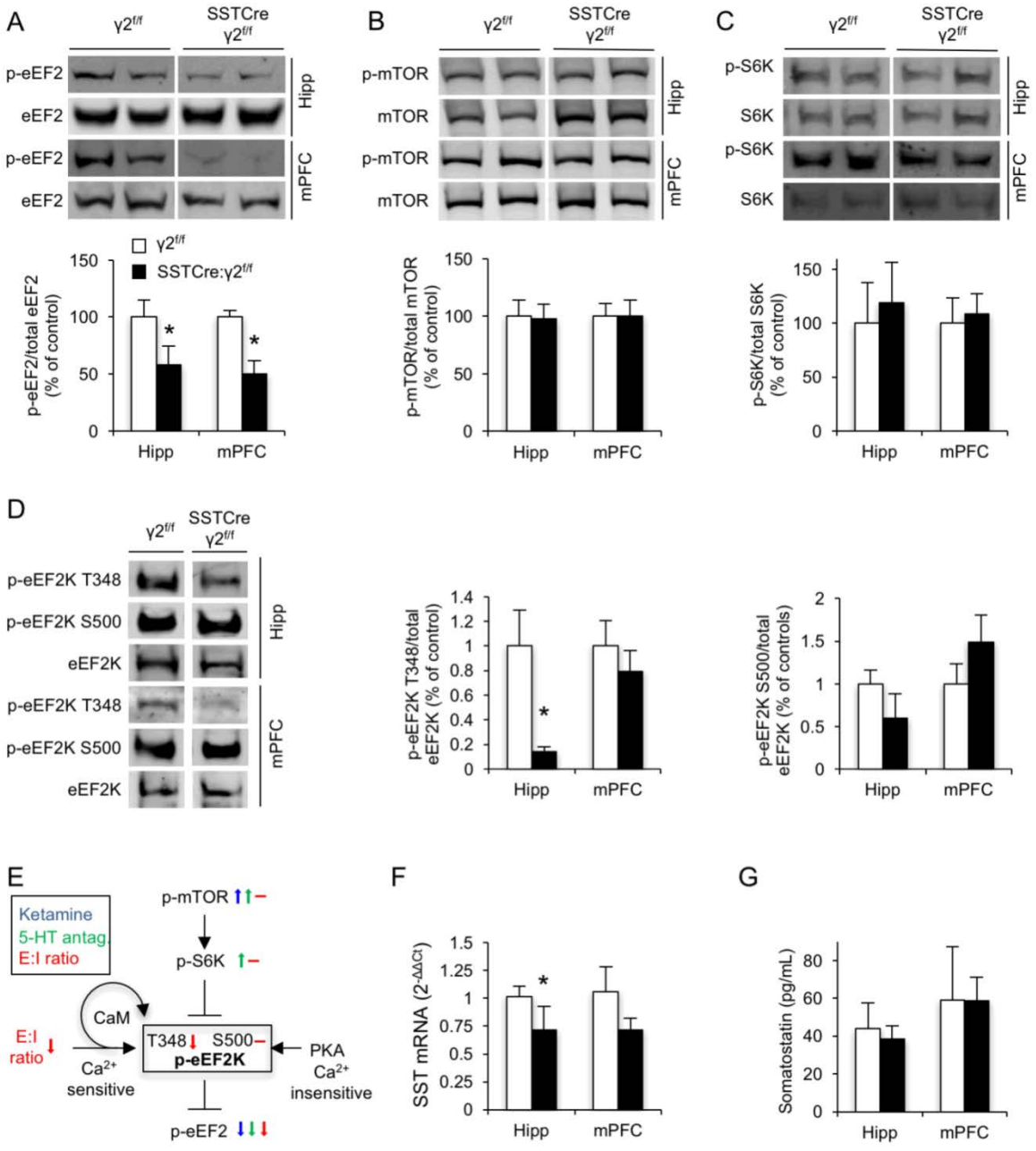
A
γ2f/f
SSTCre γ2f/f
p-eEF2
eEF2
p-eEF2
eEF2
Hipp
mPFC
γ2f/f
SSTCre:γ2f/f
p-eEF2/total eEF2 (% of control)
150
100
50
0
*
*
Hipp
mPFC
B
γ2f/f
SSTCre γ2f/f
p-mTOR
mTOR
p-mTOR
mTOR
Hipp
mPFC
p-mTOR/total mTOR (% of control)
150
100
50
0
Hipp
mPFC
C
γ2f/f
SSTCre γ2f/f
p-S6K
S6K
p-S6K
S6K
Hipp
mPFC
p-S6K/total S6K (% of control)
150
100
50
0
Hipp
mPFC
D
γ2f/f
SSTCre γ2f/f
p-eEF2K T348
p-eEF2K S500
eEF2K
p-eEF2K T348
p-eEF2K S500
eEF2K
Hipp
mPFC
p-eEF2K T348/total eEF2K (% of control)
1.4
1.2
1
0.8
0.6
0.4
0.2
0
*
Hipp
mPFC
p-eEF2K S500/total eEF2K (% of controls)
2
1.5
1
0.5
0
Hipp
mPFC
E
Ketamine
5-HT antag.
E:I ratio
p-mTOR
p-S6K
CaM
E:I ratio
Ca2+ sensitive
T348 S500
p-eEF2K
PKA
Ca2+ insensitive
p-eEF2
F
SST mRNA (2-ΔΔCt)
1.5
1.25
1
0.75
0.5
0.25
0
*
Hipp
mPFC
G
Somatostatin (pg/mL)
80
60
40
20
0
Hipp
mPFC

Reproduced from from (Fuchs et al., 2016)

Figure 6.5. SSTCre:$\gamma2^{f/f}$ mice show biochemical changes indicative of reduced intracellular Ca^{2+} signaling and increased dendritic translational elongation. (A-C) Representative western blots and summary statistics for p-eEF2, p-mTOR and p-S6K in hippocampus (hipp) and mPFC normalized to levels of the respective total proteins in the same samples. Western blots show a reduction of p-eEF2T56/total eEF2 in hippocampus (Hipp) and medial prefrontal cortex (mPFC) of SSTCre:$\gamma2^{f/f}$ vs. $\gamma2^{f/f}$ control mice ($p<0.05$, n=10-11, for both hipp and mPFC, *t*-tests) (A). The ratios of p-mTORS2448/mTOR (n=6 mice; both brain regions) (B) and of p-S6KT389/S6K (C) were unaffected by genotype (p, n.s., all four comparisons, n=6-7 per experimental group, both brain regions, Mann-Whitney). (D) Representative western blots and summary statistics of phosphorylation of eEF2K at T348 and S500, normalized to total eEF2K. A two-way ANOVA for auto-phosphorylation at T348 revealed significant main effects for genotype [$F(1,22)=10.50$, $p<0.01$], brain region [$F(1,22)=10.35$, $p<0.01$], and interaction among the two [$F(1,22)=7.69$, $p<0.05$]. Post hoc tests showed significantly reduced eEF2KT348 auto-phosphorylation in hippocampus of SSTCre:$\gamma2^{f/f}$ vs. $\gamma2^{f/f}$ controls ($p<0.01$, n=5-8) with a tendency in the same direction in mPFC (p, n.s., n=5-7 mice per experimental group, *t*-tests). By contrast, no genotype-dependent changes were evident for eEF2KS500 (p, n.s., for both brain regions; n=5-6 (hipp) and 6-8 (mPFC), Mann-Whitney). (E) Schematic of signaling cascades converging on the phospho state and activity of eEF2K as a target downstream of (i) mTOR- and S6K-mediated inhibitory phosphorylation, (ii) E:I ratio and CaM-dependent auto-phosphorylation at T348 (activating, black arrow), and (iii) Ca^{2+}-insensitive activating PKA-mediated phosphorylation at S500. Small color-coded arrows illustrate previously reported alterations in phospho-state induced by ketamine (blue 5-HT2C antagonists (green), and reported here due to a reduced synaptic E:I ratio (red, unaltered phospho-states are indicated by a horizontal dash). The unaltered phospho-states of mTOR, S6K and eEF2KS500 of SSTCre:$\gamma2^{f/f}$ mice indicate that reduced phosphorylation of eEF2 involves reduced E:I ratio- and reduced CaM-mediated autophosphorylation of eEF2K at T348. (F) SST mRNA levels quantitated by RT-PCR were reduced in hippocampus ($2^{-\Delta\Delta Ct}$, $p<0.05$) with a trend in the same direction in mPFC (p, n.s., n=5-6 mice per experimental group, Mann-Whitney). (G) SST protein levels quantitated by ELISA were not measurably affected by genotype, independent of brain region [p, n.s., n = 5-6 (hipp), 5 (mPFC), Mann-Whitney]. Data represent means ± SE. * $p<0.05$, ** $p<0.01$, *t*-tests. *$p<0.05$, *t*-tests or Mann-Whitney.

7. Hippocampal CRH neurons: Connectivity and intrinsic properties of a novel interneuron type

Previous investigations of hippocampal CRH neurons have been limited to immunostaining, *in situ* hybridization, and CRH receptor pharmacology. Apart from discovering that this population exists and that hippocampal CRH appears to be important for stress effects on learning and memory, the colocalization of the CRH neuropeptide with GAD67 mRNA suggested that they may be GABAergic interneurons. Recently we acquired a transgenic mouse line, CRH-Cre, which enables us to target this cell type for identification and activity manipulation with unprecedented precision. We therefore set out to test the hypothesis that hippocampal CRH neurons are GABAergic interneurons by characterizing their connectivity and intrinsic properties. This section contains data and figures from (Hooper and Maguire, 2015) on which I was the first author.

Rationale

Early attempts to isolate hippocampal CRH neurons were hamstrung by the available technology. Immunostaining of CRH in the hippocampus reveals a diffuse subcellular localization which makes it difficult to definitively identify its source histologically; additionally, the presence of GAD67 mRNA, while suggestive, is insufficient to prove that a cell forms functional GABAergic synapses since GAD is also present in dentate granule cells and other excitatory neurons (Sloviter et al., 1996;Cao et al., 1996;Telfeian et al., 2003). Additionally, studies relying on CRH receptor pharmacology, though informative, fail to capture the synaptic aspect of hippocampal CRH neuron activity. These studies also cannot account for the possibility of extra-hippocampal sources of CRH, or for the local activity of other CRH-family

ligands, such as Urocortin I which is also known to be expressed in hippocampus. However, the advent of Cre recombinase technology to express fluorescent proteins and other cellular tools in a cell type-specific way has paved the way for a more thorough and informative investigation of hippocampal CRH neurons. In this study we focused on the structural and functional connectivity, molecular profile, and intrinsic electrophysiological properties of these neurons, with particular emphasis on the hypothesis that they are GABAergic interneurons. Throughout these experiments, we specifically targeted CRH neurons in the dorsal hippocampus.

Does CRH-Cre expression recapitulate native CRH expression?

Our first goal was to validate the CRH-Cre model by assessing the fidelity of Cre expression to that of the native CRH peptide. We visualized cells expressing Cre by crossing the CRH-Cre line with a Cre-dependent reporter line: either GFP (green; CRH-GFP) (Figure 7.1a) or tdTomato (red; CRH-Ai9) (Figure 7.1b). In the hippocampus, reporter expression was primarily limited to somata in stratum pyramidale of area CA1 of the hippocampus (Figure 7.1a1), and extensive arborizations in area CA3 (Figure 7.1a2). I conducted immunostaining of the CRH peptide in reporter mouse brain slices and quantitatively assessed colocalization of peptide immunoreactivity with reporter fluorescence (Figure 7.1b). I found that a high proportion of reporter-positive cells also exhibited immunoreactivity (40.1±5.8%); however, a sizeable subset of CRH-immunoreactive cells did not express the reporter (37.6±6.5%). Together these data suggest that our CRH-Cre line may capture just one subpopulation of CRH-expressing neurons. Evidence to support this possibility came from immunostaining for an interneuron class marker: while none of the reporter-positive hippocampal cells demonstrated expression of the calcium-binding protein parvalbumin (PV) (0.0±0.0%), a subset of CRH-immunoreactive cells did show colocalization with PV (18.3±3.6%). Thus, we hypothesize that a separate, PV-positive subclass

of hippocampal CRH neurons exist, and that these PV-positive CRH neurons are not captured by our CRH-Cre line.

In order to provide further evidence that our CRH-Cre line captures *bona fide* hippocampal CRH neurons, single-cell PCR was performed to compare the contents of reporter-positive neurons with those of nearby reporter-negative pyramidal neurons in CA1 stratum pyramidale. Critically, 100% of reporter-positive neurons assayed expressed transcript for CRH, while 0% of pyramidal neurons expressed this transcript (Figure 7.1c1). Reporter-positive neurons also expressed transcripts of common interneuron markers including GAD65 (71.4%) and cholecystokinin (CCK; 100%) (Figure 7.1c2). A subset of reporter-positive neurons expressed the interneuron marker somatostatin (SST; 28.6%), while very few expressed PV (14.3%) and none expressed the glutamatergic neuron marker vesicular glutatmate transporter 2 (VGlut2; 0%) (Figure 7.1c2). Taken together, our single-cell PCR data and the CRH peptide immunostaining results above verify that the CRH-Cre mouse is a valid model for isolating a substantial subpopulation of hippocampal CRH neurons. Additionally, the presence of for classical interneuron marker mRNAs supports the hypothesis that hippocampal CRH neurons are GABAergic interneurons.

What is the molecular profile of hippocampal CRH neurons?

In order to assess the molecular profile of hippocampal CRH neurons at the level of protein expression, I performed immunostaining of an extensive panel of classical interneuron marker proteins (a commonly-used method to distinguish among interneuron classes) on CRH-Ai9 reporter brain sections (see Table 7.1). In agreement with the single-cell PCR results above, I found high levels of colocalization with the amino acid neurotransmitter GABA (93.1%) and the

GABA-synthesizing enzyme γ amino decarboxylase 1 (GAD1, also known as GAD67; 56.4%) (Figure 7.2a, b). Strikingly, I found no instance of colocalization between the reporter and PV (0%) (Figure 7.2c). A substantial proportion of reporter-positive neurons also expressed SST (39.5%), while smaller subsets expressed the calcium-binding proteins calbindin (26.5%) and calretinin (23.2%) (Figure 7.2d-f). Our colocalization data illustrate that this subset of hippocampal CRH neurons is uniformly GABA-positive and PV-negative, but otherwise somewhat heterogeneous with respect to molecular markers of interneuron classes.

What are the electrophysiological properties of hippocampal CRH neurons?

In addition to their molecular profile, interneuron classes can also be distinguished from one another by their intrinsic electrophysiological properties. Electrophysiological recordings were performed on visually-identified, reporter-positive hippocampal CRH neurons, and their electrophysiological profiles were compared to neighboring, reporter-negative CA1 pyramidal neurons (Figure 7.3a) (see Table 7.2). Specifically, both populations' responses to 1-second pulses of current varying from -100 pA to +100 pA in 20-pA increments were analyzed (Figure 7.3b). Phase plane plot analysis revealed no significant differences in the waveform of action potentials (APs) between neuron types (Figure 7.3c). Action potential threshold, peak, minimum, and afterhyperpolarization voltages were similar, as was the rise time of APs. Hippocampal CRH neurons were found to have a significantly depolarized resting membrane potential (-57.7±3.2 mV) compared to pyramidal neurons (-68±1.1 mV) (Figure 7.3d). Interestingly though, they were also less excitable as measured by their input resistance (CRH: 32.1±3.9 MOhm; pyramidal: 53.7±5.0 MOhm), input-output relationship (CRH: W50=91.6 pA; pyramidal: W50=54.5 pA), maximum number of APs (CRH: 16.8±4.7 APs; pyramidal: 31.0±6.3 APs), and latency to first AP (CRH: 25.8±9.0 msec; pyramidal: 12.7±2.3 msec) (n=11-13 cells, 6-7 mice per experimental

group) (Figure 7.3e-i). Unexpectedly, upon filling patched cells with biocytin for morphological analysis, CRH neurons were further revealed to be coupled together by gap junctions, as evidenced by the spread of biocytin to other reporter-positive neurons in the slice (Figure 7.3m-o); by contrast, in CA1 pyramidal neurons, biocytin remained restricted to the patched neuron as expected (Figure 7.3j-l). Together these data illustrate that, despite their proximity and superficial resemblance to pyramidal neurons, hippocampal CRH neurons possess electrophysiological properties that are markedly different from those of their pyramidal neighbors. Their apparent gap junction-coupling is of particular interest, as this feature holds exciting implications for their function in the hippocampal network.

Where do CRH neurons send their projections?

Qualitative assessment of CRH reporter brain sections revealed extensive – apparently axonal – arborizations in area CA3. In order to determine whether these arborizations actually originate from CRH neuron somata in CA1 stratum pyramidale, I conducted anterograde tract tracing to selectively label CRH neurons in CA1 and their projections (Figure 7.4a). I injected a Cre recombinase-dependent adenovirus encoding a red fluorescent protein (AAV-Flex-ChR2-tdTomato) into stratum pyramidale of area CA1 of the dorsal hippocampus. Two weeks after virus injection, I imaged brain sections containing the hippocampus and other known CRH-expressing populations. Expression of the viral fluorescent protein in 100% of injected mice mimicked the pattern of transgenic reporter expression within the hippocampus, with somata in CA1 stratum pyramidale and extensive axonal arborizations in area CA3 (Figure 7.4b-d). Also, as expected, I found no fluorescence in the BNST, CeA, or PVN, thus ruling out extra-hippocampal CRH neurons as the source of these CA3 arborizations (Figure 7.4h-j). Immunostaining for the GABA-synthesizing enzyme GAD67 revealed extensive colocalization

of GAD67 with the arborizations in CA3 (Figure 7.4e-g). These data lend further support to the notion that hippocampal CRH neurons are GABAergic interneurons, and, critically, reveal that hippocampal CRH neurons back-project from CA1 to CA3.

Do CRH neurons release GABA onto CA3 pyramidal neurons?

Though we had strong evidence across multiple experiments that hippocampal CRH neurons are GABAergic, definitive proof could only come from selectively manipulating CRH neurons' activity and recording monosynaptic responses from neurons to which they project. To this end, we generated mice (ChR/CRH) in which the light-activated cation channel Channelrhodopsin (ChR) was expressed solely in CRH neurons by crossing our CRH-Cre mouse line with a Cre-dependent Channelrhodopsin line (Figure 7.5a). Electrophysiological recordings were performed to record the firing rates of hippocampal CRH neurons or postsynaptic responses in CA3 principal neurons, using an optical fiber to selectively stimulate hippocampal CRH neurons in CA1 (Figure 7.5b; Figure 7.6a). First, we demonstrated that continuous optical stimulation was effective at increasing the firing rate of ChR-expressing CRH neurons (Figure 7.5c, d). A 100ms pulse delivered at 1 Hz was sufficient to increase the firing rate of CRH neurons from 0.2±0.3 to 6.0±1.3 Hz (Figure 7.5e3). This effect was dose-dependent, as increasing laser pulse widths progressively increased the firing rate of CRH neurons (1.1±0.1 Hz at 1 msec; 2.2±0.2 Hz at 10 msec; 7.5±0.1 Hz at 100 msec) (n=7 cells, 3 mice per experimental group) (Figure 7.5f). Next, we demonstrated that CRH neurons do indeed form functional GABAergic synapses on CA3 pyramidal neurons. Pulses of 10 msec or 100msec width delivered at 1 Hz evoked IPSCs in 100% or 74.1±8.6%, respectively, of patched CA3 pyramidal neurons (Figure 7.6g). As expected, wider laser pulses evoked IPSCs at a shorter latency (10 msec: 6.4±1.0 msec latency; 100 msec: 4.2±1.0 msec latency) and greater amplitude (10 msec: 64.4±11.1 pA; 100 msec: 100.6±17.6 pA)

(Figure 7.6e, h). Wider laser pulses also prolonged the decay time of the evoked IPSC (10 msec: 40.4±17.6 msec; 100 msec: 379.5±95.6 msec) (n=12-13 cells, 4-5 mice per experimental group) (Figure 7.6f). Importantly, the short latency onset of the IPSC indicates that the connection from CRH neuron to CA3 pyramidal neuron is monosynaptic. Additionally, IPSCs were abolished by bath application of the $GABA_AR$ antagonist Gabazine (200 μM) (n=26 cells, 6 mice per experimental group) but not by the glutamate receptor antagonist kynurenic acid (n=6 cells, 2 mice), demonstrating unequivocally that the currents are GABAergic and monosynaptic (Figure 7.6k, q). The currents were not a non-specific effect of laser stimulation, as slices from Cre-negative littermates exhibited no optically-evoked IPSCs; also, the currents were specific to CA3 as no evoked IPSCs were observed in CA1 pyramidal neurons, and they were specifically inhibitory as no evoked EPSCs were observed in either CA3 or CA1 pyramidal neurons (n=12 cells, 3-4 mice per experimental group) (Figure 7.6l-p). Together these electrophysiological data provide verify for the first time that hippocampal CRH neurons back-project to form functional GABAergic synapses on CA3 pyramidal neurons.

Significance

In this study we identified a novel hippocampal interneuron type: a subpopulation of hippocampal CRH neurons which we refer to as back-projection CRH interneurons. The significance of this finding is best appreciated in the context of Freund and Buzsaki's exhaustive 1996 review of hippocampal interneurons: after patching thousands of interneurons and identifying 21 distinct classes of interneuron, the authors state that only 2 neurons demonstrated back-projection connectivity (Freund and Buzsaki, 1996). Furthermore, these 2 previously identified back-projection interneurons are distinct from the back-projection CRH interneurons described above, as they reside in a different layer of the hippocampus (Sik et al., 1994). We

estimate that approximately 4000 back-projection CRH interneurons exist in the typical adult mouse hippocampus, and this class of interneurons has been completely overlooked – most likely because they were concealed among superficially-similar pyramidal neurons in the densely-populated stratum pyramidale. Until now, hippocampal CRH neurons have only been considered in terms of their ability to activate CRH receptors on the dendrites of hippocampal pyramidal neurons; however, our findings in this study illuminate their enormous potential impact on the excitability of the hippocampal network as a sizeable, novel population of back-projecting interneurons. Because of the unique anatomical niche they fill, we hypothesize that they may function as something analogous to a pressure release valve: basally quiet, but recruited by states of high hippocampal network excitability to drive down the activity of CA3 pyramidal neurons with powerful feedback inhibition.

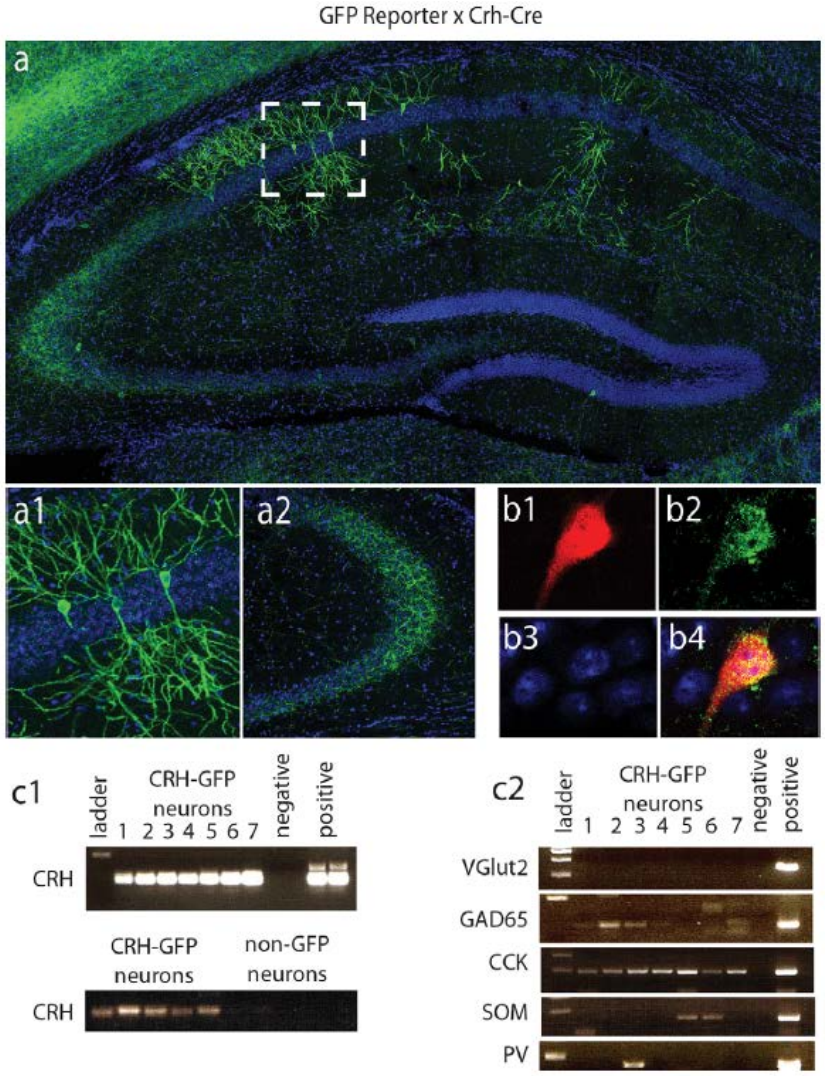

Reproduced from (Hooper and Maguire, 2015)

Figure 7.1. Characterization of hippocampal CRH neurons. a, A representative image of the hippocampus from CRH-GFP mice. a1, Higher magnification of the CA1 pyramidal cell layer highlights the morphology of hippocampal CRH neurons. a2, Higher magnification of the CA3 subregion of the hippocampus reveals dense GFPexpressing terminals surrounding the principal neurons. b, Representative image of a tdTomato-expressing hippocampal CRH neurons (red; b1) that is also immunoreactive for CRH (green; b2) (n=232 neurons, four mice). c1, Single-cell PCR detects transcript for CRH in seven individual CRH-GFP neurons in the hippocampus and in the positive controls (total brain cDNA) but not the negative control (no template) (top panel). The contents of five CRH-GFP neurons express transcript for CRH, whereas, adjacent non-GFP CA1 pyramidal neurons did not (bottom panel) (n=5–12 cells per experimental group). c2, Single cell PCR in seven individual hippocampal CRH neurons detects transcripts for GAD65, CCK, SOM, and PV, but not VGlut2.

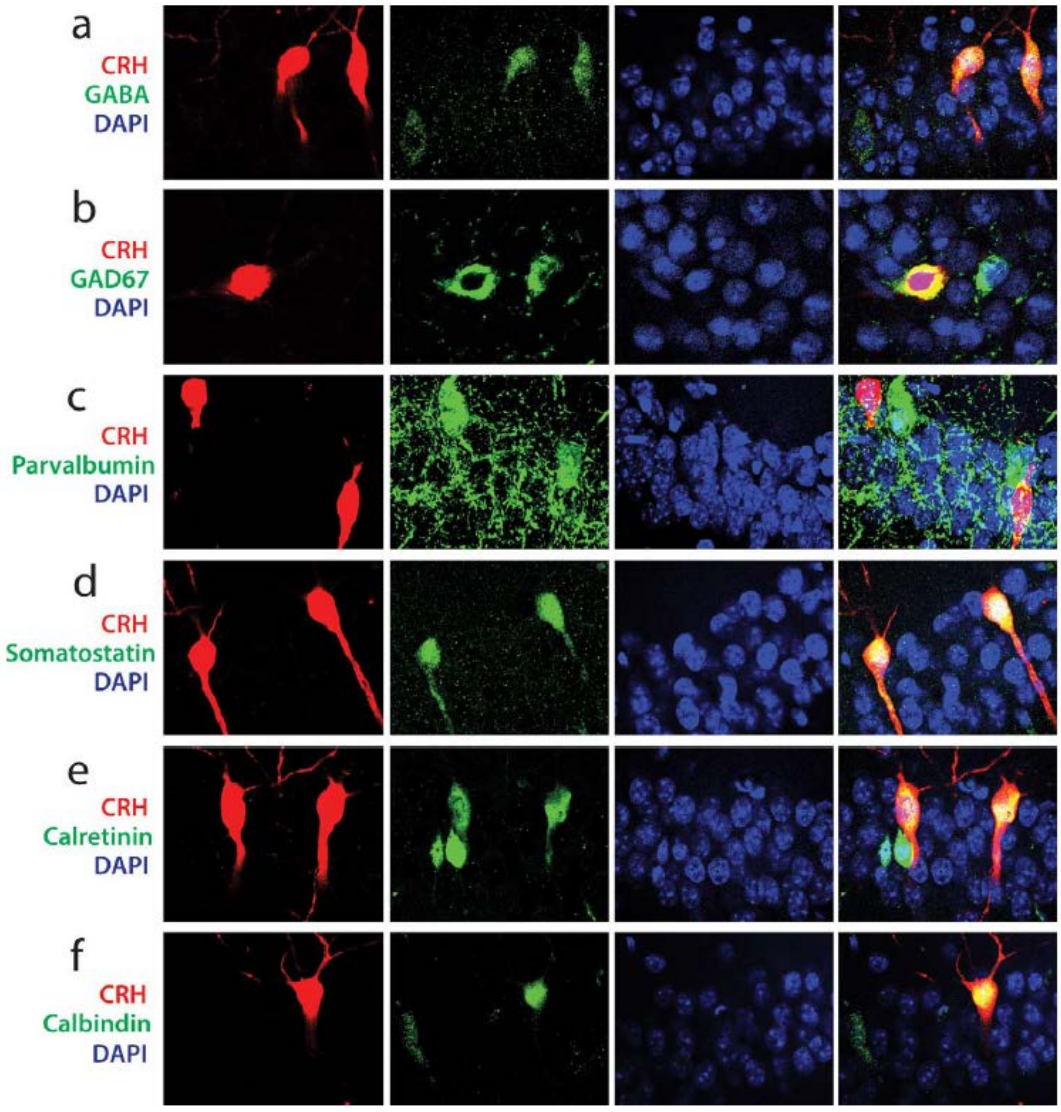

Reproduced from (Hooper and Maguire, 2015)

Figure 7.2. Molecular markers expressed by hippocampal CRH neurons. a, Representative image of GABA immunoreactivity (green) in Ai9-positive CRH neurons (red) in the CA1 region of the hippocampus. b, Representative GAD67 immunoreactivity (green) and colocalization in Ai9-positive hippocampal CRH neurons (red). c, Representative immunolabeling for parvalbumin (green) which does not overlap with Ai9 expression in CRH neurons (red). d, Representative images demonstrating the co-localization (right panel) of somatostatin (green) in Ai9-positive CRH neurons (red) in the CA1 region of the hippocampus. Representative images for calretinin (e; green) and calbindin (f; green) in Ai9-expressing CRH neurons (red) in the hippocampus. Colocalization of molecular markers and Ai9 expression is shown in the right panels. DAPI is shown in blue. N=167–290 cells, three to four mice per experimental group.

Colocalization of Interneuron Markers with Hippocampal CRH Neurons

Marker	% of CRH cells positive	Manders' coefficient	*n*
GABA	93.1 (270/290 cells)	0.739	4
GAD67	56.4 (114/202 cells)	0.688	3
Parvalbumin	0 (0/167 cells)	N/A	4
Somatostatin	39.5 (85/215 cells)	0.351	4
Calretinin	23.2 (51/220 cells)	0.314	4
Calbindin	26.5 (52/196 cells)	0.304	4
Somatostatin and calretinin	0 (0/94 cells)	N/A	4
Somatostatin and calbindin	0 (0/150 cells)	N/A	4
Calretinin and calbindin	1.29 (2/155 cells)	N/A	4

Reproduced from (Hooper and Maguire, 2015)

Table 7.1. Colocalization of interneuron markers with hippocampal CRH neurons. The percentage of hippocampal CRH neurons which express GABA, GAD67, parvalbumin, somatostatin, calretinin, and calbindin are provided with the Mander's Coefficient, characterizing the extent of the colocalization of these markers with the reporter.

Properties of Action Potentials in Hippocampal CRH Neurons and CA1 Pyramidal Neurons

Parameter	Hippocampal CRH	CA1 pyramidal
AP threshold (mV)	−44.0 ± 1.1	−42.7 ± 1.2
AP peak (mV)	63.9 ± 3.8	58.0 ± 3.5
AP rise (ms)	0.39 ± 0.04	0.32 ± 0.04
AP minimum (mV)	−62.4 ± 1.8	−65.1 ± 3.6
AHP peak (mV)	18.4 ± 1.9	22.3 ± 3.3

Reproduced from (Hooper and Maguire, 2015)

Table 7.2. Properties of action potentials in hippocampal CRH neurons and CA1 pyramidal neurons. The mean values for AP threshold, AP peak, AP rise, AP minimum, and AHP peak are provided6SEM. No statistically significant differences in the properties of the action potentials were observed between hippocampal CRH neurons and CA1 pyramidal neurons. None of the action potential parameters reached statistical significance of $p<0.05$ using a Student's t test.

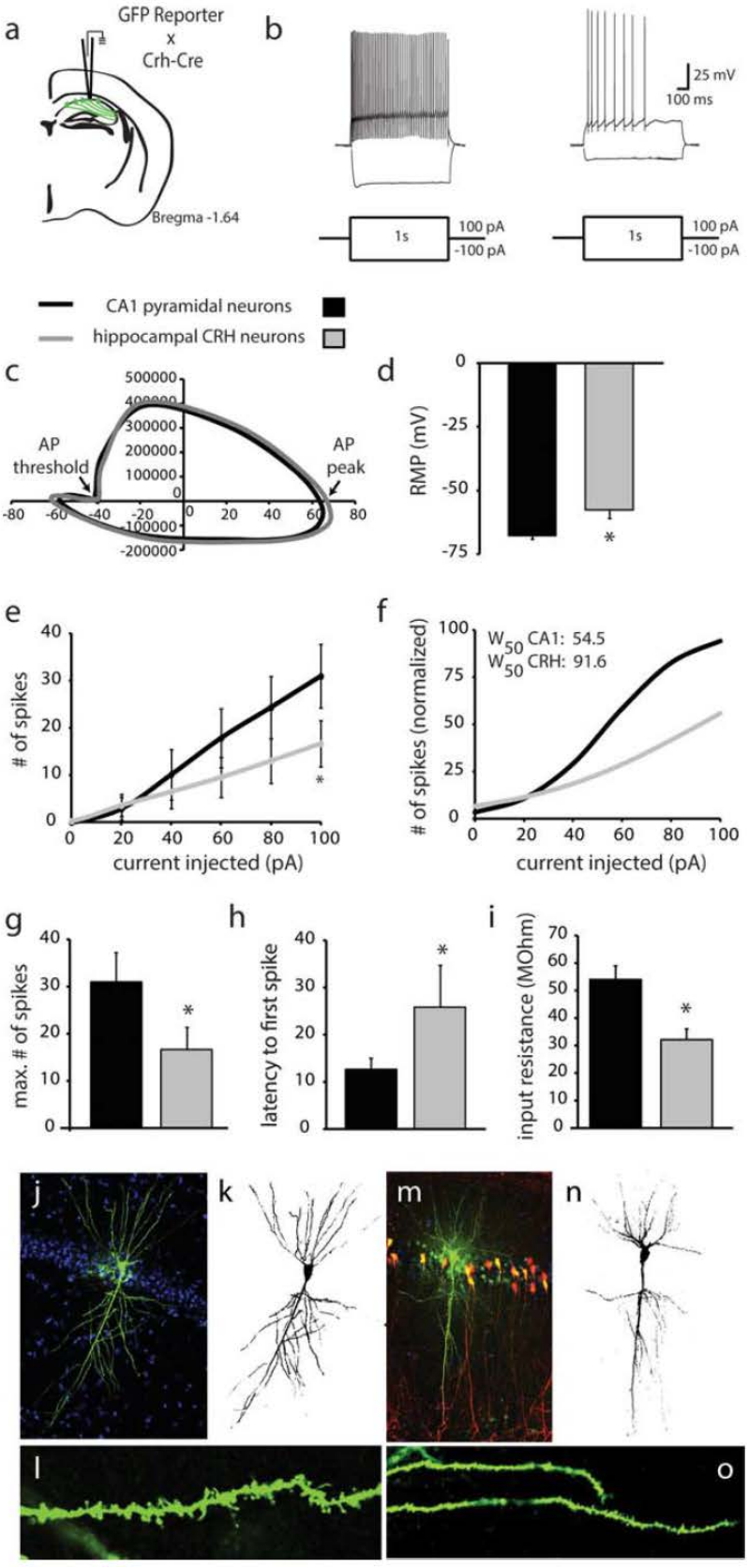
a
GFP Reporter
x
Crh-Cre
Bregma -1.64
b
25 mV
100 ms
1s
100 pA
-100 pA
CA1 pyramidal neurons
hippocampal CRH neurons
c
AP threshold
AP peak
d
RMP (mV)
e
# of spikes
current injected (pA)
f
# of spikes (normalized)
W50 CA1: 54.5
W50 CRH: 91.6
current injected (pA)
g
max. # of spikes
h
latency to first spike
i
input resistance (MOhm)
j
k
m
n
l
o

Reproduced from (Hooper and Maguire, 2015)

Figure 7.3. Electrophysiological properties of hippocampal CRH neurons. a, A diagram depicting the electrophysiological recording of hippocampal CRH neurons in CRH-GFP mice. b, Representative traces of CA1 pyramidal neurons (left panel) and hippocampal CRH neurons (right panel) in response to -100 pA and +100 pA current injections. c, Representative phase plane plots highlighting the properties of the first action potential fired in response to a +100 pA current injection in CA1 pyramidal neurons (black trace) and hippocampal CRH neurons (gray trace). d, The average resting membrane potential (RMP) is depolarized in hippocampal CRH neurons compared to CA1 pyramidal neurons. e, The average input-output curves from CA1 pyramidal neurons (black line) and hippocampal CRH neurons (gray line). f, The average input-output curves from CA1 pyramidal neurons (black line) and hippocampal CRH neurons (gray line) were fit with a Boltzman function. g, The average maximum number of action potentials fired in response to a +100 pA current injection is decreased in hippocampal CRH neurons (gray bars) compared to CA1 pyramidal neurons (black bar). h, The average latency to the first action potential is longer in hippocampal CRH neurons (gray bar) compared to CA1 pyramidal neurons (black bar). i, The average input resistance is decreased in hippocampal CRH neurons (gray bar) compared to CA1 pyramidal neurons (black bar). n=11–13 cells, six to seven mice per experimental group. * denotes statistical significance of $p<0.05$ determined using a Student's t test. j, A representative image of a CA1 pyramidal neuron filled with biocytin at x20 magnification. k, The morphology of a representative CA1 pyramidal neuron is reconstructed. l, Higher magnification (380) of a apical dendrite of a CA1 pyramidal neuron. m, A representative, biocytin filled hippocampal CRH neuron whose cell body resides in stratum pyramidale. n, Reconstruction of the representative hippocampal CRH neuron allows better appreciation of the morphology. o, Higher magnification (x80) of an apical dendrite of a hippocampal CRH neuron whose cell body resides in stratum pyramidale.

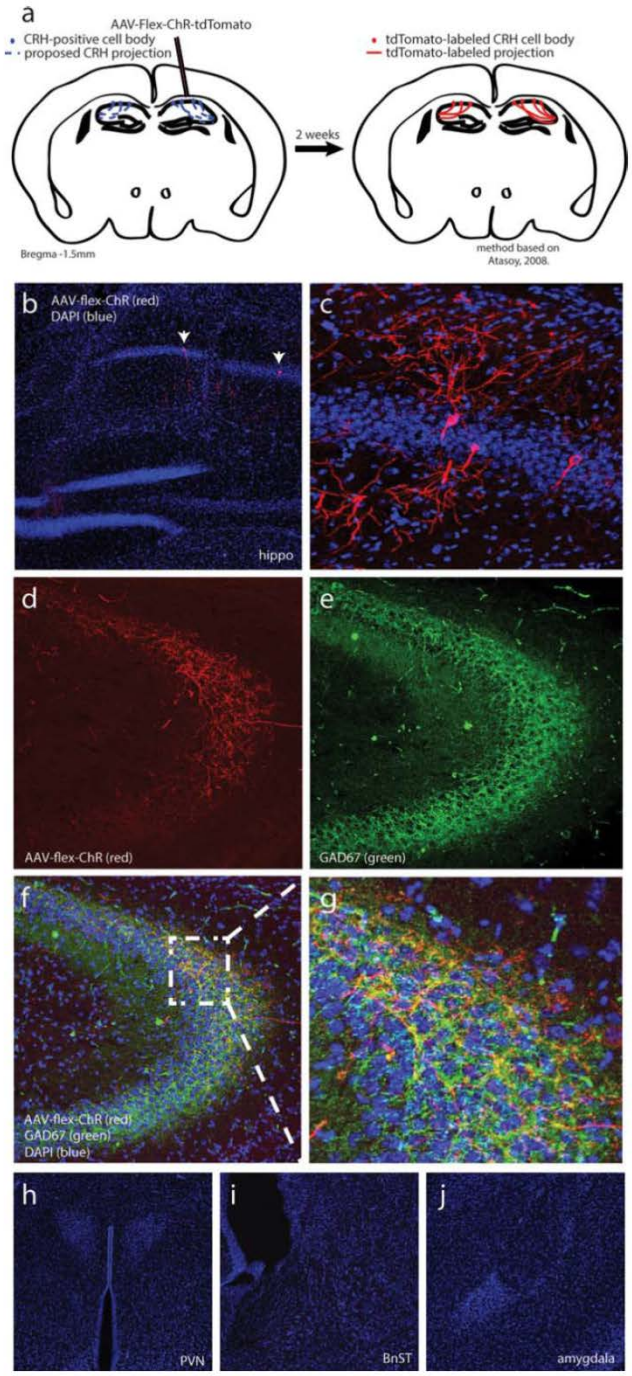

Reproduced from (Hooper and Maguire, 2015)

Figure 7.4. Unique connectivity of hippocampal CRH neurons. a, A schematic of the tract tracing method based on (Atasoy et al., 2008). AAV-Flex-ChR2-tdTomato was stereotaxically injected into the CA1 region of the hippocampus in Crh-Cre mice. After 2 weeks, the expression of tdTomato and projections of hippocampal CRH neurons were visualized using confocal microscopy. b, Representative image of AAV-Flex-ChR2-tdTomato targeting to hippocampal CRH neurons. c, CRH neurons expressing AAV-Flex-ChR2-tdTomato were observed in the CA1 pyramidal cell layer and projections were observed surrounding principal neurons in the CA3 subregion (d). Immunostaining for GAD67 (e) demonstrated colocalization of GAD67 in AAV-Flex-ChR2-tdTomatoexpressing terminals in CA3 (f–g). g, Higher magnification highlights the colocalization of GAD67 in AAV-Flex-ChR2-tdTomato expressing terminals in CA3. AAV-Flex-ChR2-tdTomato targeted to and solely expressed in hippocampal CRH neurons with cell bodies residing in the CA1 pyramidal cell layer (b, arrows) and not in other populations of CRH neurons, such as in the PVN (h), BnST (i), or amygdala (j). AAV-Flex-ChR2-tdTomato=red; DAPI=blue (n=6–10 mice).

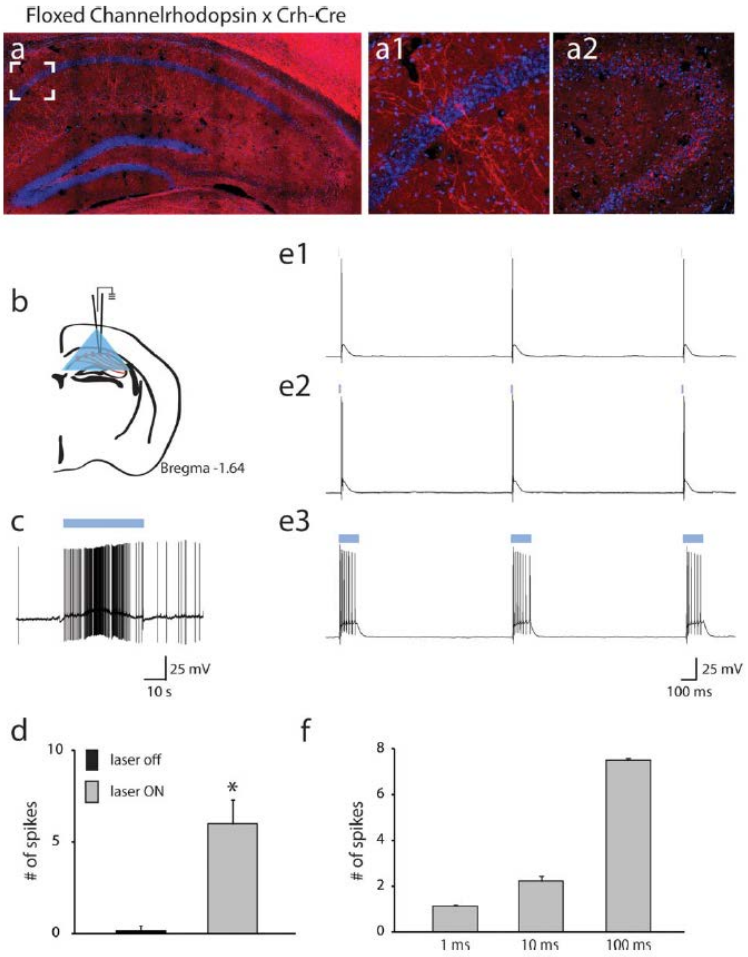

Reproduced from (Hooper and Maguire, 2015)

Figure 7.5. Optogenetic activation of hippocampal CRH neurons. a, tdTomato expression in ChR/Crh mice. a1, Higher magnification of the CA1 pyramidal cell layer highlights the expression of tdTomato in hippocampal CRH neurons, which strongly resembles the expression in the CRH-GFP mice. a2, Higher magnification of the CA3 subregion of the hippocampus reveals dense tdTomato-expressing terminals surrounding the principal neurons, similar to that observed in the CRH-GFP mice. b, A diagram depicting the electrophysiological recording and optogenetic activation of hippocampal CRH neurons in ChR/Crh mice. c, Continuous optogenetic activation increases the spontaneous firing rate of tdTomato-positive CRH neurons in ChR/Crh mice. d, The average spontaneous firing rate of tdTomato-positive CRH neurons in ChR/Crh mice in response to continuous optogenetic activation. e, Optogenetic activation at1 ms (e1), 10 ms (e2), or 100 ms (e3) at 1 Hz elicits action potentials in tdTomato-positive CRH neurons in ChR/Crh mice. f, The average number of spikes fired in response to optogenetic activation at 1, 10, or 100 ms delivered at 1 Hz. n=7 cells, three mice per experimental group. * denotes statistical significance of $p<0.05$ determined using a paired Student's t test.

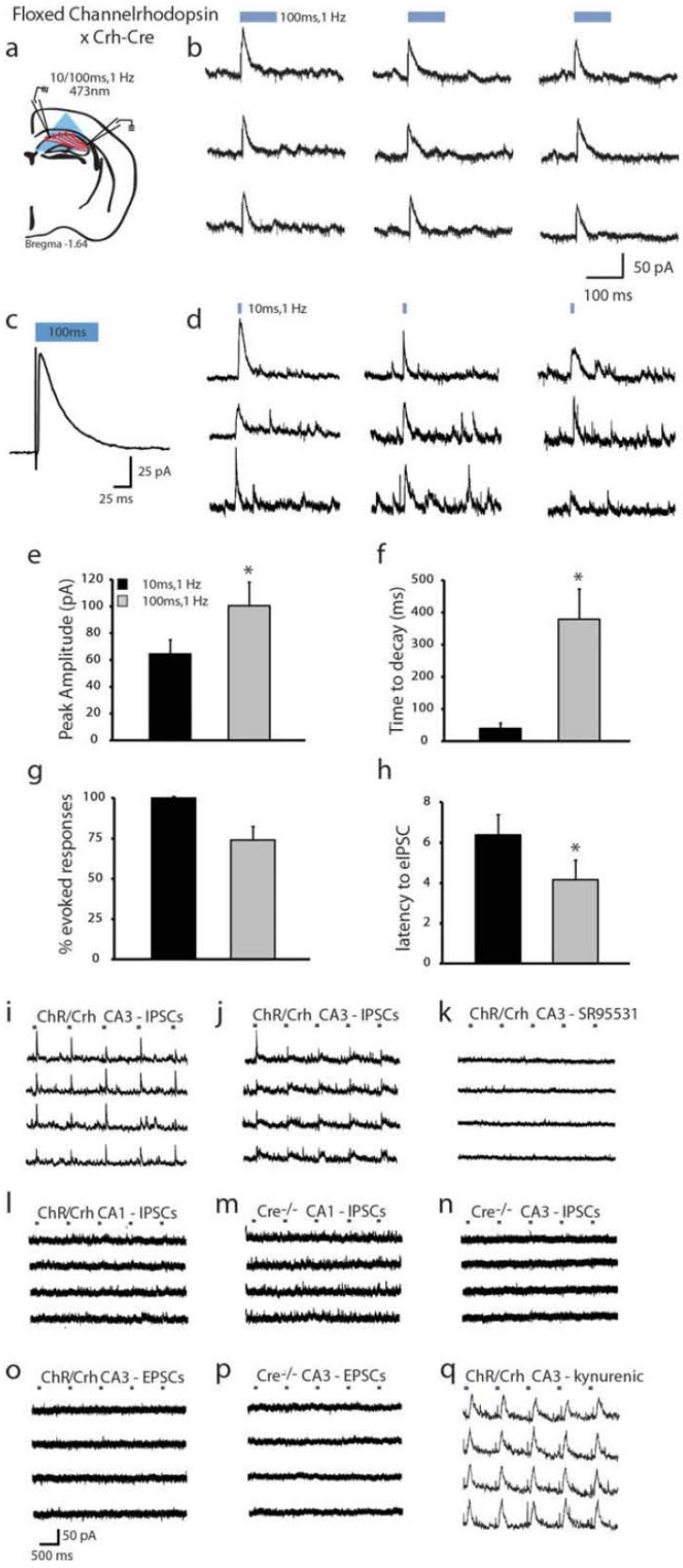
Floxed Channelrhodopsin
x Crh-Cre
a
10/100ms,1 Hz
473nm
Bregma -1.64
b
100ms,1 Hz
50 pA
100 ms
c
100ms
25 pA
25 ms
d
10ms,1 Hz
e
Peak Amplitude (pA)
10ms,1 Hz
100ms,1 Hz
f
Time to decay (ms)
g
% evoked responses
h
latency to eIPSC
i
ChR/Crh CA3 - IPSCs
j
ChR/Crh CA3 - IPSCs
k
ChR/Crh CA3 - SR95531
l
ChR/Crh CA1 - IPSCs
m
Cre-/- CA1 - IPSCs
n
Cre-/- CA3 - IPSCs
o
ChR/Crh CA3 - EPSCs
50 pA
500 ms
p
Cre-/- CA3 - EPSCs
q
ChR/Crh CA3 - kynurenic

Reproduced from (Hooper and Maguire, 2015)

Figure 7.6. Hippocampal CRH neurons make inhibitory connections onto principal neurons in CA3. a, A diagram depicting the optogenetic activation of hippocampal CRH neurons with simultaneous electrophysiological recording of principal neurons in the CA3 or CA1 region of the hippocampus in ChR/Crh mice. b, A representative traces of evoked IPSCs recorded in a CA3 pyramidal neuron in response to 100 ms, 1Hz 473nm laser pulses. c, The average evoked IPSCs recorded in a representative CA3 pyramidal neuron in response to 100 ms, 1 Hz 473-nm laser pulses. The start of the optogenetic activation is shown with a marker preceding the average evoked IPSC making it easy to appreciate the short latency to evoke the IPSC in the postsynaptic cell. d, IPSCs can also be evoked in CA3 pyramidal neurons with shorter, 10 ms, 1Hz 473-nm laser pulses. e, The average peak amplitude of evoked IPSCs recorded in CA3 pyramidal neurons in response to either 10 ms (black bar) or 100 ms (gray bar) 1 Hz 473-nm laser pulses. f, The average 10–90% time to decay is shown for IPSCs evoked with either 10 ms (black bar) or 100 ms (gray bar) 1 Hz 473-nm laser pulses. g, The average number of CA3 pyramidal cells which exhibited evoked IPSCs in response to either 10 ms (black bar) or 100 ms (gray bar) 1 Hz 473-nm laser pulses. h, The average latency to evoke an IPSC in CA3 pyramidal neurons from the beginning of optogenetic activation using either 10 ms (black bar) or 100 ms (gray bar) 1 Hz 473-nm laser pulses. n=12–13 cells, four to five mice per experimental group. * denotes statistical significance of $p<0.05$ determined using a Student's t test. i, A representative recording of evoked IPSCs in CA3 pyramidal neurons in response to 100 ms, 1 Hz 473 nm optogenetic stimulation. j, Representative traces of evoked IPSCs in CA3 pyramidal neurons in the presence of nACSF which are blocked in the presence of >200 mM SR95531 (k) (n=26 cells, 6 mice per experimental group; $p<0.0001$ compared to CA3 neurons from ChR/Crh mice). l, A representative trace demonstrating the lack of evoked IPSCs in CA1 pyramidal neurons from ChR/Crh mice in the presence of 100 ms, 1 Hz 473-nm laser pulses. Representative traces demonstrating the inability to evoke IPSCs in CA1 (m) or CA3 (n) pyramidal neurons from Cre-/- littermates in the presence of 100 ms, 1 Hz 473-nm laser pulses. o–p, Representative traces demonstrating the inability to evoke EPSCs in CA3 pyramidal neurons from ChR/Crh mice (o) or Cre-/- littermates (p) in the presence of 100 ms, 1 Hz 473-nm laser pulses (n=12 cells, three to four mice per experimental group). q, Optogenetically evoked IPSCs in CA3 pyramidal neurons were not blocked by the glutamate receptor antagonist, kynurenic acid (n=6 cells, two mice).

8. Hippocampal CRH neurons: Potent modulators of hippocampal function and excitability

In my initial work on hippocampal CRH neurons, I focused on establishing their identity as GABAergic interneurons and on characterizing their connectivity and intrinsic properties. However, as mentioned previously, the functional relevance of hippocampal CRH neurons has thus far only been assessed in terms of CRH receptor actions in the hippocampus. In order to capture their function in the hippocampal network in a more comprehensive way, here I applied a number of molecular tools to manipulate the activity of hippocampal CRH neurons. I tested the effects of these manipulations on both stress-related emotional behavior and hippocampus-dependent spatial learning and memory tasks. This section contains data and figures from a forthcoming manuscript tentatively titled "Back-projection corticotropin-releasing hormone neurons support spatial learning and potently modulate hippocampal excitability" (Hooper and Maguire, in preparation).

Rationale

Hippocampal interneurons drive the precise timing and synchrony of pyramidal neurons that underlies hippocampus-dependent learning and memory. In addition, specific classes of interneurons are specialized for distinct aspects of this function by their unique domain-selective connectivity, state-dependent changes in activity, and entrainment of populations of pyramidal neurons to oscillation frequency bands. Back-projection CRH interneurons have been suggested to be specialized for mediating stress effects on learning and memory, but to date investigators have focused on these neurons' CRH-secreting activity to the exclusion of GABA. Accordingly, I took a more open-ended approach to assessing back-projection CRH interneurons' functional

relevance, applying tools which stimulate, silence, or ablate this interneuron class selectively and employing a variety of behavioral paradigms to determine the effects of these manipulations. Throughout these experiments, I specifically targeted back-projection CRH interneurons in the dorsal hippocampus.

What brain regions innervate back-projection CRH interneurons?

A general principle of neuropsychiatry is that distinct anatomical regions are functionally specialized: straightforward examples include the precentral gyrus for coordinating contralateral motor tasks, the postcentral gyrus for processing contralateral sensory information, or the occipital cortex for processing visual information from the contralateral visual field. Given this principle, we can expect to glean critical clues regarding the function of back-projection CRH interneurons by determining the brain regions that supply this interneuron class with synaptic input. To this end, I employed a Cre recombinase-dependent monosynaptic retrograde tracing system to label neurons immediately upstream of back-projection CRH interneurons (Wall et al., 2010) (Figure 8.1a). Briefly, the first of this two-virus system (Helper) loads Cre recombinase-expressing cells with three proteins: a green fluorescent protein to label the cells, a surface receptor (TVA) that enables them to endocytose pseudorabies virus, and an envelope glycoprotein that encases pseudorabies, allowing it to infect synaptically connected cells in a retrograde-only fashion. The second virus, pseudorabies (PRV), infiltrates Helper-transduced neurons, encases itself in the envelope glycoprotein, travels one synapse upstream where, in the absence of Cre recombinase, it must remain, and finally transduces the upstream neuron with a red fluorescent protein (RFP) transgene to label the upstream neuron. I stereotaxically injected the Helper virus bilaterally into area CA1 of the hippocampi of adult CRH-Cre mice, waited 3 weeks to allow Helper transduction of CRH neurons, then injected PRV bilaterally to the same

coordinates. After waiting an additional 4 weeks for PRV infection and transduction of upstream neurons, I collected and processed the brains, then imaged sections throughout the entire brain to identify GFP-labeled, Helper-transduced CRH neurons and RFP-labeled, PRV-transduced neurons directly upstream of them (n=9 mice) (see Table 8.1). As expected, Helper virus expression was largely confined to stratum pyramidale of CA1 where back-projection CRH interneurons reside (Figure 8.1b). Moderate expression of PRV was identified in the dentate gyrus (Figure 8.1c) and stratum pyramidale of CA1 (not shown). None of the PRV-labeled neurons in CA1 demonstrated colocalization with the Helper virus GFP marker, suggesting that these upstream neurons in CA1 are pyramidal cells and not back-projection CRH interneurons. Unexpectedly, robust PRV expression was found widely throughout neocortical regions (Figure 8.1d). The largest populations of PRV-labeled neurons were in layer 2/3 of primary and secondary somatosensory, auditory, and visual cortex; however, PRV expression was not confined to these areas but rather found at least sparsely in every neocortical region examined. The diffuse distribution of upstream neurons throughout neocortex makes it difficult to postulate the specific functional significance of these synaptic inputs. However, these retrograde tracing results reveal yet another intriguing unique feature of back-projection CRH interneurons: their apparent primary source of synaptic input bypasses the dentate gyrus to project directly from neocortex to CA1.

How do back-projection CRH interneurons modulate their activity in response to stress and in other brain states?

One obvious indicator that a class of neurons is functionally relevant to a given state is a significant change in their level of activity during said state. Accordingly, I applied a variety of stimuli to CRH-Ai9 mice, whose CRH neurons are labeled with tdTomato, then stained

hippocampal brain sections for the immediate early gene c-fos, a transcription factor which is translated and translocated to the nucleus along a well-defined time course in response to periods of high neuronal activity (Caputto and Guido, 2000). Using confocal microscopy, I measured the colocalization of c-fos immunofluorescence with the CRH reporter and expressed population activity as a ratio of c-fos- and reporter-positive neurons to total report-positive neurons (n=2-4 mice per experimental group) (see Figure 8.2a). In agreement with our electrophysiological characterization in the previous study, back-projection CRH neurons demonstrate low levels of activity basally (8.33±2.34% colocalization) (Figure 8.2b). In order to validate the approach of c-fos colocalization as an indicator of high activity, I applied *in vivo* optical stimulation of back-projection CRH interneurons in ChR/CRH mice, which express Channelrhodopsin and a red fluorescent protein marker specifically in CRH neurons. Optical stimulation was sufficient to significantly elevate back-projection CRH interneuron levels of c-fos (29.20±3.69% colocalization)) compared to their basal levels, indicating that this technique is sensitive to increases in activity (Figure 8.2c). Surprisingly, after the acute stress of one 30-minute restraint, the activity of CRH neurons did not change significantly (1.85±2.56% colocalization). Similarly, the chronic stress paradigm of 14 consecutive daily 30-minute restraint sessions did not alter the induction of c-fos in these neurons either (6.76±4.36% colocalization). In contrast, CRH neurons in the PVN did demonstrate significantly greater induction of c-fos following acute stress compared to unstressed controls (Figure 8.2e), affirming that our restraint protocols activate the HPA axis as expected. I next tested whether a different form of psychological stress might significantly recruit back-projection CRH interneurons by applying the fear acquisition paradigm, wherein mice receive two aversive foot shocks paired with loud auditory tones. This approach resulted in a trend toward a slight increase in c-fos induction (11.59±1.47% colocalization) compared to minimally-handled controls. Finally, I induced acute

seizures using the systemic KA model, and found that, in addition to an obvious widespread induction of c-fos among pyramidal neurons, c-fos expression is also greatly increased in back-projection CRH interneurons following seizures (60.77±15.11% colocalization) compared to saline-injected controls (2.66±1.05% colocalization) (n=4 mice per experimental group; $p<0.01$ using an unpaired Student's *t*-test) (Figure 8.2d). Together these data reveal an unexpected dearth of stress-reactivity among back-projection CRH interneurons, and massive activation of this population during provoked seizures. While surprising, these data can be interpreted to support our previously-stated hypothesis that back-projection CRH interneurons are functionally specialized to constrain the excitability of the hippocampal network, rather than specifically mediating stress effects on emotional behavior and information processing.

Do back-projection CRH interneurons play a role in modulating stress-reactive behaviors?

Pharmacology of the CRH receptor in the hippocampus previously revealed an association between hippocampal CRH and stress effects on learning and memory (Chen et al., 2010;Chen et al., 2012). I therefore tested the hypothesis that manipulating back-projection CRH interneuron activity would significantly impact emotional, stress-reactive behavior. I began by assessing anxiety-like behavior in the open field, light-dark box, and elevated plus maze paradigms. First I activated dorsal hippocampal back-projection CRH interneurons using an optical fiber implanted in the hippocampus of ChR/CRH mice to activate ChR with a 473 nm laser with 50 msec pulses delivered at 20 Hz. Laser activation of back-projection CRH interneurons during the open field test had no effect on locomotor activity (2330±136 basic movements) or anxiety-like behavior (22.15±3.24% time in center) compared to Cre-negative controls who received laser but did not express ChR (2459±115 basic movements; 21.31±2.84% time in center) (n=11-14 mice per experimental group). Similarly, in the elevated plus maze,

optical stimulation of back-projection CRH interneurons did not significantly alter locomotor activity (599±59 basic movements) or anxiety-like behavior (9.30±4.31% time in open arm) compared to Cre-negative controls (663±55 basic movements; 14.30±5.20% time in open arm) (n=10 mice per experimental condition). Next, I silenced back-projection CRH interneurons using Cre-dependent inhibitory designer receptors exclusively activated by designer drugs (G_i-DREADDs), virally expressed by stereotaxic injection into area CA1 of CRH-Cre mice. In the open field test, activation of G_i-DREADDs by the selective ligand CNO to silence back-projection CRH interneurons had no effect on anxiety-like behavior (17.40±1.99% time in center), compared to controls that received CNO but lacked DREADDs (13.25±2.16% time in center). Surprisingly though, silencing back-projection CRH interneurons resulted in a striking locomotor hyperactivity phenotype (Gi-DREADD: 3696±242 basic movements; control: 2605±169 basic movements) (n=12-16 mice per experimental group) (Figure 8.3a). Similar results were obtained in the light-dark box paradigm, where silencing CRH neurons had no significant impact on anxiety-like behavior (31.59±2.83% time in light compartment) but caused a significant increase in locomotor activity (2435±115 basic movements) compared to controls (21.96±6.34% time in light compartment; 1788±74 basic movements) (n=12-16 mice per experimental group) (Figure 8.3b). Finally I applied a Cre recombinase-dependent diphtheria toxin A subunit-encoding virus (AAV-DTA) to selectively kill back-projection CRH neurons by stereotaxic injection to the CA1 region of CRH-Cre mice. In the open field, while this manipulation had no effect on anxiety-like behavior (19.71±1.92% time in center) compared to controls (19.37±2.09% time in center), it did produce a subtle, non-significant trend toward locomotor hyperactivity (AAV-DTA: 3267±187 basic movements; control: 3011±163 basic movements) (n=13 mice per experimental group). Likewise, in the light-dark box, selectively killing back-projection CRH interneurons had no impact on anxiety-like behavior (AAV-DTA:

22.42±3.90% time in light compartment; control: 20.30±3.02% time in light compartment) and a slight trend toward increased locomotor activity (AAV-DTA: 2061±144 basic movements; control: 1888±94.7 basic movements) (n=13 mice per experimental group). Together these data indicate that manipulating back-projection CRH interneuron activity does not give rise to any alterations in anxiety-like behavior, while suppressing their activity transiently or permanently have differential effects on locomotor activity. The latter observation might be explained by compensatory adjustments within the relevant circuits that are only brought on by the chronic manipulation.

Since depression-like behavior is also altered in stress states, I next assessed the effect of manipulating back-projection CRH interneurons in the forced swim test, a model of depression-like behavior. Silencing this population had no impact on the latency to the first bout of immobility (86.7±5.0 sec) or the total time spent immobile (193.9±10.1 sec) compared to controls (98.4±13.4 sec latency; 197.8±8.7 sec total immobility), nor did selective ablation (AAV-DTA: 65.3±11.7 sec latency, 209.0±20.4 sec total immobility; control: 72.9±14.4 sec latency; 218.4±15.7 sec total immobility) (n=9-12 mice per experimental group) (Figure 8.3c, d). Together, these experiments on anxiety-like and depression-like behavior suggest that back-projection CRH interneurons are not critical for mediating stress effects on emotional behavior generally, but reveal that transiently removing them from the network has a profound impact on locomotor activity. The finding that a hippocampal-specific manipulation can produce a hyperactivity phenotype – as opposed to impacting the cognitive processes required for successful navigation, or emotional states related to locomotor activity – is novel so far as I can tell. Thus, the specific circuit-level mechanism underlying this behavioral effect is currently unknown, but a promising avenue for further exploration is the putative "control system" that

inhibits basal locomotor tone, connecting the entorhinal cortex to the olfactory bulb by way of the hippocampus, septum, and prefrontal cortex (Viggiano, 2008).

Do back-projection CRH interneurons play a role in hippocampus-dependent learning and memory?

Given the singular importance of inhibitory neurotransmission in cognition, I anticipated that manipulating back-projection CRH interneurons could impact performance of hippocampus-dependent learning and memory tasks. I therefore assessed the effect of manipulating this population on memory acquisition in a fear conditioning experiment, where both the context of the fear conditioning chamber and the cue of a loud auditory tone are paired with aversive foot shocks. Optogenetic stimulation of back-projection CRH interneurons during fear acquisition had no effect on mice's subsequent contextual (37.55±7.37% freezing) or cued (23.20±4.20% freezing) memory retrieval compared to Cre-negative controls (context: 33.60±6.33% freezing; cued: 16.46±3.65% freezing) (n=12-14 mice per experimental group). Similarly, Gi-DREADD-mediated silencing of back-projection CRH interneurons during acquisition did not significantly impact contextual (25.78±4.35% freezing) or cued (28.13±5.51% freezing) memory retrieval compared to AAV-GFP-injected controls (context: 35.50±7.39% freezing; cued: 39.84±5.34% freezing) (n=13-15 mice per experimental group). Additionally, selective ablation of this interneuron population had no effect on contextual (25.83±4.30% freezing) or cued (35.72±7.12% freezing) fear memory retrieval compared to controls (context: 34.22±5.01% freezing; cued: 36.63±6.37% freezing) (n=13 mice per experimental group). However, both the acute (Gi-DREADD) and chronic (AAV-DTA) suppression approaches produced trends toward impaired performance in the contextual memory retrieval task, and the previous revelation of a locomotor hyperactivity phenotype in the open field and light-dark box urged

caution in interpreting the results of this learning and memory paradigm. Therefore, I followed up on this experiment by using an alternative spatial learning paradigm that internally controls for changes in locomotor activity, the object recognition memory (ORM) test. In agreement with the locomotor hyperactivity effect observed in the open field and light-dark box, ORM revealed an increase in total object explorations caused by both acute and chronic suppression of CRH interneurons that both acute (G_i-DREADD: 85±6 explorations; control: 71±7 explorations) and chronic suppression of CRH interneurons (AAV-DTA: 76±6 explorations; control: 66±8 explorations) caused an increase in total object explorations (n=9-13 mice per experimental group). Furthermore, while the ratio of novel-to-familiar exploration was similar between experimental and control mice in the 24-hour retention test, the 3-hour retention test revealed a trend toward a memory deficit specifically among AAV-DTA mice (1.01±0.10) compared to controls (1.45±0.24) (Figure 8.4b). The time-dependence of this effect may reflect differences in task difficulty: while memory of the familiar object is quite robust at 24 hours, control animals show a significant but comparatively weak preference for the novel object at 3 hours, indicating that familiarity is not as ingrained and thus perhaps more vulnerable to disruption at this earlier retention interval. Considering that back-projection CRH interneurons are just one of over 20 classes of hippocampal interneuron, it is remarkable that their selective removal from the network is sufficient to significantly impair spatial learning and memory, highlighting their importance in hippocampal network function.

How does back-projection CRH interneuron activity modulate acute seizure susceptibility?

My experiments thus far revealed no strong links between back-projection CRH interneuron activity and stress-related behavior, casting doubt on the hypothesis that this population might mediate stress effects on seizure susceptibility. However, hippocampal interneurons are known

to be disproportionately impacted by epileptic sclerosis (Marx et al., 2013), and interneuron-precursor grafts into the hippocampus demonstrate potent anti-epileptic properties (Hunt et al., 2013), so CRH interneurons' impact on seizure susceptibility remained an important question. Therefore, we applied EEG recording in conjunction with optogenetic stimulation, chemogenetic inhibition, or selective ablation of back-projection CRH interneurons to the systemic KA model of acute seizures. Interestingly, preliminary data from optogenetic stimulation of CRH interneurons indicates a robust anti-convulsant effect, markedly reducing the total time of electrographic seizures across the 2-hour recording period compared to Cre-negative controls even in a single cohort (n=2 mice per experimental group; $p<0.05$ using a Student's unpaired *t*-test) (Figure 8.5a). Silencing CRH interneurons with Gi-DREADD demonstrated a trend toward the opposite effect, increasing the duration of each episode of epileptiform activity (685.14±291.64 sec) compared to AAV-GFP controls (397.21±166.40 sec) (n=8-11 mice per experimental group) (Figure 8.5b). Similarly, selectively ablating this population with AAV-DTA resulted in a trend toward a slight increase in the average duration of each episode of epileptiform activity (396.69±109.17 sec) compared to controls (312.04±185.97 sec) as well as a trend toward an increase in the total time spent seizing (AAV-DTA: 50.05±7.42%; control: 28.28±8.74%; $p=0.078$ using a Student's unpaired *t*-test) (n=9-10 mice per experimental group) (Figure 8.5c). Importantly, a subset of control animals in the silencing and ablation experiments exhibited long periods of low-frequency interictal spikes. Because these spikes were included in my analysis of total epileptiform activity, this subset positively skewed the control groups' average seizure durations. Even without correcting for this however, the divergent effects of activating or suppressing CRH interneurons on the severity of acute seizures are clear and congruent with the anticipated effects of respectively increasing or

decreasing GABAergic constraint of area CA3. Once again, our results highlight the potency of this single class of interneurons in influencing the excitability of the hippocampal network.

What is the circuit-level mechanism underlying back-projection CRH interneurons' impact on excitability?

Back-projection CRH interneurons' unique connectivity, combined with their apparent critical role in modulating hippocampal excitability, suggest that their functional relevance in the trisynaptic circuit is tied to their inhibitory constraint of the mossy fiber-CA3 pathway. In order to test this hypothesis at the level of the circuit and bridge our earlier optogenetics-patch clamp experiments and recent *in vivo* findings, I used a field recording approach in conjunction with optogenetics. In acute hippocampal slices from ChR/CRH mice and Cre-negative littermates, I electrically stimulated the mossy fiber-CA3 pathway at a constant intensity and increasing pulse widths while recording the population response from stratum radiatum of CA3 to generate an input-output curve. After a 5 minute "recovery" period to avoid complications of short-term plasticity induction, I generated another input-output curve, this time in the presence of laser stimulation. Finally, I compared the peak field excitatory postsynaptic potentials (fEPSPs) and the parameters of the two input-output curves. As expected, Cre-negative control slices demonstrated no effect of laser stimulation on peak fEPSP (laser off: -26±7.1 μV; laser on: -26±9.0 μV) or input-output curve half-width (laser off: 124.0±10.6 μsec; laser on: 123.6±13.5 μsec). On the other hand, in ChR/CRH slices, laser stimulation profoundly suppressed the peak fEPSP (laser off: -22±7.7 μV; laser on: -14±6.7 μV) without impacting the input-output half-width (laser off: 128.4±10.3 μsec; laser on: 126.2±16.3 μsec). This indicates that back-projection CRH interneurons potently suppress excitability of the mossy fiber-CA3 pathway, not by altering the excitability of the afferent fibers themselves, but by acting as a gain modulator, flatly

suppressing the amplitude of the postsynaptic response through potent hyperpolarizing or shunting inhibition.

Significance

Taken together, our results demonstrate that CRH interneurons' unique back-projecting connectivity place them in a critical role for restraining the excitability of the hippocampal network, and that modulation of their activity is potentially important for both physiological functions like learning and memory, and pathological mechanisms such as seizure susceptibility. Surprisingly, the modulation of CRH interneurons' activity appears to be largely uncoupled from stress signaling, though more work is needed to rule out the possibility that the population is specialized to detect certain types or features of stressors. Additionally, we do not yet know if back-projection CRH interneurons synchronize or entrain their postsynaptic targets to any hippocampal oscillations, and this too will be a critical aspect of their functional relevance to information processing and memory consolidation. Finally, it is possible that GABAergic signaling from this population dictates its functional relevance only under certain states, while in other states CRH signaling plays a distinct and critical role. Indeed, the question of how synaptic and peptidergic signaling from an individual neuron class either cooperate or compete is one that we have not yet begun to address in any neuronal population, let alone in back-projection CRH interneurons.

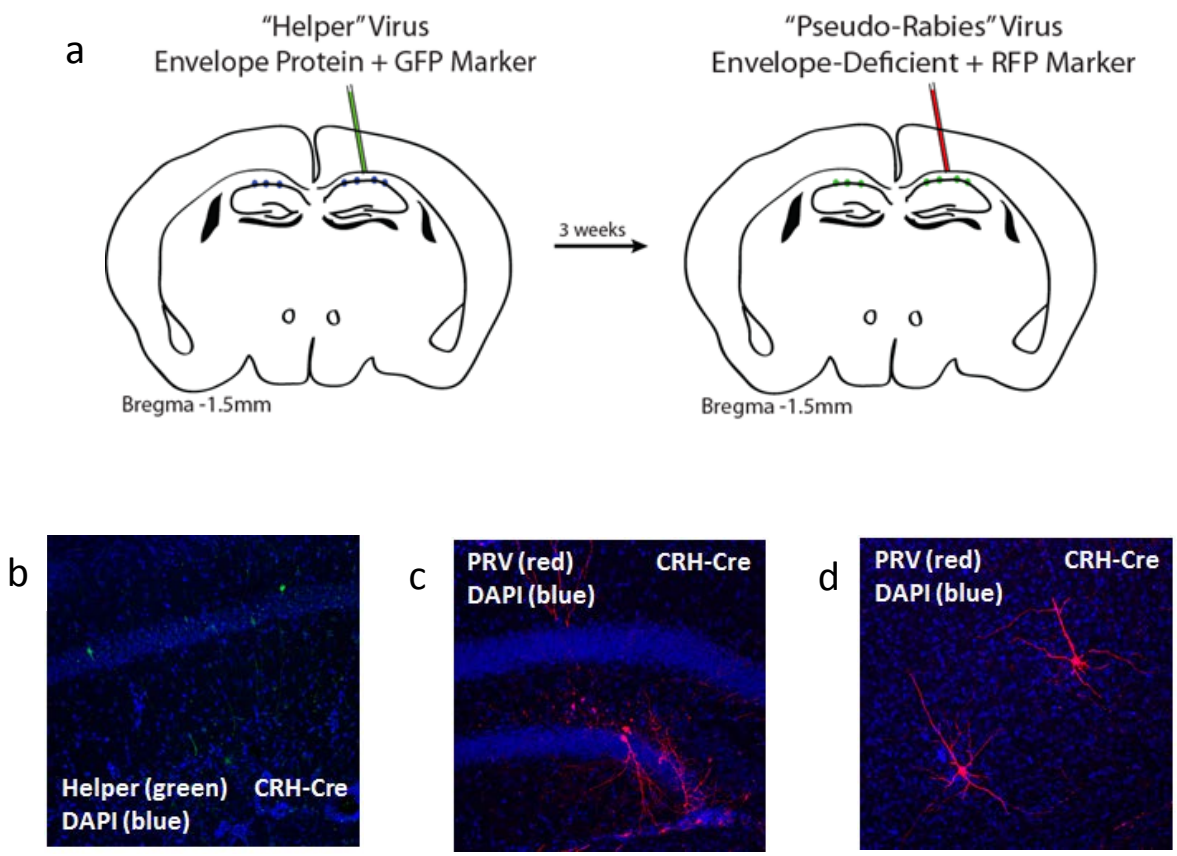

Figure 8.1. Identification of synaptic afferents to back-projections CRH interneurons . (a) Schematic illustrating monosynaptic retrograde tracing approach. Helper virus was injected into the CA1 region of CRH-Cre mice. After a 3-week interval to allow Helper expression, the Helper-dependent Pseudorabies virus was injected into the same site to label neurons one synapse upstream of back-projection CRH interneurons. (b) Representative images of Helper virus-encoded GFP in CA1 stratum pyramidale (left), and Pseudorabies virus-encoded RFP in the dentate gyrus (middle) and layer 2/3 primary somatosensory cortex (right) (n=9 mice).

	Helper-positive	Pseudorabies-positive
Hippocampus - CA1	100% (14)	88.9% (4)
Hippocampus - CA3	0	55.6% (1)
Hippocampus - Dentate Gyrus	77.8% (2)	88.9% (4)
Neocortex	0	100% (20)
Fimbria	0	33.3% (*)
Septal Nucleus	0	33.3% (*)

Table 8.1. Summary of back-projection CRH neuron monosynaptic retrograde tracing results. Results are reported as the percentage of injected CRH-Cre mice (n=9) demonstrating expression in each region; in parentheses is the median number of virus-positive cells, and * denotes brain regions where virus expression was limited to fibers rather than cell bodies. The majority of Helper-labeled neurons were identified in stratum pyramidale of CA1, while most Pseudorabies-transduced upstream neurons resided throughout neocortex.

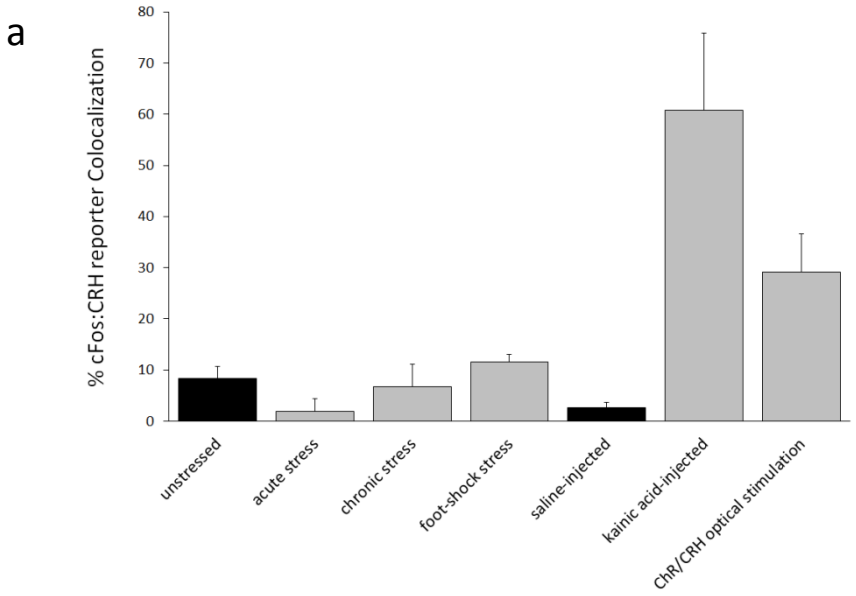
a
% cFos:CRH reporter Colocalization
80
70
60
50
40
30
20
10
0
unstressed
acute stress
chronic stress
foot-shock stress
saline-injected
kainic acid-injected
ChR/CRH optical stimulation

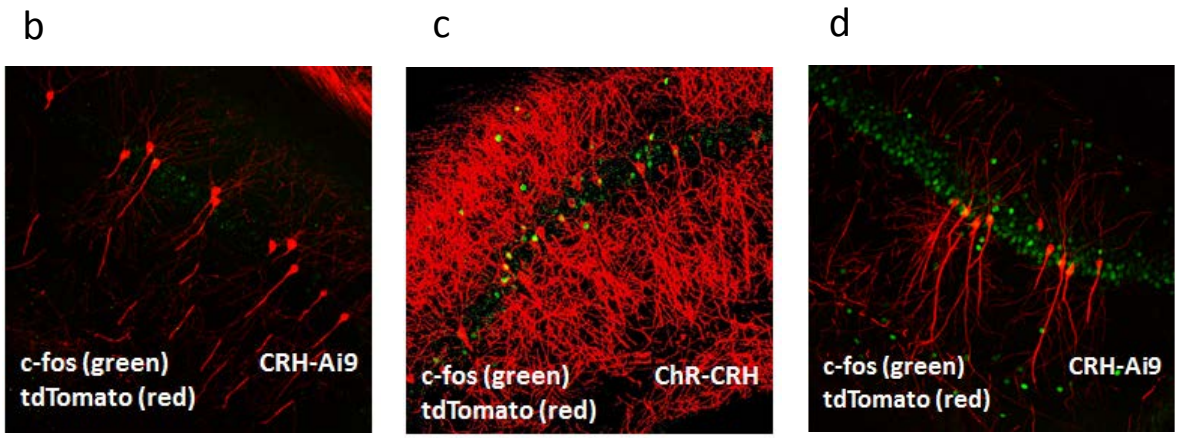
b
c-fos (green)
tdTomato (red)
CRH-Ai9
c
c-fos (green)
tdTomato (red)
ChR-CRH
d
c-fos (green)
tdTomato (red)
CRH-Ai9

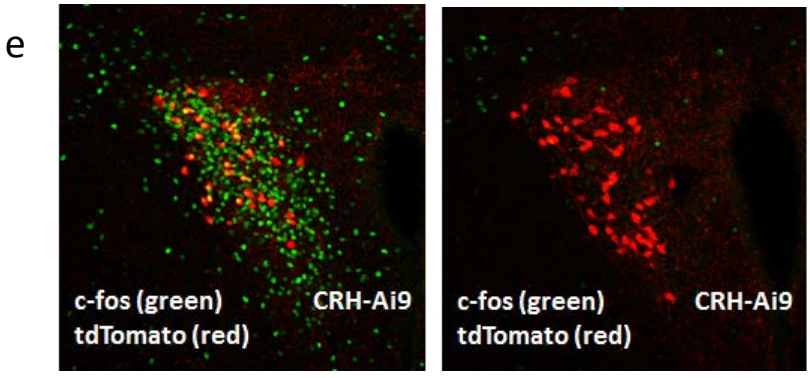
e
c-fos (green)
tdTomato (red)
CRH-Ai9
c-fos (green)
tdTomato (red)
CRH-Ai9

Figure 8.2. Induction of activity marker c-fos in CRH neurons. (a) Summary of c-fos:CRH reporter colocalization by experimental condition. (b-d) Representative confocal images of back-projection CRH neurons (red) demonstrate low basal c-fos induction (green) (a) and robust induction of c-fos by either optical stimulation (b) or KA-induced acute seizures (c). (e) Representative images of PVN CRH neurons (red) following acute restraint stress (left) or from minimally-handled control mice (right). c-fos (green) in the PVN is heavily induced by acute stress.

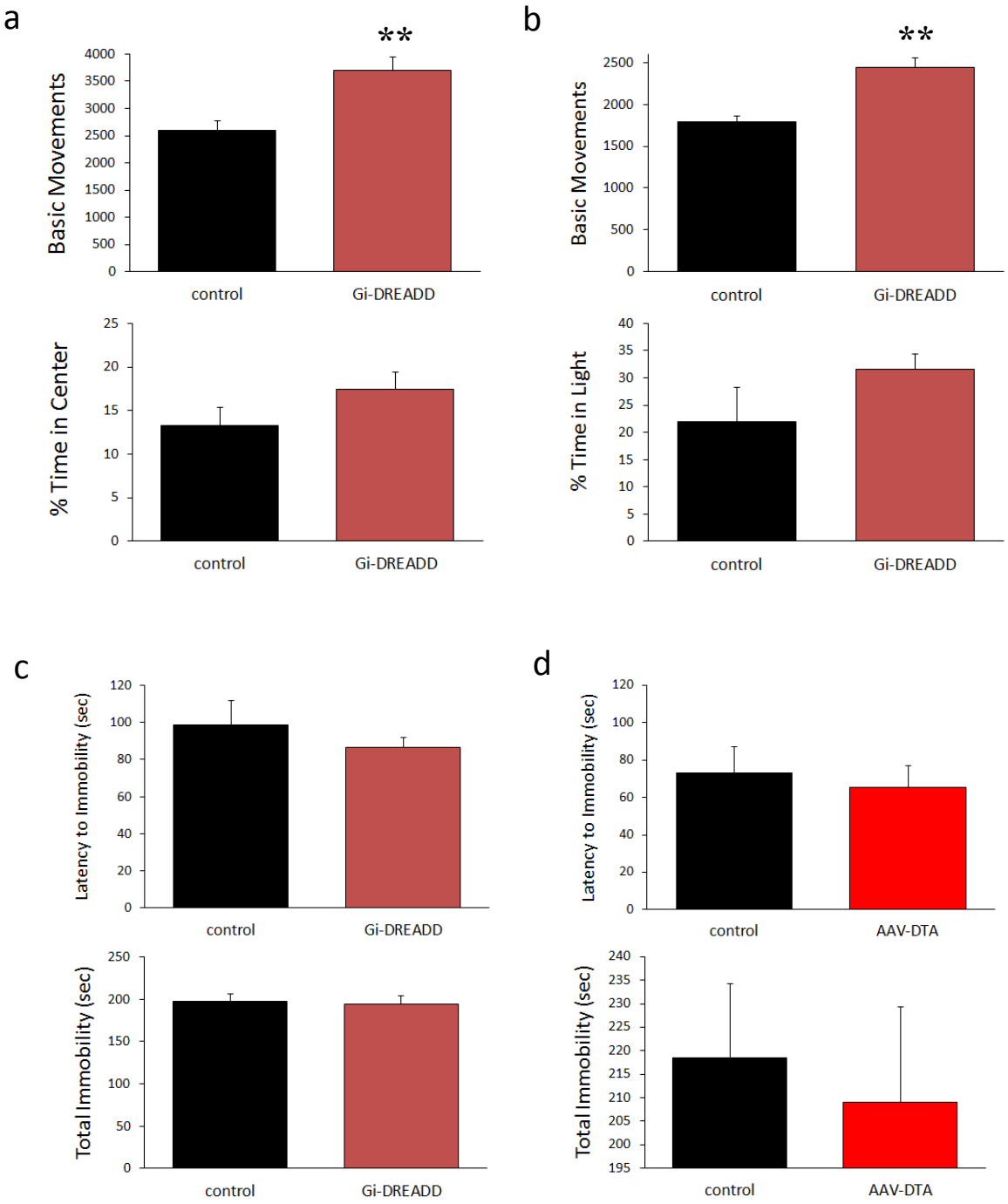
a
**
Basic Movements
4000
3500
3000
2500
2000
1500
1000
500
0
control
Gi-DREADD
% Time in Center
25
20
15
10
5
0
control
Gi-DREADD
b
**
Basic Movements
2500
2000
1500
1000
500
0
control
Gi-DREADD
% Time in Light
40
35
30
25
20
15
10
5
0
control
Gi-DREADD
c
Latency to Immobility (sec)
120
100
80
60
40
20
0
control
Gi-DREADD
Total Immobility (sec)
250
200
150
100
50
0
control
Gi-DREADD
d
Latency to Immobility (sec)
120
100
80
60
40
20
0
control
AAV-DTA
Total Immobility (sec)
240
235
230
225
220
215
210
205
200
195
control
AAV-DTA

Figure 8.3. Silencing back-projection CRH neurons spares emotional behavior and causes locomotor hyperactivity. (a) Results of open field test reveal that selectively silencing back-projection CRH interneurons significantly increased locomotor activity (top) but did not influence anxiety-like behavior (bottom) (n=12-16 mice per experimental group). (b) Results from light-dark box paradigm reveal silencing with G_i-DREADDs produces a significant locomotor hyperactivity phenotype with no effect on anxiety-like behavior compared to AAV-GFP-injected controls. (c) Forced swim test results showed no effect of G_i-DREADD silencing on depression-like behavior (n=9-12 mice per experimental group). (d) Forced swim test results following AAV-DTA-mediated selective ablation of back-projection CRH interneurons revealed no effect on depression-like behavior compared to AAV-GFP controls (n=9 mice per experimental group). ** denotes statistical significance at $p<0.01$

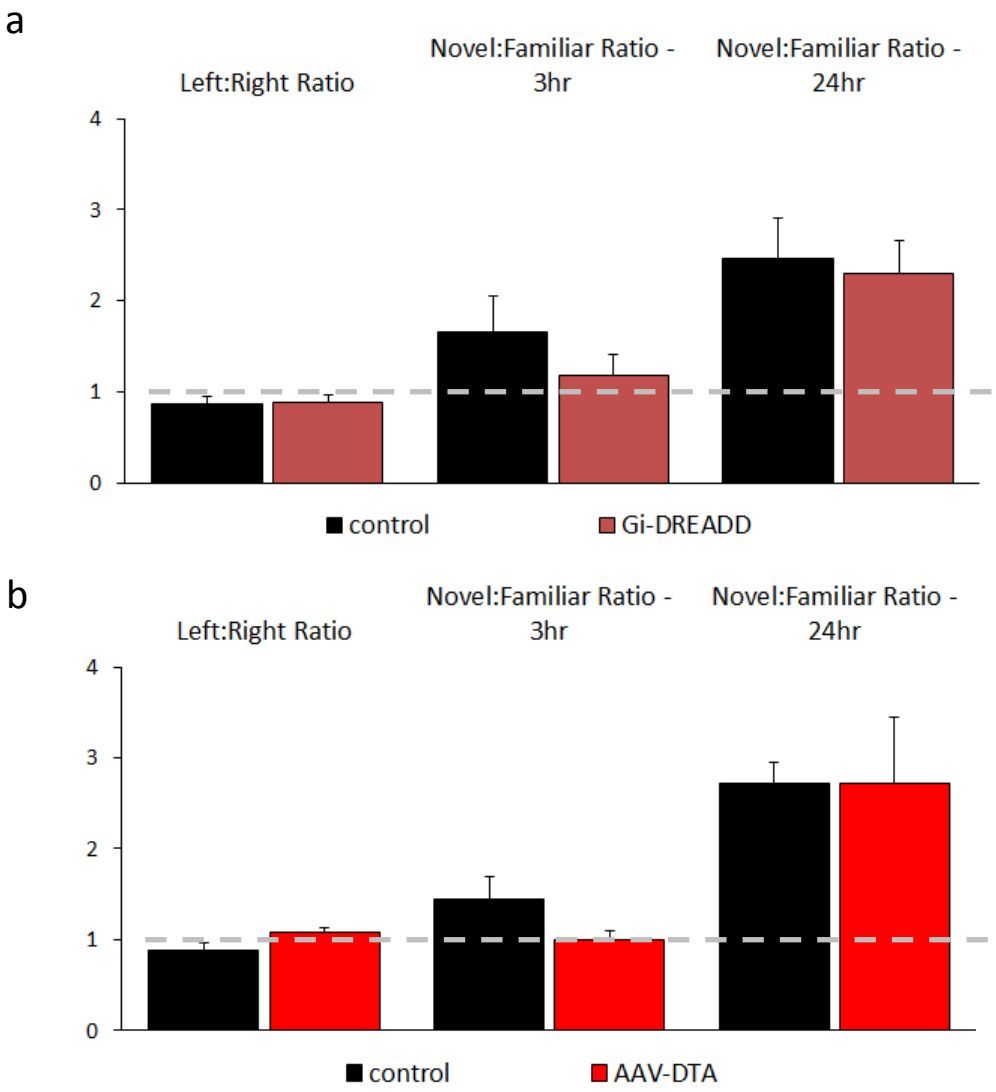

Figure 8.4. Ablating back-projection CRH interneurons impairs object recognition memory. (a) Results of object recognition memory test after selective silencing of CRH neurons during training by G_i-DREADD. Selective silencing did not impact left:right preference or memory at 24 hr, but produced a moderate, non-significant reduction in performance at 3 hr (n=9-12 mice per experimental group). (b) Results of object recognition memory test after selective ablation of CRH neurons by AAV-DTA. Selective ablation did not impact the preference for one side of the enclosure over the other (left:right ratio) or spatial memory at the 24 hr retention interval, but reduced novel object discrimination to the level of chance (grey dashed line) at the 3 hr retention interval (n=9 mice per experimental group) (p=0.071; power=0.55).

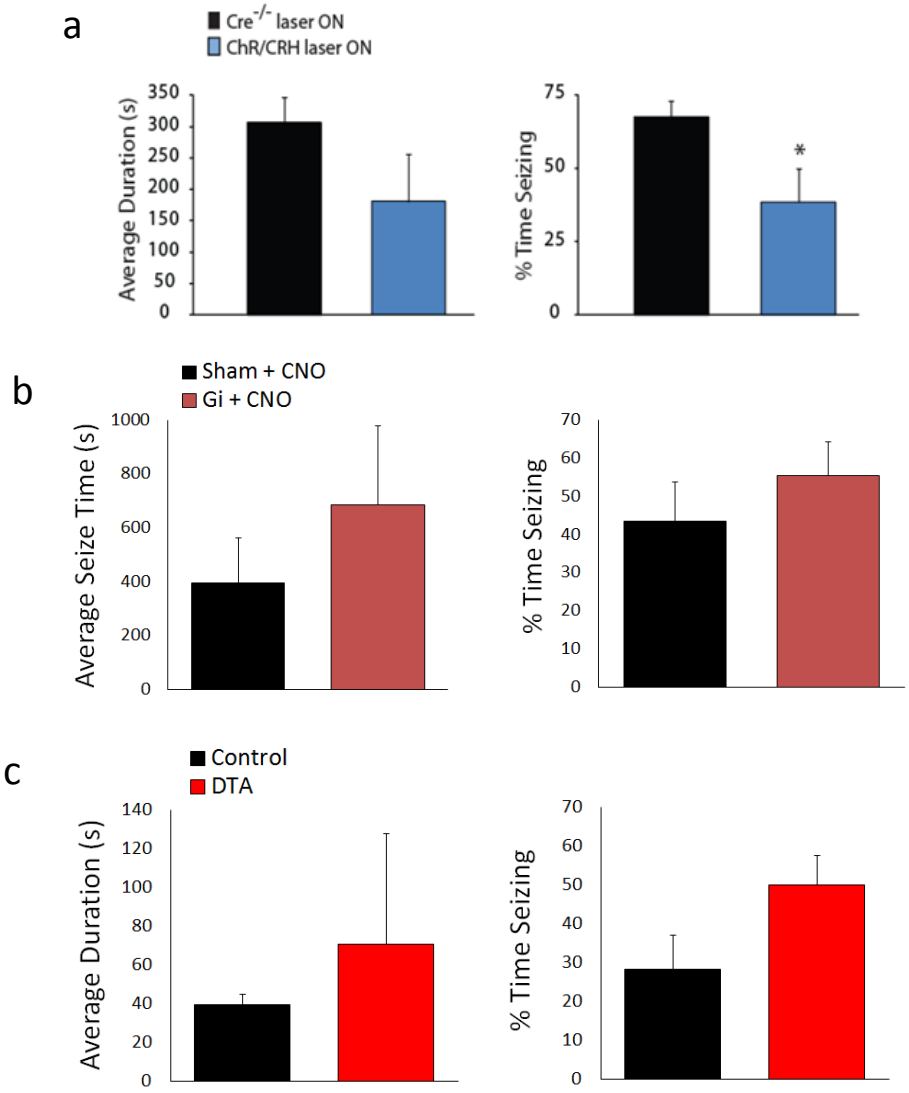

Figure 8.5. Back-projection CRH interneuron activity is anti-convulsant in the KA model. (a) Preliminary KA-induced seizure susceptibility results indicate that optogenetic stimulation of back-projection CRH interneurons reduces the total time seizing (right) (n=2 mice per experimental group). (b) Mice undergoing KA-induced seizures while CRH neurons are selectively silenced by G_i-DREADD exhibit trends toward longer seizures (left) and increased total time seizing (right) (n=8-11 mice per experimental group). (c) Mice undergoing KA-induced seizures following selective ablation of CRH neurons by AAV-DTA demonstrate a trend toward an increase in time seizing (right) compared to AAV-GFP-injected controls (n=9-10 mice per experimental group).

a

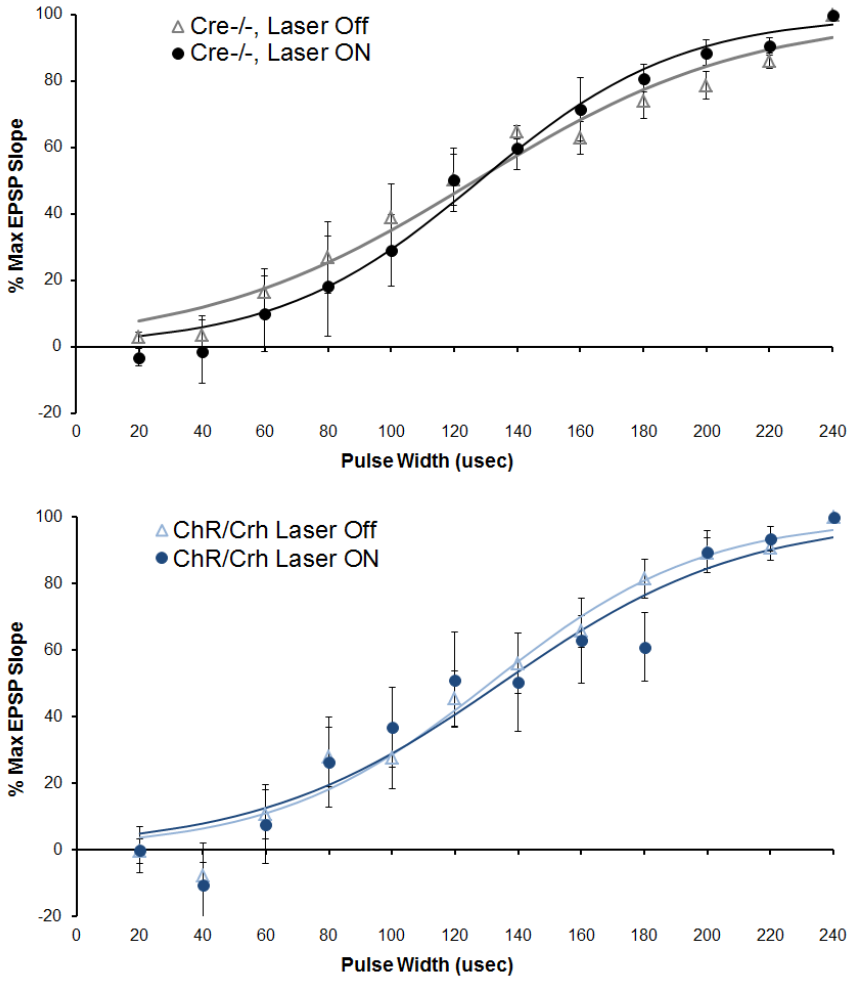
Cre-/-, Laser Off
Cre-/-, Laser ON
% Max EPSP Slope
Pulse Width (usec)
ChR/Crh Laser Off
ChR/Crh Laser ON
% Max EPSP Slope
Pulse Width (usec)

b

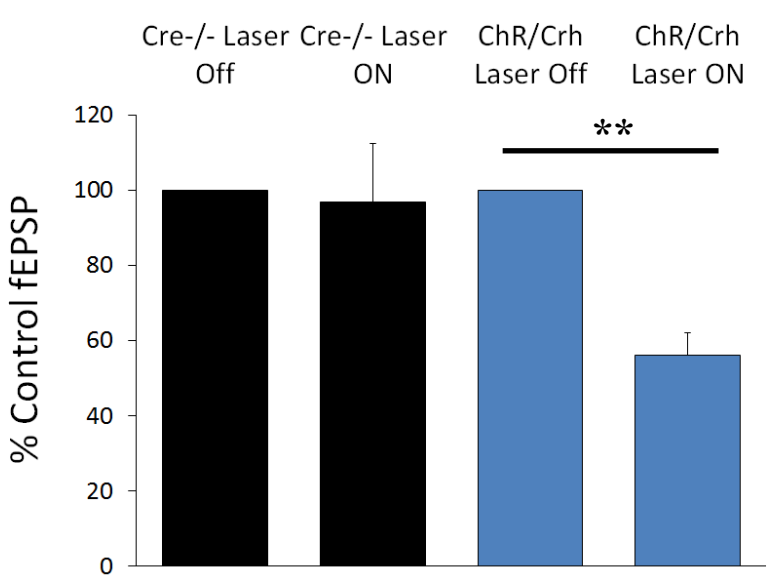
Cre-/- Laser Off
Cre-/- Laser ON
ChR/Crh Laser Off
ChR/Crh Laser ON
**
% Control fEPSP

Figure 8.6. Back-projection CRH interneuron activation suppresses mossy fiber-CA3 postsynaptic response amplitude. (a) Input-output data (points) fit with Boltzmann functions (curves), from Cre-negative control slices (top) and ChR/CRH slices (bottom), both of which received laser stimulation throughout generation of the second input-output curve. There was no change in input-output relationship within each genotype, demonstrating that optical stimulation of CRH neurons does not affect excitability of afferent mossy fibers. (b) Summary of peak amplitudes of electrically evoked fEPSP across genotypes and laser stimulation conditions. While Cre-negative fEPSPs were unaffected by laser stimulation, ChR/CRH slices demonstrate a striking reduction in peak amplitude (n=5-7 slices, 4 mice per experimental group). ** denotes statistical significance at $p<0.01$ using a paired Student's *t*-test

Conclusions and Future Directions

9.1. Inhibitory neurotransmission in the paraventricular nucleus of the hypothalamus

Significance

Our investigation of the relationship between seizure susceptibility and HPA axis activity highlights KCC2 as a highly attractive drug target. Substantial clinical evidence implicates HPA axis dysregulation not only in the co-occurrence of psychiatric disorders with epilepsy but also as a direct link to seizure susceptibility (de Kloet et al., 2005;Tellez-Zenteno et al., 2007), while our results implicate KCC2 as a critical molecular substrate of this link. Thus, drugs that are capable of rescuing or enhancing KCC2 function in the PVN directly – or acting indirectly through targets that serve the common goal of normalizing chloride homeostasis – should be actively pursued for their potential impact on stress-related pathological conditions including seizure susceptibility.

Collectively the results of my manipulations of KCC2 transporter function suggest an intriguing disconnect between developmental and adult-specific knockout in the PVN: stress-related functions are spared in the CRH-KCC2 developmental knockout, perhaps through compensatory changes in K^+/Cl^- cotransporter or $GABA_AR$ expression, scaling down of excitatory inputs, or structural rewiring that shifts stress signaling control to AVP neurons; however, such compensation is evidently less possible in the adult-specific, viral knockout, as the neuroendocrine response to stress is exacerbated, emotional behavior is abnormal, and body weight homeostasis is perturbed. The effects on metabolism are especially interesting in light of the novel projection I identified from PVN CRH neurons to the tuberal nucleus of the lateral hypothalamus, which is implicated in stress effects on feeding (Kremer, 1992). Enhanced

synaptic output from CRH neurons to the tuberal nucleus resulting from erosion of inhibitory constraint of the PVN could provide a straightforward, glucocorticoid-independent mechanistic explanation for the metabolic phenotype I observed. Considering the problem of using C-terminal domain-directed antibodies to detect changes in a C-terminal domain-truncated protein, however, the first step forward is to use alternative strategies such as perforated patch clamp electrophysiology to validate that KCC2 is indeed functionally impaired by our transgenic and viral transport knockout approaches.

Reconciling findings with previous studies

My approach to selectively manipulate inhibitory efficacy through KCC2 function in the PVN is novel, so there is little basis for conflict with previous studies. Additionally, the resulting disruptions in stress-related physiology and behavior are consistent with predictions that arise from the widely-accepted importance of effective inhibitory constraint of the PVN and particularly its transient reversal in adaptive stress signaling (Gao et al., 2016;Hewitt et al., 2009;Wamsteeker and Bains, 2010). There is still some debate regarding the importance of KCC2 functional expression in setting the chloride gradient versus restoring the gradient following chloride influx, given the impact of impermeant anions on ionic homeostasis (Glykys et al., 2014). However, I understand this debate to be more a matter of as-yet undetermined differences among brain regions in their developmental maturation of KCC2 function. For hypothalamic CRH neurons this developmental profile is well-established (Watanabe and Fukuda, 2015), so there is no apparent potential for conflict over KCC2's importance in determining GABA's hyperpolarizing or depolarizing action in the mature PVN.

Future directions

Mechanism of Antalarmin and bumetanide effects. We demonstrated that both the CRH receptor antagonist Antalarmin and the NKCC1 antagonist bumetanide blocked seizure-induced HPA axis activation and attenuated vulnerability to a second dose of KA. The most parsimonious explanation for these effects, given our understanding of HPA axis circuitry, are actions at corticotroph CRH receptor and PVN CRH neuron GABAergic inhibitory efficacy, respectively. However, we cannot decisively rule out drug actions at sites outside the pituitary and PVN, considering the widespread expression of CRHRs and NKCC1 throughout the brain (Millan et al., 1986;Kanaka et al., 2001) and periphery (Simard et al., 2010;Vasiadi et al., 2012;Shiozaki et al., 2014;Sun et al., 2016). Thus additional experiments using regional- or cell-specific manipulations of CRHRs and NKCC1 will be needed to ascertain the precise circuit-level mechanism of these drugs' efficacy against HPA axis exacerbation of seizure susceptibility. Of note, our laboratory recently demonstrated that intrahippocampal bumetanide effectively attenuated seizure severity in the KA model (Sivakumaran and Maguire, 2016). However, the possibility of a direct anticonvulsant action of bumetanide through hippocampal actions appears unlikely for the study described in Section 3, since the dose of systemic bumetanide used here did not significantly attenuate electrographic seizures induced by a single dose of 20 mg/kg KA, whereas the same dose of bumetanide was clearly able to reduce seizure-induced CORT and attenuate susceptibility to a second 10 mg/kg KA dose.

Manipulation of KCC2 transport function. Many of the results from my efforts to manipulate KCC2 function specifically in the PVN are still preliminary and demand additional follow-up in the future. For example, while we have identified putative collateral projections from PVN CRH neurons to the tuberal nucleus, we have not yet validated these as functional connections, and

the molecular profile of the postsynaptic targets of these connections will provide vital clues to their functional relevance. The evident lack of a dramatic effect on basal CORT levels is also preliminary, and this experiment must be repeated to be statistically robust. Furthermore, my results from indirect calorimetry indicating a potential effect of impaired PVN inhibitory efficacy on metabolism are extremely preliminary and must be explored further before any strong conclusions are drawn – especially considering the discrepancies in locomotor behavior between this paradigm and tests of anxiety-like behavior.

A more general concern is the lack of cell-type specificity in our adult knockout model, as viral Cre also presumably excises KCC2 transport from AVP-expressing parvocellular neuroendocrine cells and the other cell populations within the PVN, impairing inhibitory constraint of a potentially wide variety of PVN- but not CRH-specific functions. Fortunately we have recently acquired a novel virus (from Dr. Kerry Ressler at Harvard Medical School) that will allow us to overcome this limitation: a lentivirus encoding Cre recombinase under control of the CRH promoter, thus adding cell-specificity to the temporal- and spatial-specific viral approach that has so far been more effective than the transgenic model. These forthcoming studies will open up two equally intriguing possibilities: we may see similar effects on emotional behavior and body weight homeostasis, which would confirm that inhibitory constraint of PVN CRH neurons is critical to these functions; alternatively, we may uncover divergent effects between the cell-specific and -nonspecific approaches, which in turn could lead directly to uncovering the functional relevance of other cell types within the PVN.

GR and MR signaling as mechanisms for PVN KCC2 manipulation effects. There is one important and as-yet untested assumption built into both of my investigations of KCC2 in the

PVN: presumably excitatory GABA on PVN CRH neurons leads to an increase in circulating CORT, which in turn acts to produce the observed phenotypes through MR and GR signaling pathways. Over 250 genes containing glucocorticoid response elements (GREs) have been identified in adipocytes alone (Yu et al., 2010), and while the molecular mechanism of GR binding to GREs has been thoroughly characterized (Kadmiel and Cidlowski, 2013), surprisingly little is known about the specific genes whose expression is suppressed by GR to mediate CORT-dependent stress effects. Additionally, most studies of GR-mediated genomic effects have focused in peripheral systems on circadian fluctuations in CORT (Polidarova et al., 2016;Smith et al., 2016;Oster et al., 2016), and I have not yet directly probed GR or MR occupancy, expression, gene regulation, or rapid non-genomic actions, but here I will propose hypotheses about the specific actions of CORT in my investigations.

The main clinical uses of targeting GRs – for example, in rheumatoid arthritis and chronic obstructive pulmonary disease – derive from their peripheral anti-inflammatory and immunosuppressive actions (Buttgereit, 2012;Greulich et al., 2016;Kadmiel and Cidlowski, 2013). Indeed, these peripheral effects are precisely the obstacles to drug development targeting GRs in stress-related disorders or even basic research of the same: while it would presumably be beneficial to transiently block the excessive brain GR signaling resulting from trauma or chronic stress, there is currently no way to do this without also dangerously interfering with tonic peripheral GR actions. Of relevance to my manipulations of PVN KCC2 function, peripheral GR signaling has well-characterized effects on metabolism, acting to maintain circulating glucose levels by promoting protein degradation and suppressing insulin-induced glucose uptake (Kuo et al., 2013). These actions of GR suggest another potential mechanism underlying KCC2 knockout-mediated effects on body weight homeostasis: persistently elevated CORT could lead

to reduced weight gain through atrophy of peripheral tissue systems. Peripheral administration of GR antagonists is problematic for the reasons stated above, but in the future I could test this hypothesis by examining peripheral expression of GRE-containing genes that are thought to mediate CORT-induced tissue atrophy, such as Pik3r1, FoxO3, and MuRF1 (Kuo et al., 2013).

Hippocampal CORT is known to be important for stress effects on learning and memory (Joels and Baram, 2009), though once again, the specific genomic actions of GRs and MRs mediating these effects remain largely unknown. Nevertheless, in future studies it will be important to determine by microdialysis whether manipulating KCC2 expression in the PVN has a significant impact on basal hippocampal CORT levels: exogenous CORT has been shown to influence dendritic morphology and synaptic plasticity in the hippocampus (Kim and Diamond, 2002;Joels et al., 2007), so protracted elevation of hippocampal CORT is a promising candidate to explain the trend I observed toward a deficit in contextual fear memory following viral KCC2 knockout.

9.2. Inhibitory neurotransmission in the hippocampus

Significance

Our findings on tonic inhibition in the dentate gyrus following chronic stress adds to a growing list of cellular mechanisms that mediate stress effects on circuits throughout the brain: in this case, the critical substrate for gating information flowing into the hippocampal network. Similarly, our results from selectively disinhibiting neocortical and hippocampal somatostatin interneurons raise additional questions about these two distinct somatostatin interneuron populations, but nevertheless highlight a novel, critical role for these interneurons in emotional behavior. However, because these projects were tangential to my primary aim of studying hippocampal CRH interneurons, for further discussion of the significance of these findings I refer the reader to the respective publications (Lee et al., 2016) (Fuchs et al., 2016).

Turning to my investigation of hippocampal CRH: the identification of back-projection CRH interneurons as a novel interneuron type with unique connectivity could stand alone as a significant finding, as this broadens our conception of inhibitory neurotransmission in the hippocampus. Specifically, this class of interneurons is unique in that it primarily receives synaptic input directly from the neocortex, and projects across regions from CA1 to CA3 – against the usual flow of information through the trisynaptic circuit. Additionally, our biocytin labeling results suggest that CRH interneurons are electrically coupled together via gap junctions. This holds additional implications for their ability to function not just as individual units but as a concerted syncytium, similar to fast-spiking PV-positive basket cells, possibly entraining large populations of CA3 principal cells to rhythmic oscillations (Fukuda and Kosaka, 2000). The functional relevance of CRH interneurons to hippocampus-dependent memory is attested by the results of selectively removing them from the network with AAV-DTA. Finally, the observed

effects on locomotor activity – silencing or ablating this population produces a hyperactivity phenotype – is interesting as this implies additional functional connectivity to networks involved in controlling arousal, motivation, or behavioral inhibition.

Reconciling findings with previous studies

In our hands CRH neurons in the dorsal hippocampus exhibit a very low spontaneous firing rate basally. Accordingly, immunostaining reveals low levels of CRH throughout the hippocampus basally, in contrast to the BNST and CeA where CRH expression is more obvious. Acute stress causes an increase in hippocampal CRH neurons' spontaneous firing rate (Jamie Maguire, unpublished observations), and exogenous application of CRH increases the firing rate of hippocampal pyramidal neurons (Aldenhoff et al., 1983). Previous studies have quite logically assumed increased local concentrations of CRH in the hippocampus as indicative of increased hippocampal CRH interneuron activity (Chen et al., 2012). Surprisingly, I do not observe any striking change in CRH immunoreactivity in the hippocampus following acute restraint stress. This apparent disconnect in our results does, however, allow for a straightforward explanation: that relevant changes in CRH concentration are indeed occurring, but at a low enough range of concentrations that our methods are not sufficiently sensitive to detect them.

The major differences between our findings and previous work on this population, though, are the localization and molecular profile of hippocampal CRH neurons. Previous studies relying on immunostaining indicated that CRH neurons are dispersed throughout the hippocampal fields and express PV but not CCK (Yan et al., 1998;Chen et al., 2012;Chen et al., 2015); in our hands, CRH neurons are almost exclusively located in stratum pyramidale of CA1, none express PV at the protein level, and all express CCK at the mRNA level. One way to

reconcile these data is to concede that ours may be just one sub-population out of several distinct hippocampal CRH interneuron classes, hence the striking disparities in placement and molecular profile. There is currently a good deal of interest in this question as two recent publications from separate groups examined CRH reporter expression in the hippocampus and each reported strikingly different findings depending on the reporter line used (Chen et al., 2015;Kono et al., 2016). Particularly on the strength of our single-cell PCR data (see Section 7), I am convinced that the hippocampal CRH neuron population I have described above consists of *bona fide* CRH neurons with consistent profiles and critical functional relevance – however, I am quite open to the possibility of multiple distinct hippocampal CRH neuron sub-classes and interested in following up on this possibility through a more detailed analysis of the anatomical distribution of CRH reporter expression from each of the available lines.

Future directions

Intrinsic properties. My characterization of CRH interneurons' intrinsic properties, while thorough, remains incomplete. While we confirmed the presence of CCK in CRH interneurons at the mRNA level, we did not have a reliable CCK antibody to confirm this at the protein level. We have since identified a CCK antibody that works well for immunostaining, so I plan to follow up on this. The presence of CCK would be interesting not only for its own sake, but also because in other cortical interneuron classes, CCK expression reliably indicates the presence of cannabinoid receptor 1 (CB1R) (Eggan et al., 2010;Jappy et al., 2016). The presence of CB1R would have exciting implications for modulation of CRH interneurons' activity considering the known importance of hippocampal endocannabinoids in stress-related behavior (Dow-Edwards and Silva, 2016). On the subject of receptors, I am also broadly interested in assessing CRH interneurons' expression of neurotransmitter and neuromodulator receptors, including their

profile of glutamate and $GABA_A$ receptor subunits. Lastly, I will follow up on my connectivity experiments by testing hypotheses that were suggested but by no means definitively demonstrated in (Hooper and Maguire, 2014): that spines are absent from hippocampal CRH neuron dendrites; that gap junctions couple hippocampal CRH neurons together; and that hippocampal CRH neurons specifically innervate the perisomatic domain (versus other subcellular compartments) of CA3 pyramidal neurons.

Spatial learning and memory. While suggestive regarding their importance in hippocampus-dependent learning and memory, my object recognition memory results (see Section 8) raise the question of why ablating CRH interneurons impacted object memory at 3 hours but not at 24 hours. There are several potential explanations for this discrepancy: first, that CRH interneuron ablation produces a marginal effect on memory that can only be appreciated in the more demanding and thus more vulnerable 3 hour task; second, that since all animals were tested at both time points, the improved performance at 24 hours simply reflects additional "training" from the 3 hour test trial; third, that CRH interneurons are relevant to memory formation (or retrieval) within a relatively short time window; or fourth, that one of the novel objects is more salient to the mouse, thereby giving rise to a more robust memory. I plan to follow up on these initial findings by testing future cohorts at only one time point each, and by counterbalancing the two different novel objects across experimental groups.

State-dependence of activity. The lack of a robust effect on stress-reactive behaviors suggests that hippocampal CRH neurons' role in the network is not as simple as a stress state 'toggle'. However, selectively removing these neurons from the network had striking consequences for spatial memory and seizure susceptibility, highlighting their important place in the trisynaptic

circuit. Furthermore, field recording results reveal their potency in suppressing the excitability of area CA3, and taken together with our evidence that they are gap junction-coupled with one another, they are well-placed to be a critical component for preventing excessive excitability through the network, perhaps by clamping the excitability of CA3 to a homeostatic range. It will therefore be essential to identify under what physiological and pathological conditions this population mobilizes into high activity. An ideal approach to this question would be activity monitoring in freely-behaving animals, for example with CRH-specific expression of the fluorescent calcium indicator GCaMP and implantation of a mini-microscope capable of imaging the CA1 region.

CRH and non-neuronal cells. Another topic not directly addressed by our investigations in the hippocampus is the role of CRH signaling through non-neuronal cell types. Previous studies have demonstrated that microglia express CRHRs, and that microglial CRHR1 signaling is involved in regulating the inflammatory response to focal ischemia in the neocortex (Stevens et al., 2003), as well as neuropathic pain in the dorsal horn of the spinal cord (Kim et al., 2011). Very little investigation has been done on this topic though, and any manipulation of local CRH concentration – as, presumably, in our activity manipulations of CRH interneurons – will have consequences for microglia function.

CRH release *versus* GABA release. Finally, among the questions these investigations raise, the least-studied concern synaptic versus peptidergic function. Compared to synaptic vesicle exocytosis, the calcium-dependence of secretory granules has been sparsely studied. The main technical limitation that prevents measurement of endogenous peptidergic currents in receptor-expressing neurons is the time course of the impacted currents: leak potassium channels are

modulated by many second messenger systems, and under physiological conditions we would expect many of these modulatory systems to be modulating potassium conductance in parallel. As a result, disentangling the specific actions of CRHR1 signaling on leak potassium currents even in an acute slice model is impractical. Thus, even though our network excitability results are consistent with commensurate changes in GABAergic signaling in CA3, we cannot account for parallel changes that we are causing in CRHR1 signaling. Future studies need to elucidate the cellular mechanisms of secretory granule formation, transport, and fusion just as past studies have done for synaptic vesicles. One technique that holds promise for resolving peptidergic currents is the "sniffer patch" approach: cultured cells (for example, Chinese hamster ovary cells) can be transduced with CRHR1 and applied in an outside-out configuration to the tip of a recording electrode, which could then be moved, for example, over area CA3 to detect changes in CRH concentration with good temporal and spatial resolution. This method could even be taken a step further by designing a synthetic ionotropic receptor with a CRH-binding domain of CRHR1 to greatly improve temporal resolution.

Reference List

Aguilera G, Rabadan-Diehl C, Nikodemova M (2001) Regulation of pituitary corticotropin releasing hormone receptors. Peptides 22:769-774.

Albrechet-Souza L, Hwa LS, Han X, Zhang EY, DeBold JF, Miczek KA (2015) Corticotropin Releasing Factor Binding Protein and CRF2 Receptors in the Ventral Tegmental Area: Modulation of Ethanol Binge Drinking in C57BL/6J Mice. Alcohol Clin Exp Res 39:1609-1618.

Albus K, Wahab A, Heinemann U (2008) Standard antiepileptic drugs fail to block epileptiform activity in rat organotypic hippocampal slice cultures. Br J Pharmacol 154:709-724.

Aldenhoff JB, Gruol DL, Rivier J, Vale W, Siggins GR (1983) Corticotropin releasing factor decreases postburst hyperpolarizations and excites hippocampal neurons. Science 221:875-877.

Allers K, Essue BM, Hackett ML, Muhunthan J, Anderson CS, Pickles K, Scheibe F, Jan S (2015) The economic impact of epilepsy: a systematic review. BMC Neurol 15:245.

Andres AL, Regev L, Phi L, Seese RR, Chen Y, Gall CM, Baram TZ (2013) NMDA receptor activation and calpain contribute to disruption of dendritic spines by the stress neuropeptide CRH. J Neurosci 33:16945-16960.

Anne C, Gasnier B (2014) Vesicular neurotransmitter transporters: mechanistic aspects. Curr Top Membr 73:149-174.

Arruda-Carvalho M, Clem RL (2014) Pathway-selective adjustment of prefrontal-amygdala transmission during fear encoding. J Neurosci 34:15601-15609.

Artigas F (2001) Limitations to enhancing the speed of onset of antidepressants - are rapid action antidepressants possible? Hum Psychopharmacol 16:29-36.

Atasoy D, Aponte Y, Su HH, Sternson SM (2008) A FLEX switch targets Channelrhodopsin-2 to multiple cell types for imaging and long-range circuit mapping. J Neurosci 28:7025-7030.

Atkinson HC, Wood SA, Castrique ES, Kershaw YM, Wiles CC, Lightman SL (2008) Corticosteroids mediate fast feedback of the rat hypothalamic-pituitary-adrenal axis via the mineralocorticoid receptor. Am J Physiol Endocrinol Metab 294:E1011-E1022.

Balamurugan E, Aggarwal M, Lamba A, Dang N, Tripathi M (2013) Perceived trigger factors of seizures in persons with epilepsy. Seizure 22:743-747.

Bale TL, Contarino A, Smith GW, Chan R, Gold LH, Sawchenko PE, Koob GF, Vale WW, Lee KF (2000) Mice deficient for corticotropin-releasing hormone receptor-2 display anxiety-like behaviour and are hypersensitive to stress. Nat Genet 24:410-414.

Behan DP, De Souza EB, Lowry PJ, Potter E, Sawchenko P, Vale WW (1995) Corticotropin releasing factor (CRF) binding protein: a novel regulator of CRF and related peptides. Front Neuroendocrinol 16:362-382.

Ben-Ari Y, Khalilov I, Kahle KT, Cherubini E (2012) The GABA excitatory/inhibitory shift in brain maturation and neurological disorders. Neuroscientist 18:467-486.

Bergstrom HC (2016) The neurocircuitry of remote cued fear memory. Neurosci Biobehav Rev 71:409-417.

Bernardis LL, Bellinger LL (1993) The lateral hypothalamic area revisited: neuroanatomy, body weight regulation, neuroendocrinology and metabolism. Neurosci Biobehav Rev 17:141-193.

Bittencourt JC, Sawchenko PE (2000) Do centrally administered neuropeptides access cognate receptors?: an analysis in the central corticotropin-releasing factor system. J Neurosci 20:1142-1156.

Blaesse P, Airaksinen MS, Rivera C, Kaila K (2009) Cation-chloride cotransporters and neuronal function. Neuron 61:820-838.

Blaesse P, Guillemin I, Schindler J, Schweizer M, Delpire E, Khiroug L, Friauf E, Nothwang HG (2006) Oligomerization of KCC2 correlates with development of inhibitory neurotransmission. J Neurosci 26:10407-10419.

Blank T, Nijholt I, Eckart K, Spiess J (2002) Priming of long-term potentiation in mouse hippocampus by corticotropin-releasing factor and acute stress: implications for hippocampus-dependent learning. J Neurosci 22:3788-3794.

Bloom FE, Battenberg EL, Rivier J, Vale W (1982) Corticotropin releasing factor (CRF): immunoreactive neurones and fibers in rat hypothalamus. Regul Pept 4:43-48.

Borsini F, Meli A (1988) Is the forced swimming test a suitable model for revealing antidepressant activity? Psychopharmacology (Berl) 94:147-160.

Boyson CO, Holly EN, Shimamoto A, Albrechet-Souza L, Weiner LA, DeBold JF, Miczek KA (2014) Social stress and CRF-dopamine interactions in the VTA: role in long-term escalation of cocaine self-administration. J Neurosci 34:6659-6667.

Burdakov D, Karnani MM, Gonzalez A (2013) Lateral hypothalamus as a sensor-regulator in respiratory and metabolic control. Physiol Behav 121:117-124.

Burgos-Robles A, Vidal-Gonzalez I, Quirk GJ (2009) Sustained conditioned responses in prelimbic prefrontal neurons are correlated with fear expression and extinction failure. J Neurosci 29:8474-8482.

Burgoyne RD, Morgan A (2003) Secretory granule exocytosis. Physiol Rev 83:581-632.

Buttgereit F (2012) A fresh look at glucocorticoids how to use an old ally more effectively. Bull NYU Hosp Jt Dis 70 Suppl 1:26-29.

Cai X, Kallarackal AJ, Kvarta MD, Goluskin S, Gaylor K, Bailey AM, Lee HK, Huganir RL, Thompson SM (2013) Local potentiation of excitatory synapses by serotonin and its alteration in rodent models of depression. Nat Neurosci 16:464-472.

Cao Y, Wilcox KS, Martin CE, Rachinsky TL, Eberwine J, Dichter MA (1996) Presence of mRNA for glutamic acid decarboxylase in both excitatory and inhibitory neurons. Proc Natl Acad Sci U S A 93:9844-9849.

Caputto BL, Guido ME (2000) Immediate early gene expression within the visual system: light and circadian regulation in the retina and the suprachiasmatic nucleus. Neurochem Res 25:153-162.

Cardin JA, Carlen M, Meletis K, Knoblich U, Zhang F, Deisseroth K, Tsai LH, Moore CI (2010) Targeted optogenetic stimulation and recording of neurons in vivo using cell-type-specific expression of Channelrhodopsin-2. Nat Protoc 5:247-254.

Casillas-Espinosa PM, Hicks A, Jeffreys A, Snutch TP, O'Brien TJ, Powell KL (2015) Z944, a Novel Selective T-Type Calcium Channel Antagonist Delays the Progression of Seizures in the Amygdala Kindling Model. PLoS One 10:e0130012.

Cenquizca LA, Swanson LW (2007) Spatial organization of direct hippocampal field CA1 axonal projections to the rest of the cerebral cortex. Brain Res Rev 56:1-26.

Chamma I, Chevy Q, Poncer JC, Levi S (2012) Role of the neuronal K-Cl co-transporter KCC2 in inhibitory and excitatory neurotransmission. Front Cell Neurosci 6:5.

Chen N, Liu C, Yan N, Hu W, Zhang JG, Ge Y, Meng FG (2013a) A macaque model of mesial temporal lobe epilepsy induced by unilateral intrahippocampal injection of kainic Acid. PLoS One 8:e72336.

Chen Y, Andres AL, Frotscher M, Baram TZ (2012) Tuning synaptic transmission in the hippocampus by stress: the CRH system. Front Cell Neurosci 6:13.

Chen Y, Bender RA, Frotscher M, Baram TZ (2001) Novel and transient populations of corticotropin-releasing hormone-expressing neurons in developing hippocampus suggest unique functional roles: a quantitative spatiotemporal analysis. J Neurosci 21:7171-7181.

Chen Y, Brunson KL, Adelmann G, Bender RA, Frotscher M, Baram TZ (2004) Hippocampal corticotropin releasing hormone: pre- and postsynaptic location and release by stress. Neuroscience 126:533-540.

Chen Y, Dube CM, Rice CJ, Baram TZ (2008) Rapid loss of dendritic spines after stress involves derangement of spine dynamics by corticotropin-releasing hormone. J Neurosci 28:2903-2911.

Chen Y, Kramar EA, Chen LY, Babayan AH, Andres AL, Gall CM, Lynch G, Baram TZ (2013b) Impairment of synaptic plasticity by the stress mediator CRH involves selective destruction of thin dendritic spines via RhoA signaling. Mol Psychiatry 18:485-496.

Chen Y, Molet J, Gunn BG, Ressler K, Baram TZ (2015) Diversity of Reporter Expression Patterns in Transgenic Mouse Lines Targeting Corticotropin-Releasing Hormone-Expressing Neurons. Endocrinology 156:4769-4780.

Chen Y, Rex CS, Rice CJ, Dube CM, Gall CM, Lynch G, Baram TZ (2010) Correlated memory defects and hippocampal dendritic spine loss after acute stress involve corticotropin-releasing hormone signaling. Proc Natl Acad Sci U S A 107:13123-13128.

Chudotvorova I, Ivanov A, Rama S, Hubner CA, Pellegrino C, Ben-Ari Y, Medina I (2005) Early expression of KCC2 in rat hippocampal cultures augments expression of functional GABA synapses. J Physiol 566:671-679.

Cook CJ (2004) Stress induces CRF release in the paraventricular nucleus, and both CRF and GABA release in the amygdala. Physiol Behav 82:751-762.

Cota VR, Drabowski BM, de Oliveira JC, Moraes MF (2016) The epileptic amygdala: Toward the development of a neural prosthesis by temporally coded electrical stimulation. J Neurosci Res 94:463-485.

Coulter DA, Carlson GC (2007) Functional regulation of the dentate gyrus by GABA-mediated inhibition. Prog Brain Res 163:235-243.

Couve A, Moss SJ, Pangalos MN (2000) GABAB receptors: a new paradigm in G protein signaling. Mol Cell Neurosci 16:296-312.

Cryan JF, Mombereau C, Vassout A (2005) The tail suspension test as a model for assessing antidepressant activity: review of pharmacological and genetic studies in mice. Neurosci Biobehav Rev 29:571-625.

Curia G, Longo D, Biagini G, Jones RS, Avoli M (2008) The pilocarpine model of temporal lobe epilepsy. J Neurosci Methods 172:143-157.

Cushman JD, Moore MD, Olsen RW, Fanselow MS (2014) The role of the delta GABA(A) receptor in ovarian cycle-linked changes in hippocampus-dependent learning and memory. Neurochem Res 39:1140-1146.

Czeh B, Varga ZK, Henningsen K, Kovacs GL, Miseta A, Wiborg O (2015) Chronic stress reduces the number of GABAergic interneurons in the adult rat hippocampus, dorsal-ventral and region-specific differences. Hippocampus 25:393-405.

Dayas CV, Buller KM, Day TA (2001) Medullary neurones regulate hypothalamic corticotropin-releasing factor cell responses to an emotional stressor. Neuroscience 105:707-719.

de Andrade JS, Abrao RO, Cespedes IC, Garcia MC, Nascimento JO, Spadari-Bratfisch RC, Melo LL, da Silva RC, Viana MB (2012) Acute restraint differently alters defensive responses and fos immunoreactivity in the rat brain. Behav Brain Res 232:20-29.

de Andrade JS, Cespedes IC, Abrao RO, Dos Santos TB, Diniz L, Britto LR, Spadari-Bratfisch RC, Ortolani D, Melo-Thomas L, da Silva RC, Viana MB (2013) Chronic unpredictable mild

stress alters an anxiety-related defensive response, Fos immunoreactivity and hippocampal adult neurogenesis. Behav Brain Res 250:81-90.

De Francesco PN, Valdivia S, Cabral A, Reynaldo M, Raingo J, Sakata I, Osborne-Lawrence S, Zigman JM, Perello M (2015) Neuroanatomical and functional characterization of CRF neurons of the amygdala using a novel transgenic mouse model. Neuroscience 289:153-165.

de Kloet ER, Joels M, Holsboer F (2005) Stress and the brain: from adaptation to disease. Nat Rev Neurosci 6:463-475.

de Kloet ER, Vreugdenhil E, Oitzl MS, Joels M (1998) Brain corticosteroid receptor balance in health and disease. Endocr Rev 19:269-301.

Deeb TZ, Lee HH, Walker JA, Davies PA, Moss SJ (2011) Hyperpolarizing GABAergic transmission depends on KCC2 function and membrane potential. Channels (Austin) 5:475-481.

Deeb TZ, Maguire J, Moss SJ (2012) Possible alterations in GABAA receptor signaling that underlie benzodiazepine-resistant seizures. Epilepsia 53 Suppl 9:79-88.

Dow-Edwards D, Silva L (2016) Endocannabinoids in brain plasticity: Cortical maturation, HPA axis function and behavior. Brain Res.

Dravet C, Oguni H (2013) Dravet syndrome (severe myoclonic epilepsy in infancy). Handb Clin Neurol 111:627-633.

Drolet G, Rivest S (2001) Corticotropin-releasing hormone and its receptors; an evaluation at the transcription level in vivo. Peptides 22:761-767.

Duric V, Clayton S, Leong ML, Yuan LL (2016) Comorbidity Factors and Brain Mechanisms Linking Chronic Stress and Systemic Illness. Neural Plast 2016:5460732.

Duvarci S, Pare D (2007) Glucocorticoids enhance the excitability of principal basolateral amygdala neurons. J Neurosci 27:4482-4491.

Earnheart JC, Schweizer C, Crestani F, Iwasato T, Itohara S, Mohler H, Luscher B (2007) GABAergic control of adult hippocampal neurogenesis in relation to behavior indicative of trait anxiety and depression states. J Neurosci 27:3845-3854.

Eggan SM, Melchitzky DS, Sesack SR, Fish KN, Lewis DA (2010) Relationship of cannabinoid CB1 receptor and cholecystokinin immunoreactivity in monkey dorsolateral prefrontal cortex. Neuroscience 169:1651-1661.

Eichenbaum H (2013) What H.M. taught us. J Cogn Neurosci 25:14-21.

Erler P, Monaghan JR (2015) The link between injury-induced stress and regenerative phenomena: A cellular and genetic synopsis. Biochim Biophys Acta 1849:454-461.

Fanselow MS, Kim JJ (1992) The benzodiazepine inverse agonist DMCM as an unconditional stimulus for fear-induced analgesia: implications for the role of GABAA receptors in fear-related behavior. Behav Neurosci 106:336-344.

Feodorova YN, Sarafian VS (2012) Psychological stress--cellular and molecular mechanisms. Folia Med (Plovdiv) 54:5-13.

Fisher RS, Acevedo C, Arzimanoglou A, Bogacz A, Cross JH, Elger CE, Engel J, Jr., Forsgren L, French JA, Glynn M, Hesdorffer DC, Lee BI, Mathern GW, Moshe SL, Perucca E, Scheffer IE, Tomson T, Watanabe M, Wiebe S (2014) ILAE official report: a practical clinical definition of epilepsy. Epilepsia 55:475-482.

Forray MI, Gysling K (2004) Role of noradrenergic projections to the bed nucleus of the stria terminalis in the regulation of the hypothalamic-pituitary-adrenal axis. Brain Res Brain Res Rev 47:145-160.

Foy MR, Stanton ME, Levine S, Thompson RF (1987) Behavioral stress impairs long-term potentiation in rodent hippocampus. Behav Neural Biol 48:138-149.

Freund TF, Buzsaki G (1996) Interneurons of the hippocampus. Hippocampus 6:347-470.

Fuchs T, Jefferson SJ, Hooper A, Yee P-HP, Maguire J, Luscher B (2016) Disinhibition of somatostatin-positive GABAergic interneurons results in an anxiolytic and antidepressant-like brain state. Mol Psychiatry.

Fukuda T, Kosaka T (2000) Gap junctions linking the dendritic network of GABAergic interneurons in the hippocampus. J Neurosci 20:1519-1528.

Fuzesi T, Daviu N, Wamsteeker Cusulin JI, Bonin RP, Bains JS (2016) Hypothalamic CRH neurons orchestrate complex behaviours after stress. Nat Commun 7:11937.

Gafford GM, Ressler KJ (2015) GABA and NMDA receptors in CRF neurons have opposing effects in fear acquisition and anxiety in central amygdala vs. bed nucleus of the stria terminalis. Horm Behav 76:136-142.

Gallopin T, Geoffroy H, Rossier J, Lambolez B (2006) Cortical sources of CRF, NKB, and CCK and their effects on pyramidal cells in the neocortex. Cereb Cortex 16:1440-1452.

Gao Y, Zhou JJ, Zhu Y, Kosten T, Li DP (2016) Chronic Unpredictable Mild Stress Induces Loss of GABA Inhibition in Corticotrophin-Releasing Hormone-Expressing Neurons Through NKCC1 Upregulation. Neuroendocrinology.

Ghasemi A, Zahediasl S (2012) Normality tests for statistical analysis: a guide for non-statisticians. Int J Endocrinol Metab 10:486-489.

Glykys J, Dzhala V, Egawa K, Balena T, Saponjian Y, Kuchibhotla KV, Bacskai BJ, Kahle KT, Zeuthen T, Staley KJ (2014) Local impermeant anions establish the neuronal chloride concentration. Science 343:670-675.

Goldenberg MM (2010) Overview of drugs used for epilepsy and seizures: etiology, diagnosis, and treatment. P T 35:392-415.

Greenberg PE, Fournier AA, Sisitsky T, Pike CT, Kessler RC (2015) The economic burden of adults with major depressive disorder in the United States (2005 and 2010). J Clin Psychiatry 76:155-162.

Greenberg PE, Sisitsky T, Kessler RC, Finkelstein SN, Berndt ER, Davidson JR, Ballenger JC, Fyer AJ (1999) The economic burden of anxiety disorders in the 1990s. J Clin Psychiatry 60:427-435.

Gregus A, Wintink AJ, Davis AC, Kalynchuk LE (2005) Effect of repeated corticosterone injections and restraint stress on anxiety and depression-like behavior in male rats. Behav Brain Res 156:105-114.

Greulich F, Hemmer MC, Rollins DA, Rogatsky I, Uhlenhaut NH (2016) There goes the neighborhood: Assembly of transcriptional complexes during the regulation of metabolism and inflammation by the glucocorticoid receptor. Steroids 114:7-15.

Griffin A, Krasniak C, Baraban SC (2016) Advancing epilepsy treatment through personalized genetic zebrafish models. Prog Brain Res 226:195-207.

Guerrini R, Marini C, Mantegazza M (2014) Genetic epilepsy syndromes without structural brain abnormalities: clinical features and experimental models. Neurotherapeutics 11:269-285.

Hart PC, Bergner CL, Smolinsky AN, Dufour BD, Egan RJ, Laporte JL, Kalueff AV (2010) Experimental models of anxiety for drug discovery and brain research. Methods Mol Biol 602:299-321.

Hashimoto K, Makino S, Asaba K, Nishiyama M (2001) Physiological roles of corticotropin-releasing hormone receptor type 2. Endocr J 48:1-9.

Hatch RJ, Reid CA, Petrou S (2014) Enhanced in vitro CA1 network activity in a sodium channel beta1(C121W) subunit model of genetic epilepsy. Epilepsia 55:601-608.

Hemley CF, McCluskey A, Keller PA (2007) Corticotropin releasing hormone--a GPCR drug target. Curr Drug Targets 8:105-115.

Herman JP, Cullinan WE, Watson SJ (1994) Involvement of the bed nucleus of the stria terminalis in tonic regulation of paraventricular hypothalamic CRH and AVP mRNA expression. J Neuroendocrinol 6:433-442.

Herman JP, Mueller NK, Figueiredo H (2004) Role of GABA and glutamate circuitry in hypothalamo-pituitary-adrenocortical stress integration. Ann N Y Acad Sci 1018:35-45.

Herman JP, Ostrander MM, Mueller NK, Figueiredo H (2005) Limbic system mechanisms of stress regulation: hypothalamo-pituitary-adrenocortical axis. Prog Neuropsychopharmacol Biol Psychiatry 29:1201-1213.

Heuermann RJ, Jaramillo TC, Ying SW, Suter BA, Lyman KA, Han Y, Lewis AS, Hampton TG, Shepherd GM, Goldstein PA, Chetkovich DM (2016) Reduction of thalamic and cortical Ih by deletion of TRIP8b produces a mouse model of human absence epilepsy. Neurobiol Dis 85:81-92.

Hewitt SA, Wamsteeker JI, Kurz EU, Bains JS (2009) Altered chloride homeostasis removes synaptic inhibitory constraint of the stress axis. Nat Neurosci 12:438-443.

Hirtz D, Thurman DJ, Gwinn-Hardy K, Mohamed M, Chaudhuri AR, Zalutsky R (2007) How common are the "common" neurologic disorders? Neurology 68:326-337.

Hiscock JJ, Murphy S, Willoughby JO (2000) Confocal microscopic estimation of GABAergic nerve terminals in the central nervous system. J Neurosci Methods 95:1-11.

Holter SM, Einicke J, Sperling B, Zimprich A, Garrett L, Fuchs H, Gailus-Durner V, Hrabe de AM, Wurst W (2015a) Tests for Anxiety-Related Behavior in Mice. Curr Protoc Mouse Biol 5:291-309.

Holter SM, Garrett L, Einicke J, Sperling B, Dirscherl P, Zimprich A, Fuchs H, Gailus-Durner V, Hrabe de AM, Wurst W (2015b) Assessing Cognition in Mice. Curr Protoc Mouse Biol 5:331-358.

Hooper A, Maguire J (2014) Characterizing a novel interneuron subtype in the hippocampus expressing corticotropin-releasing hormone. in preparation.

Howard MW, Eichenbaum H (2015) Time and space in the hippocampus. Brain Res 1621:345-354.

Hunt RF, Girskis KM, Rubenstein JL, Alvarez-Buylla A, Baraban SC (2013) GABA progenitors grafted into the adult epileptic brain control seizures and abnormal behavior. Nat Neurosci 16:692-697.

Hwa LS, Holly EN, DeBold JF, Miczek KA (2016) Social stress-escalated intermittent alcohol drinking: modulation by CRF-R1 in the ventral tegmental area and accumbal dopamine in mice. Psychopharmacology (Berl) 233:681-690.

Ikonomidou C, Kaindl AM (2011) Neuronal death and oxidative stress in the developing brain. Antioxid Redox Signal 14:1535-1550.

Ionescu DF, Luckenbaugh DA, Niciu MJ, Richards EM, Slonena EE, Vande Voort JL, Brutsche NE, Zarate CA, Jr. (2014) Effect of baseline anxious depression on initial and sustained antidepressant response to ketamine. J Clin Psychiatry 75:e932-e938.

Janak PH, Tye KM (2015) From circuits to behaviour in the amygdala. Nature 517:284-292.

Jankord R, Herman JP (2008) Limbic regulation of hypothalamo-pituitary-adrenocortical function during acute and chronic stress. Ann N Y Acad Sci 1148:64-73.

Jappy D, Valiullina F, Draguhn A, Rozov A (2016) GABABR-Dependent Long-Term Depression at Hippocampal Synapses between CB1-Positive Interneurons and CA1 Pyramidal Cells. Front Cell Neurosci 10:4.

Joels M (2011) Impact of glucocorticoids on brain function: relevance for mood disorders. Psychoneuroendocrinology 36:406-414.

Joels M, Baram TZ (2009) The neuro-symphony of stress. Nat Rev Neurosci 10:459-466.

Joels M, Karst H, Krugers HJ, Lucassen PJ (2007) Chronic stress: implications for neuronal morphology, function and neurogenesis. Front Neuroendocrinol 28:72-96.

Juruena MF (2014) Early-life stress and HPA axis trigger recurrent adulthood depression. Epilepsy Behav 38:148-159.

Kadmiel M, Cidlowski JA (2013) Glucocorticoid receptor signaling in health and disease. Trends Pharmacol Sci 34:518-530.

Kahle KT, Deeb TZ, Puskarjov M, Silayeva L, Liang B, Kaila K, Moss SJ (2013) Modulation of neuronal activity by phosphorylation of the K-Cl cotransporter KCC2. Trends Neurosci 36:726-737.

Kanaka C, Ohno K, Okabe A, Kuriyama K, Itoh T, Fukuda A, Sato K (2001) The differential expression patterns of messenger RNAs encoding K-Cl cotransporters (KCC1,2) and Na-K-2Cl cotransporter (NKCC1) in the rat nervous system. Neuroscience 104:933-946.

Kandratavicius L, Balista PA, Lopes-Aguiar C, Ruggiero RN, Umeoka EH, Garcia-Cairasco N, Bueno-Junior LS, Leite JP (2014) Animal models of epilepsy: use and limitations. Neuropsychiatr Dis Treat 10:1693-1705.

Karst H, Berger S, Turiault M, Tronche F, Schutz G, Joels M (2005) Mineralocorticoid receptors are indispensable for nongenomic modulation of hippocampal glutamate transmission by corticosterone. Proc Natl Acad Sci U S A 102:19204-19207.

Keifer OP, Jr., Hurt RC, Ressler KJ, Marvar PJ (2015) The Physiology of Fear: Reconceptualizing the Role of the Central Amygdala in Fear Learning. Physiology (Bethesda) 30:389-401.

Keller-Wood M (2015) Hypothalamic-Pituitary--Adrenal Axis-Feedback Control. Compr Physiol 5:1161-1182.

Kessler RC, Petukhova M, Sampson NA, Zaslavsky AM, Wittchen H-U (2012) Twelve-month and lifetime prevalence and lifetime morbid risk of anxiety and mood disorders in the United States. Int J Methods Psychiatr Res 21:169-184.

Kim EH, Ryu DH, Hwang S (2011) The expression of corticotropin-releasing factor and its receptors in the spinal cord and dorsal root ganglion in a rat model of neuropathic pain. Anat Cell Biol 44:60-68.

Kim JJ, Diamond DM (2002) The stressed hippocampus, synaptic plasticity and lost memories. Nat Rev Neurosci 3:453-462.

Klausberger T, Somogyi P (2008) Neuronal Diversity and Temporal Dynamics: The Unity of Hippocampal Circuit Operations. Science 321:53-57.

Kolber BJ, Muglia LJ (2009) Defining brain region-specific glucocorticoid action during stress by conditional gene disruption in mice. Brain Res 1293:85-90.

Kono J, Konno K, Talukder AH, Fuse T, Abe M, Uchida K, Horio S, Sakimura K, Watanabe M, Itoi K (2016) Distribution of corticotropin-releasing factor neurons in the mouse brain: a study using corticotropin-releasing factor-modified yellow fluorescent protein knock-in mouse. Brain Struct Funct.

Krashes MJ, Koda S, Ye C, Rogan SC, Adams AC, Cusher DS, Maratos-Flier E, Roth BL, Lowell BB (2011) Rapid, reversible activation of AgRP neurons drives feeding behavior in mice. J Clin Invest 121:1424-1428.

Kremer HP (1992) The hypothalamic lateral tuberal nucleus: normal anatomy and changes in neurological diseases. Prog Brain Res 93:249-261.

Kuo T, Harris CA, Wang JC (2013) Metabolic functions of glucocorticoid receptor in skeletal muscle. Mol Cell Endocrinol 380:79-88.

Laxer KD, Trinka E, Hirsch LJ, Cendes F, Langfitt J, Delanty N, Resnick T, Benbadis SR (2014) The consequences of refractory epilepsy and its treatment. Epilepsy Behav 37:59-70.

LeDoux JE (1992) Brain mechanisms of emotion and emotional learning. Curr Opin Neurobiol 2:191-197.

Lee V, MacKenzie G, Hooper A, Maguire J (2016) Reduced tonic inhibition in the dentate gyrus contributes to chronic stress-induced impairments in learning and memory. Hippocampus 26:1276-1290.

Lee V, Maguire J (2013) Impact of inhibitory constraint of interneurons on neuronal excitability. Journal of Neurophysiology.

Lee V, Sarkar J, Maguire J (2014) Loss of Gabrd in CRH neurons blunts the corticosterone response to stress and diminishes stress-related behaviors. Psychoneuroendocrinology 41:75-88.

Levesque M, Avoli M (2013) The kainic acid model of temporal lobe epilepsy. Neurosci Biobehav Rev 37:2887-2899.

Lewis DA, Lund JS (1990) Heterogeneity of chandelier neurons in monkey neocortex: corticotropin-releasing factor- and parvalbumin-immunoreactive populations. J Comp Neurol 293:599-615.

Li N, Lee B, Liu RJ, Banasr M, Dwyer JM, Iwata M, Li XY, Aghajanian G, Duman RS (2010) mTOR-dependent synapse formation underlies the rapid antidepressant effects of NMDA antagonists. Science 329:959-964.

Lin LC, Sibille E (2013) Reduced brain somatostatin in mood disorders: a common pathophysiological substrate and drug target? Front Pharmacol 4:110.

Lovejoy DA, de LL (2013) Evolution and phylogeny of the corticotropin-releasing factor (CRF) family of peptides: expansion and specialization in the vertebrates. J Chem Neuroanat 54:50-56.

Lu NZ, Wardell SE, Burnstein KL, Defranco D, Fuller PJ, Giguere V, Hochberg RB, McKay L, Renoir JM, Weigel NL, Wilson EM, McDonnell DP, Cidlowski JA (2006) International Union of Pharmacology. LXV. The pharmacology and classification of the nuclear receptor superfamily: glucocorticoid, mineralocorticoid, progesterone, and androgen receptors. Pharmacol Rev 58:782-797.

Luscher B, Fuchs T (2015) GABAergic control of depression-related brain states. Adv Pharmacol 73:97-144.

Mackenzie G, Maguire J (2014) Chronic stress compromises GABAergic inhibition in the hippocampus and increases seizure susceptibility.

Maguire J, Mody I (2007) Neurosteroid synthesis-mediated regulation of GABA(A) receptors: relevance to the ovarian cycle and stress. J Neurosci 27:2155-2162.

Maguire J, Salpekar JA (2013) Stress, seizures, and hypothalamic-pituitary-adrenal axis targets for the treatment of epilepsy. Epilepsy Behav 26:352-362.

Makara GB (1992) The relative importance of hypothalamic neurons containing corticotropin-releasing factor or vasopressin in the regulation of adrenocorticotropic hormone secretion. Ciba Found Symp 168:43-51.

Maras PM, Baram TZ (2012) Sculpting the hippocampus from within: stress, spines, and CRH. Trends Neurosci 35:315-324.

Marx M, Haas CA, Haussler U (2013) Differential vulnerability of interneurons in the epileptic hippocampus. Front Cell Neurosci 7:167.

McEwen BS (2000) Effects of adverse experiences for brain structure and function. Biological Psychiatry 48:721-731.

McHugh TJ, Jones MW, Quinn JJ, Balthasar N, Coppari R, Elmquist JK, Lowell BB, Fanselow MS, Wilson MA, Tonegawa S (2007) Dentate gyrus NMDA receptors mediate rapid pattern separation in the hippocampal network. Science 317:94-99.

McKlveen JM, Myers B, Herman JP (2015) The medial prefrontal cortex: coordinator of autonomic, neuroendocrine and behavioural responses to stress. J Neuroendocrinol 27:446-456.

Mercado A, Broumand V, Zandi-Nejad K, Enck AH, Mount DB (2006) A C-terminal domain in KCC2 confers constitutive K+-Cl- cotransport. J Biol Chem 281:1016-1026.

Meyer AC, Dua T, Ma J, Saxena S, Birbeck G (2010) Global disparities in the epilepsy treatment gap: a systematic review. Bull World Health Organ 88:260-266.

Micioni Di Bonaventura MV, Ciccocioppo R, Romano A, Bossert JM, Rice KC, Ubaldi M, St LR, Gaetani S, Massi M, Shaham Y, Cifani C (2014) Role of bed nucleus of the stria terminalis corticotrophin-releasing factor receptors in frustration stress-induced binge-like palatable food consumption in female rats with a history of food restriction. J Neurosci 34:11316-11324.

Miklos IH, Kovacs KJ (2002) GABAergic innervation of corticotropin-releasing hormone (CRH)-secreting parvocellular neurons and its plasticity as demonstrated by quantitative immunoelectron microscopy. Neuroscience 113:581-592.

Millan MA, Jacobowitz DM, Hauger RL, Catt KJ, Aguilera G (1986) Distribution of corticotropin-releasing factor receptors in primate brain. Proc Natl Acad Sci U S A 83:1921-1925.

Miret M, Ayuso-Mateos JL, Sanchez-Moreno J, Vieta E (2013) Depressive disorders and suicide: Epidemiology, risk factors, and burden. Neurosci Biobehav Rev 37:2372-2374.

Mody I, Maguire J (2011) The reciprocal regulation of stress hormones and GABA(A) receptors. Front Cell Neurosci 6:4.

Morisot N, Rouibi K, Contarino A (2015) CRF2 Receptor Deficiency Eliminates the Long-Lasting Vulnerability of Motivational States Induced by Opiate Withdrawal. Neuropsychopharmacology 40:1990-2000.

Moss SJ, Smart TG (2001) Constructing inhibitory synapses. Nat Rev Neurosci 2:240-250.

Nemeroff CB, Widerlov E, Bissette G, Walleus H, Karlsson I, Eklund K, Kilts CD, Loosen PT, Vale W (1984) Elevated concentrations of CSF corticotropin-releasing factor-like immunoreactivity in depressed patients. Science 226:1342-1344.

Nicolaides NC, Kyratzi E, Lamprokostopoulou A, Chrousos GP, Charmandari E (2015) Stress, the stress system and the role of glucocorticoids. Neuroimmunomodulation 22:6-19.

O'Toole KK, Hooper A, Wakefield S, Maguire J (2014) Seizure-induced disinhibition of the HPA axis increases seizure susceptibility. Epilepsy Res 108:29-43.

Oster H, Challet E, Ott V, Arvat E, de Kloet ER, Dijk DJ, Lightman S, Vgontzas A, Van CE (2016) The functional and clinical significance of the 24-h rhythm of circulating glucocorticoids. Endocr Rever20151080.

Pacak K, Palkovits M, Kopin IJ, Goldstein DS (1995) Stress-induced norepinephrine release in the hypothalamic paraventricular nucleus and pituitary-adrenocortical and sympathoadrenal activity: in vivo microdialysis studies. Front Neuroendocrinol 16:89-150.

Panich U, Sittithumcharee G, Rathviboon N, Jirawatnotai S (2016) Ultraviolet Radiation-Induced Skin Aging: The Role of DNA Damage and Oxidative Stress in Epidermal Stem Cell Damage Mediated Skin Aging. Stem Cells Int 2016:7370642.

Park JT, Shahid AM, Jammoul A (2015) Common pediatric epilepsy syndromes. Pediatr Ann 44:e30-e35.

Partridge JG, Forcelli PA, Luo R, Cashdan JM, Schulkin J, Valentino RJ, Vicini S (2016) Stress increases GABAergic neurotransmission in CRF neurons of the central amygdala and bed nucleus stria terminalis. Neuropharmacology 107:239-250.

Petraglia F, Florio P, Gallo R, Salvestroni C, Lombardo M, Genazzani AD, Di CC, Stomati M, D'Ambrogio G, Artini PG (1996) Corticotropin-releasing factor-binding protein: origins and possible functions. Horm Res 45:187-191.

Pirker S, Schwarzer C, Wieselthaler A, Sieghart W, Sperk G (2000) GABA(A) receptors: Immunocytochemical distribution of 13 subunits in the adult rat brain. Neuroscience 101:815-850.

Poleszak E, Wosko S, Serefko A, Wlaz A, Kasperek R, Dudka J, Wrobel A, Nowak G, Wlaz P (2014) The effects of ifenprodil on the activity of antidepressant drugs in the forced swim test in mice. Pharmacol Rep 66:1031-1036.

Polidarova L, Houdek P, Sladek M, Novosadova Z, Pacha J, Sumova A (2016) Mechanisms of hormonal regulation of the peripheral circadian clock in the colon. Chronobiol Int1-16.

Pytka K, Dziubina A, Mlyniec K, Dziedziczak A, Zmudzka E, Furgala A, Olczyk A, Sapa J, Filipek B (2016) The role of glutamatergic, GABA-ergic, and cholinergic receptors in depression and antidepressant-like effect. Pharmacol Rep 68:443-450.

Rani V, Deep G, Singh RK, Palle K, Yadav UC (2016) Oxidative stress and metabolic disorders: Pathogenesis and therapeutic strategies. Life Sci 148:183-193.

Rashid S, Lewis GF (2005) The mechanisms of differential glucocorticoid and mineralocorticoid action in the brain and peripheral tissues. Clin Biochem 38:401-409.

Ren Z, Pribiag H, Jefferson SJ, Shorey M, Fuchs T, Stellwagen D, Luscher B (2016) Bidirectional Homeostatic Regulation of a Depression-Related Brain State by Gamma-Aminobutyric Acidergic Deficits and Ketamine Treatment. Biol Psychiatry 80:457-468.

Ren Z, Sahir N, Murakami S, Luellen BA, Earnheart JC, Lal R, Kim JY, Song H, Luscher B (2015) Defects in dendrite and spine maturation and synaptogenesis associated with an anxious-depressive-like phenotype of GABAA receptor-deficient mice. Neuropharmacology 88:171-179.

Ressler KJ (2010) Amygdala activity, fear, and anxiety: modulation by stress. Biol Psychiatry 67:1117-1119.

Reul JM, de Kloet ER (1985) Two receptor systems for corticosterone in rat brain: microdistribution and differential occupation. Endocrinology 117:2505-2511.

Roland BL, Sawchenko PE (1993) Local origins of some GABAergic projections to the paraventricular and supraoptic nuclei of the hypothalamus in the rat. J Comp Neurol 332:123-143.

Rotondo F, Butz H, Syro LV, Yousef GM, Di IA, Restrepo LM, Quintanar-Stephano A, Berczi I, Kovacs K (2016) Arginine vasopressin (AVP): a review of its historical perspectives, current research and multifunctional role in the hypothalamo-hypophysial system. Pituitary 19:345-355.

Rush AJ, Crismon ML, Toprac MG, Trivedi MH, Rago WV, Shon S, Altshuler KZ (1998) Consensus guidelines in the treatment of major depressive disorder. J Clin Psychiatry 59 Suppl 20:73-84.

Sarkar J, Wakefield S, Mackenzie G, Moss SJ, Maguire J (2011) Neurosteroidogenesis Is Required for the Physiological Response to Stress: Role of Neurosteroid-Sensitive GABAA Receptors. J Neurosci 31:18198-18210.

Sarkisova K, van LG (2011) The WAG/Rij strain: a genetic animal model of absence epilepsy with comorbidity of depression [corrected]. Prog Neuropsychopharmacol Biol Psychiatry 35:854-876.

Sawchenko PE, Swanson LW (1982) Immunohistochemical identification of neurons in the paraventricular nucleus of the hypothalamus that project to the medulla or to the spinal cord in the rat. J Comp Neurol 205:260-272.

Saxena A, Sampson JR (2015) Epilepsy in Tuberous Sclerosis: Phenotypes, Mechanisms, and Treatments. Semin Neurol 35:269-276.

Schweizer C, Balsiger S, Bluethmann H, Mansuy IM, Fritschy JM, Mohler H, Luscher B (2003) The gamma 2 subunit of GABA(A) receptors is required for maintenance of receptors at mature synapses. Mol Cell Neurosci 24:442-450.

Shiozaki A, Nako Y, Ichikawa D, Konishi H, Komatsu S, Kubota T, Fujiwara H, Okamoto K, Kishimoto M, Marunaka Y, Otsuji E (2014) Role of the Na (+)/K (+)/2Cl(-) cotransporter NKCC1 in cell cycle progression in human esophageal squamous cell carcinoma. World J Gastroenterol 20:6844-6859.

Shors TJ, Dryver E (1994) Effect of stress and long-term potentiation (LTP) on subsequent LTP and the theta burst response in the dentate gyrus. Brain Res 666:232-238.

Sik A, Ylinen A, Penttonen M, Buzsaki G (1994) Inhibitory CA1-CA3-hilar region feedback in the hippocampus. Science 265:1722-1724.

Silayeva L, Deeb TZ, Hines RM, Kelley MR, Munoz MB, Lee HH, Brandon NJ, Dunlop J, Maguire J, Davies PA, Moss SJ (2015) KCC2 activity is critical in limiting the onset and severity of status epilepticus. Proc Natl Acad Sci U S A 112:3523-3528.

Silberman Y, Winder DG (2013) Emerging role for corticotropin releasing factor signaling in the bed nucleus of the stria terminalis at the intersection of stress and reward. Front Psychiatry 4:42.

Simard M, Cote M, Provost PR, Tremblay Y (2010) Expression of genes related to the hypothalamic-pituitary-adrenal axis in murine fetal lungs in late gestation. Reprod Biol Endocrinol 8:134.

Sivakumaran S, Maguire J (2016) Bumetanide reduces seizure progression and the development of pharmacoresistant status epilepticus. Epilepsia 57:222-232.

Sloviter RS, Dichter MA, Rachinsky TL, Dean E, Goodman JH, Sollas AL, Martin DL (1996) Basal expression and induction of glutamate decarboxylase and GABA in excitatory granule cells of the rat and monkey hippocampal dentate gyrus. J Comp Neurol 373:593-618.

Smith SM, Vale WW (2006) The role of the hypothalamic-pituitary-adrenal axis in neuroendocrine responses to stress. Dialogues Clin Neurosci 8:383-395.

Smith SS, Dole NS, Franceschetti T, Hrdlicka HC, Delany AM (2016) microRNA-433 Dampens Glucocorticoid Receptor Signaling, Impacting Circadian Rhythm and Osteoblastic Gene Expression. J Biol Chem.

Soghomonian JJ, Martin DL (1998) Two isoforms of glutamate decarboxylase: why? Trends Pharmacol Sci 19:500-505.

Sperling MR, Schilling CA, Glosser D, Tracy JI, Asadi-Pooya AA (2008) Self-perception of seizure precipitants and their relation to anxiety level, depression, and health locus of control in epilepsy. Seizure 17:302-307.

Stevens SL, Shaw TE, Dykhuizen E, Lessov NS, Hill JK, Wurst W, Stenzel-Poore MP (2003) Reduced cerebral injury in CRH-R1 deficient mice after focal ischemia: a potential link to microglia and atrocytes that express CRH-R1. J Cereb Blood Flow Metab 23:1151-1159.

Sudhof TC, Rizo J (2011) Synaptic vesicle exocytosis. Cold Spring Harb Perspect Biol 3.

Sun PL, Jin Y, Park SY, Kim H, Park E, Jheon S, Kim K, Lee CT, Chung JH (2016) Expression of Na+-K+-2Cl- cotransporter isoform 1 (NKCC1) predicts poor prognosis in lung adenocarcinoma and EGFR-mutated adenocarcinoma patients. QJM 109:237-244.

Swaab DF, Hofman MA, Lucassen PJ, Purba JS, Raadsheer FC, Van de Nes JA (1993) Functional neuroanatomy and neuropathology of the human hypothalamus. Anat Embryol (Berl) 187:317-330.

Swanson LW, Sawchenko PE, Rivier J, Vale WW (1983) Organization of Ovine Corticotropin-Releasing Factor Immunoreactive Cells and Fibers in the Rat Brain: An Immunohistochemical Study. Neuroendocrinology 36:165-186.

Szilagyi T, Orban-Kis K, Horvath E, Metz J, Pap Z, Pavai Z (2011) Morphological identification of neuron types in the rat hippocampus. Rom J Morphol Embryol 52:15-20.

Takagi H (2000) Roles of ion channels in EPSP integration at neuronal dendrites. Neurosci Res 37:167-171.

Tatum WO (2012) Mesial temporal lobe epilepsy. J Clin Neurophysiol 29:356-365.

Telfeian AE, Tseng HC, Baybis M, Crino PB, Dichter MA (2003) Differential expression of GABA and glutamate-receptor subunits and enzymes involved in GABA metabolism between electrophysiologically identified hippocampal CA1 pyramidal cells and interneurons. Epilepsia 44:143-149.

Tellez-Zenteno JF, Hernandez-Ronquillo L (2012) A review of the epidemiology of temporal lobe epilepsy. Epilepsy Res Treat 2012:630853.

Tellez-Zenteno JF, Patten SB, Jette N, Williams J, Wiebe S (2007) Psychiatric comorbidity in epilepsy: a population-based analysis. Epilepsia 48:2336-2344.

Thierry AM, Gioanni Y, Degenetais E, Glowinski J (2000) Hippocampo-prefrontal cortex pathway: anatomical and electrophysiological characteristics. Hippocampus 10:411-419.

Tian N, Cui W, Zack M, Kobau R, Fowler KA, Hesdorffer DC (2016) Suicide among people with epilepsy: A population-based analysis of data from the U.S. National Violent Death Reporting System, 17 states, 2003-2011. Epilepsy Behav 61:210-217.

Uebelacker LA, Weisberg R, Millman M, Yen S, Keller M (2013) Prospective study of risk factors for suicidal behavior in individuals with anxiety disorders. Psychol Med 43:1465-1474.

Ulrich-Lai YM, Herman JP (2009) Neural regulation of endocrine and autonomic stress responses. Nat Rev Neurosci 10:397-409.

Vale W, Spiess J, Rivier C, Rivier J (1981) Characterization of a 41-residue ovine hypothalamic peptide that stimulates secretion of corticotropin and beta-endorphin. Science 213:1394-1397.

Vargas-Perez H, Bahi A, Bufalino MR, Ting AK, Maal-Bared G, Lam J, Fahmy A, Clarke L, Blanchard JK, Larsen BR, Steffensen S, Dreyer JL, van der Kooy D (2014) BDNF signaling in the VTA links the drug-dependent state to drug withdrawal aversions. J Neurosci 34:7899-7909.

Vasiadi M, Therianou A, Sideri K, Smyrnioti M, Sismanopoulos N, Delivanis DA, Asadi S, Katsarou-Katsari A, Petrakopoulou T, Theoharides A, Antoniou C, Papadavid E, Stavrianeas N, Kalogeromitros D, Theoharides TC (2012) Increased serum CRH levels with decreased skin CRHR-1 gene expression in psoriasis and atopic dermatitis. J Allergy Clin Immunol 129:1410-1413.

Venza M, Visalli M, Beninati C, De Gaetano GV, Teti D, Venza I (2015) Cellular Mechanisms of Oxidative Stress and Action in Melanoma. Oxid Med Cell Longev 2015:481782.

Vertes RP (2006) Interactions among the medial prefrontal cortex, hippocampus and midline thalamus in emotional and cognitive processing in the rat. Neuroscience 142:1-20.

Viggiano D (2008) The hyperactive syndrome: metanalysis of genetic alterations, pharmacological treatments and brain lesions which increase locomotor activity. Behav Brain Res 194:1-14.

Vollenweider I, Smith KS, Keist R, Rudolph U (2011) Antidepressant-like properties of alpha2-containing GABA(A) receptors. Behav Brain Res 217:77-80.

Walker D, Yang Y, Ratti E, Corsi M, Trist D, Davis M (2009) Differential effects of the CRF-R1 antagonist GSK876008 on fear-potentiated, light- and CRF-enhanced startle suggest preferential involvement in sustained vs phasic threat responses. Neuropsychopharmacology 34:1533-1542.

Wall NR, Wickersham IR, Cetin A, De La Parra M, Callaway EM (2010) Monosynaptic circuit tracing in vivo through Cre-dependent targeting and complementation of modified rabies virus. Proc Natl Acad Sci U S A 107:21848-21853.

Wamsteeker JI, Bains JS (2010) A synaptocentric view of the neuroendocrine response to stress. Eur J Neurosci 32:2011-2021.

Watanabe M, Fukuda A (2015) Development and regulation of chloride homeostasis in the central nervous system. Front Cell Neurosci 9:371.

Weninger SC, Dunn AJ, Muglia LJ, Dikkes P, Miczek KA, Swiergiel AH, Berridge CW, Majzoub JA (1999) Stress-induced behaviors require the corticotropin-releasing hormone (CRH) receptor, but not CRH. Proc Natl Acad Sci U S A 96:8283-8288.

West MJ, Gundersen HJ (1990) Unbiased stereological estimation of the number of neurons in the human hippocampus. J Comp Neurol 296:1-22.

Whissell PD, Eng D, Lecker I, Martin LJ, Wang DS, Orser BA (2013) Acutely increasing deltaGABA(A) receptor activity impairs memory and inhibits synaptic plasticity in the hippocampus. Front Neural Circuits 7:146.

Wise RA, Morales M (2010) A ventral tegmental CRF-glutamate-dopamine interaction in addiction. Brain Res 1314:38-43.

Yan HC, Cao X, Das M, Zhu XH, Gao TM (2010) Behavioral animal models of depression. Neurosci Bull 26:327-337.

Yan XX, Toth Z, Schultz L, Ribak CE, Baram TZ (1998) Corticotropin-releasing hormone (CRH)-containing neurons in the immature rat hippocampal formation: light and electron microscopic features and colocalization with glutamate decarboxylase and parvalbumin. Hippocampus 8:231-243.

Yang L, Zhao Y, Wang Y, Liu L, Zhang X, Li B, Cui R (2015a) The Effects of Psychological Stress on Depression. Curr Neuropharmacol 13:494-504.

Yang XD, Liao XM, Uribe-Marino A, Liu R, Xie XM, Jia J, Su YA, Li JT, Schmidt MV, Wang XD, Si TM (2015b) Stress during a critical postnatal period induces region-specific structural abnormalities and dysfunction of the prefrontal cortex via CRF1. Neuropsychopharmacology 40:1203-1215.

Yu CY, Mayba O, Lee JV, Tran J, Harris C, Speed TP, Wang JC (2010) Genome-wide analysis of glucocorticoid receptor binding regions in adipocytes reveal gene network involved in triglyceride homeostasis. PLoS One 5:e15188.

Zhang Y, Sheng H, Qi J, Ma B, Sun J, Li S, Ni X (2012) Glucocorticoid acts on a putative G protein-coupled receptor to rapidly regulate the activity of NMDA receptors in hippocampal neurons. Am J Physiol Endocrinol Metab 302:E747-E758.